The formation of the ophiolitic terrane of SW Norway – relationships between immature island arc volcanic sequences and trondhjemitic complexes on Bømlo

By Simen Saltvedt

Thesis for Master degree

In Geochemistry and Geobiology

Department of Earth Science

University of Bergen

September 2021

Abstract

Single zircon U/Pb dating, geochemistry, and field descriptions from trondhjemitic and tonalitic intrusions, intruding the Lykling Ophiolite Complex, provide new insights into the origin and evolution of the Early Ordovician ophiolitic terrane of SW Norway. A pluton of trondhjemite and (partly) tonalite, differentiated in the residual melt of ophiolite gabbro, intruded the Lykling Ophiolite Complex at 484 ± 6 Ma.

Major- and trace element analyses revealed that dacitic volcanics from the overlying Geitung Unit exhibits similar geochemical characteristics as the trondhjemites and tonalites indicating they are the intrusive and extrusive parts of the same magmatic event. Evidence for internal variations within the Geitung Unit points to a transitional phase where immature island arc dacites and trondhjemites evolved to more mature island arc magma than reported earlier. Two generations of basaltic dikes are reported in the Lykling Ophiolite Complex, where the older generation is related to the development of the ophiolite complex. The second-generation basaltic dikes are correlated with other volcanic groups and complexes on Bømlo; the Siggjo Complex, the Vikafjord Group and the Vardafjell Gabbro. All these lithologies are sourced from the same magma, and formed in a similar type of environment.

Zircon REE was used to reconstruct crustal thicknesses for two different lithologies at different stages in the island arc evolution. A trondhjemite and a siltstone from the Geitung Unit revealed crustal thicknesses of 55 and 66 km respectively. These thicknesses are highly contested compared to the modern-day equivalent, the Mariana Arc, in the western Pacific. Crustal thickness findings may be imprecise due to the applicability of this method in this type of formation setting.

Acknowledgements

First and foremost, I would like to thank my supervisor Professor Rolf Birger Pedersen for letting me work on such an interesting project and for valuable feedback during the writing process. I would also thank my co-supervisor Håvard H. Stubseid for feedback on the thesis and assistance in the field and in the preparation phase.

Furthermore, I would like to thank everyone involved with the lab work. I am grateful to Ida M. Gabrielsen for all the help in preparing samples for major- and trace element geochemistry as well as geochronology. A big thanks to Leif Erik Ryland Pedersen for all the help given in preparing and analyzing samples for U/Pb geochronology.

Particularly I would like to thank Matz S. Slotnes, Trond Fjellet and Frida R. Forsberg for being excellent field companions, as well as providing useful discussions during the writing process. Thank you to Øystein B. Asserson and the rest of the "Black Smoker" study room for making the last 2 (and a half) years unforgettable.

Finally, I would like to thank my girlfriend, Helene, and the rest of my family for immense support throughout my whole education, and for always being there with non-scientific help.

Bergen, 24.09.21

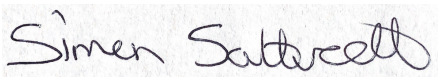

Simen Saltvedt

Table of contents

1. Introduction

The coastal regions of SW Norway comprise ophiolites, island arc complexes and closely associated lithologies belonging to the outboard terrane that constitute the upper allochthon of the nappe sequence of the Caledonian Orogeny (Figure 1.1). Bømlo, a place where such accreted oceanic realms are located, lies between Bergen to the north and Haugesund to the south. The geological history of Bømlo have been extensively researched over the last few decades (e.g. Sturt & Thon, 1978; Furnes, 1980; Brekke et al., 1984; Furnes, 1985; Nordås et al., 1985; Dunning & Pedersen, 1988; Pedersen & Hertogen, 1990, Pedersen et al., 1992; Pedersen & Dunning, 1997; Fonneland, 2002; Viken, 2017; Stubseid, 2017), and have been correlated to similar lithologies on the island of Karmøy, as well as in Gullfjellet, close to Bergen (Pedersen & Dunning, 1988; Pedersen et al., 1992). On Bømlo, a trondhjemitic and tonalitic complex intrude the Lykling Ophiolite Complex. Thus far, these plutonics have been limited in explorations and both age and affinity are hitherto unknown. This thesis elucidates the origin of these plutonics and provide new insights into the evolution of the ophiolitic terrane these rocks are a part of. Age and affinity of these rocks are unearthed through U/Pb dating of trondhjemites, and whole rock major- and trace element analyses.

In recent years, new analytical approaches and applications for zircon exploitations have been explored. Rare earth elements (REE) within the relatively high resilient zircons have been found to represent crystallization environments and magmatic sources of the rocks they occupy (Belousova et al., 2002), and to determine crustal thicknesses (Tang et al., 2021). In this thesis, these relatively new approaches are applied to the trondhjemitic intrusions on Bømlo revealing formation environment and crustal thicknesses of the island arc in its early, pre-collisional phase.

This study addresses our current understanding of the ophiolitic terrane and expands upon it bringing new findings to the heavily investigated area. This was carried out by combining field descriptions with several analytical methods. Geochemical analyses (major- and trace elements) were used for classifications of the different rocks, as well as helping to understand which environments they were formed in. Single zircon U/Pb dating of granitic plutons were used to provide absolute ages, and zircon rare earth element (REE) analyses used to determine

crustal thicknesses. Together all these analytical methods add to our current knowledge surrounding the origin and evolution of the Early Ordovician ophiolitic terrane in SW Norway.

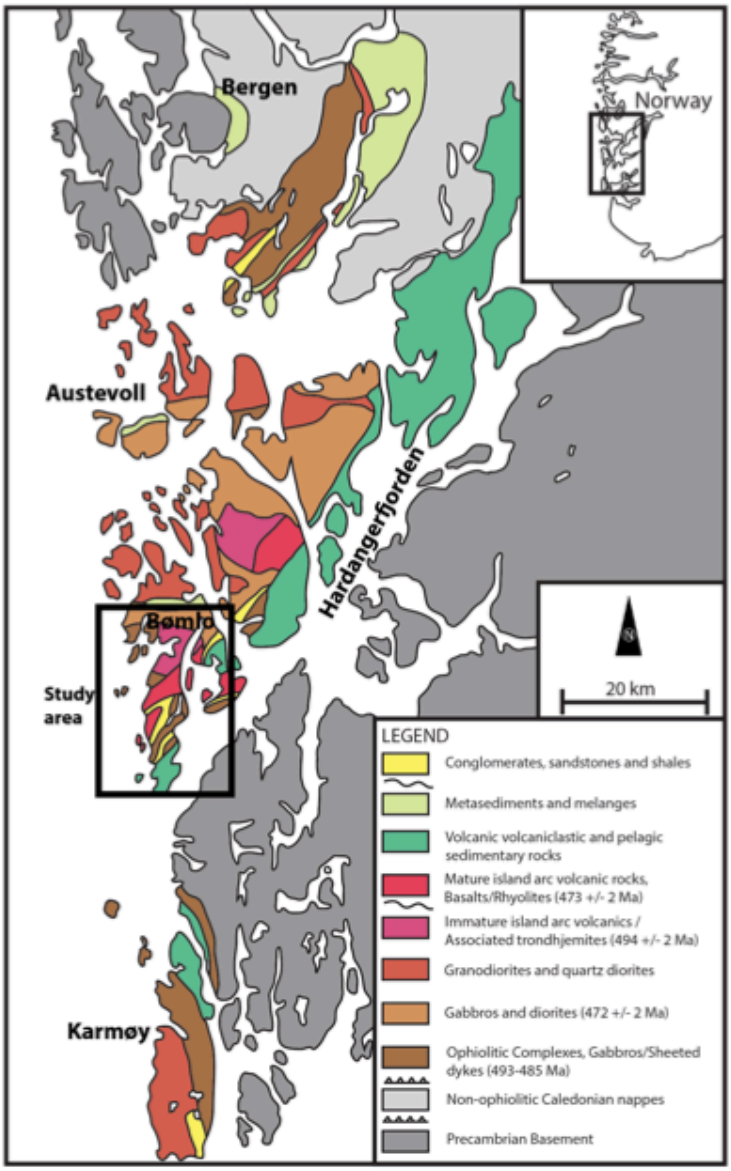

Figure 1.1. Geological map of the ophiolitic terrane in SW Norway with the study area marked with a black square box. Figure from Viken (2017).

2. Regional geology

2.1 Scandinavian Caledonides

Evolution of the Caledonian orogeny and tectonostratigraphy

The Scandinavian Caledonides is an early Paleozoic orogenic belt formed by the subduction of the Baltic margin beneath the Laurentian continent (Roberts & Gee, 1985). The orogeny was initiated in the Neoproterozoic when the two paleocontinents Baltica and Laurentia rifted apart, opening the Iapetus Ocean. Convergence in Ordovician and Silurian times led to the closing of the Iapetus Ocean and accretion of oceanic terranes onto the Laurentian margin before the main continent-continent collision between the two landmasses (Roberts, 2003; Corfu et al., 2007). This collision caused rapid subduction of the Baltic margin down to approximately 120 km depth where an equally rapid exhumation followed, and initiated extensional tectonics and orogenic collapse (Roberts, 2003).

During the collision, far-travelled nappes piled on top of the Precambrian Fennoscandian Basement. These nappes have been tectonostratigraphically divided into several north-south trending tectonic elements (Corfu et al., 2007); an autochthon-parautochthonous basement with various allochthonous segments (Roberts & Gee, 1985). The Allochthonous elements are are a series of nappes divided into the Lower-, Middle-, Upper-, and Uppermost Allochthon. The allochthons represent exotic landmasses that were thrust on to the continent from the west during collision (Stephens & Gee, 1989). The subdivision of the allochthons is based on their continental affinity. The Lower- and Middle Allochthon are thought to derive from the Pre-Caledonian margin of Baltica, while the Upper Allochthon represents the outermost margin as well as exotic terranes from outboard oceanic domains (e.g. ophiolite complexes and ocean island arcs). The Uppermost Allochthon has its origin from the Laurentian margin (Stephens et al., 1985)

The regional scale setting of the Caledonian orogeny is characterized by a w-dipping A-type subduction of the Baltic Shield beneath Laurentia in Silurian times (Griffin et al., 1985). Fossen (1992) subdivided the autochthon-parautochthon unit into three major tectonic components; 1) The Baltic Shield which constitutes the Precambrian basement of the Baltic continent; 2) a decollement zone in the late Precambrian to lower Paleozoic sediments; 3) an orogenic nappe wedge exposed above the decollement zone. The sediments of the decollement zone comprised

of mostly mechanically weak rocks such as phyllites and phyllonites acting as basal thruster to the far-travelled nappes that were emplaced onto the Baltic Shield (Fossen, 1992). The autochthonous Baltic Shield of the Precambrian basement crops out in central southern Norway in what is called the Hardangervidda section (Andersen & Andresen, 1994) (Figure 2.1).

The Lower Allochthon is mainly dominated by a Late Precambrian to Early Paleozoic sedimentary cover that have undergone detachments and folding that can be followed throughout the length of the mountain belt (Roberts & Gee, 1985). In some areas, Precambrian crystalline rocks from the Baltican basement is present (Fossen & Hurich, 2005), but these are constricted to the interior of the orogen (Roberts & Gee, 1985). Detrital zircon analysis of schists and phyllites exposed in both the parautochthon and the Lower Allochthon revealed both Timanian and Fennoscandian origins (Slama & Pedersen, 2015). Slama & Pedersen (2015) further indicate that the Timanian orogen may have shed detritus across larger areas towards both hinterland and foreland of the Baltic continent. The crystalline interior of the allochthon can be located in the southeastern part of Norway where it crops out adjacent to the sedimentary cover (Pedersen et al., 1992) (Figure 2.1).

The Middle Allochthon is overlying the Lower Allochthon and comprises heavily deformed crystalline rocks and unfossiliferous metasandstones. In parts these are extensively intruded by dolerites (Roberts & Gee, 1985). Primarily the Middle Allochthon include Precambrian crystalline rocks native to Baltica (Corfu & Roffeis, 2012), and are differentiated from the underlying nappe because there is no correlation with the crystalline basin of the autochthonous units. Several far-travelled nappes however belong to this allochthon, e.g. The Jotun, Bergsdalen and Lindås Nappe (Hossack & Cooper, 1986). The Middle Allochthon is situated on the eastern border of Norway (Pedersen et al., 1992) (Figure 2.1).

The Upper Allochthon is exposed in several locations along the coast from western Norway to the northern section of the country. This allochthon comprises the Upper and Lower Ordovician outboard terranes including the transported ophiolites and island-arc sequences. Several tectonic and magmatic units have been recognized within this allochthon (Roberts & Gee, 1985). The lower parts of the allochthon also include Precambrian basement lithologies rifted off the margin of Baltica (Andersen & Andresen, 1994). Most notably are the ophiolite complexes in and around Bergen, Bømlo and Karmøy. These ophiolite complexes are discussed in detail further in this thesis.

The Uppermost Allochthon only crops out in northern Norway where complexes of nappes dominated by gneisses, schists and granitoids dominate (Roberts & Gee, 1985). These are generally assumed to be of Laurentian affinity due to their preserved structures from the Taconian orogeny (Roberts et al., 2002).

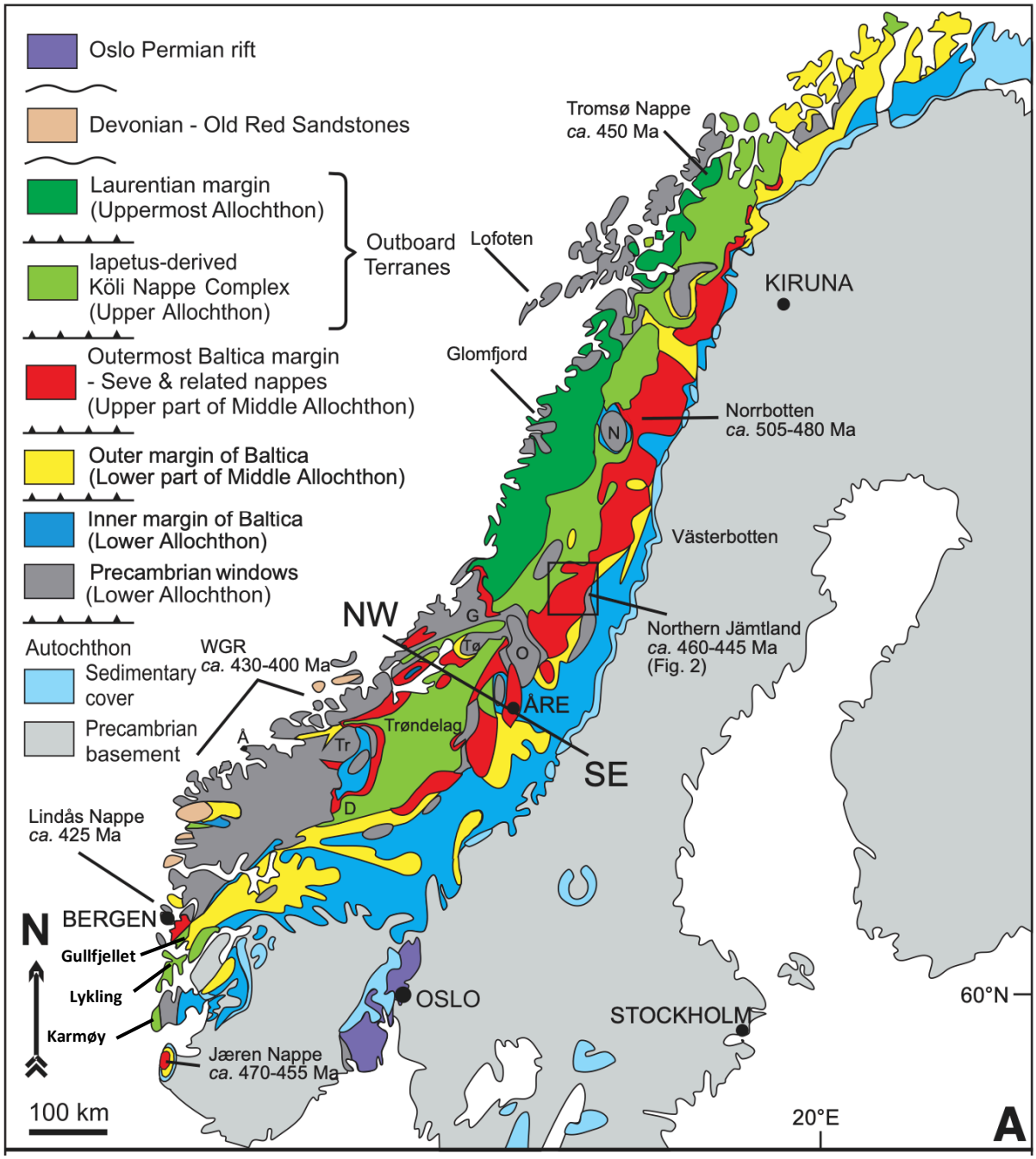

Figure 2.1. Tectonostratigraphical map of the Scandinavian Caledonides. Modified from Gee et al. (2013).

The allochthonous subdivision of the Scandinavian Caledonides was introduced by Gee et al. (1985) and Roberts & Gee (1985), and since then our understanding of the orogen have developed significantly. Some have criticized this categorization as an oversimplification inhibiting further understandings of the complex tectonic evolution (Corfu et al., 2014; Corfu et al., 2014). However, in this thesis the classifications presented by Gee et al. (1985) will be used.

2.2 The ophiolitic terrane of south-western Norway and associated early Silurian sedimentary sequences

The Upper Allochthon of the Scandinavian Caledonides hosts an array of ophiolites and island-arc sequences (Furnes, 1979; Stephens et al., 1985; Pedersen et al., 1988), and these complexes give insight to the evolution of the pre-continent-continent collision in Silurian times. Dunning and Pedersen (1988) proposed a subdivision of the ophiolitic terrane into two separate ages of formation. The older complexes revealed Tremadocian-Arenigian age (Early Ordovician) while the younger complexes show age signatures closer to Ashgillian age (Late Ordovician). The ophiolitic terrane of south-western Norway belongs to the older grouping and are backed up by geochronological and geochemical analyses as well as field relations (Pedersen et al., 1988). Ophiolites of south-western Norway include the Gullfjellet Complex within the Bergen Arc, the Lykling Ophiolite Complex on the islands of Bømlo and Stord, as well as the Karmøy Ophiolite Complex. Same formation and accretionary history were proposed for all three of these complexes as they show similarities in several areas: Plagiogranites within the Karmøy and Gullfjellet ophiolites yield similar U/Pb zircon ages within the analytical uncertainties (493 +7/-4 Ma and 489 ± 3 Ma respectively). The two ophiolite complexes are also intruded by arc-related plutons of tonalite and trondhjemite that also revealed similar ages (485 ± 2 Ma and 482 +6/-4 Ma) (Dunning & Pedersen, 1988). The minimum age of the Lykling ophiolite was constrained by dating the unconformably overlying Geitung Unit, which comprise an immature island-arc volcanic sequence. The intruding trondhjemite and tonalite into this ophiolite complex have a previously unknown age and affinity. All these complexes are also characterized by later intruding granitic complexes (the Sunnhordland Batholith and the West Karmøy Igneous Complex) and overlain by younger Silurian sediment deposits. Together they share a common geologic history where all complexes are remnant terranes of the oceanic

domain of the Iapetus Ocean that was closed during collision between Laurentia and Baltica (Dunning & Pedersen, 1988).

Gullfjellet Ophiolite Complex

The Gullfjellet Ophiolite Complex constitutes one of the major complexes from the Caledonian allochthonous sequence of the Major Bergen Arc (Furnes et al., 1982; Ingdahl, 1989 and references therein). A plutonic zone of olivine-bearing cumulates comprises the lower part of the complex. Overlain by layered metagabbros that gradually passes upwards into isotropic gabbro towards the top. The upper part of the complex comprises a NE-SW oriented sheeted dyke complex and pillow lavas. (Sturt & Thon, 1978)

Analysis of zircons separated from the ophiolite by Dunning & Pedersen (1988) yielded 489 ± 3 Ma as the crystallization age of the plagiogranites and the enclosing gabbro magma chamber of the ophiolite. Another arc-related crosscutting tonalite was dated to 482 +6/-4 Ma (Dunning & Pedersen, 1988).

Unconformably above Gullfjellet Ophiolite Complex lies the Ulven Group, a sedimentary sequence of Upper Ordovician to Lower Silurian age. The group comprises mainly quartzites, conglomerates and fossil bearing phyllites, and provenance studies conducted on these sediments revealed age signatures of Early Proterozoic to Middle Proterozoic (1800 Ma – 900 Ma) indicating a deposition after ophiolitic accretion (Fonneland, 2002).

Karmøy Ophiolite Complex and the Torvastad Group

The Karmøy Ophiolite Complex is the southernmost ophiolite present in south-western Norway. Dunning & Pedersen (1988) categorized the Karmøy ophiolite as a product of two distinct spreading events. First event, the Karmøy Axis Sequence (KAS), produced layered gabbro grading upwards into isotropic gabbro, finally transitioning into sheeted dykes and pillow lavas. The sheeted dykes of the KAS are referred to as the Feøy Sheeted Complex. The KAS is the oldest unit of the complex. Furthermore, this sequence is crosscut by plutonic and hypabyssal rocks whose trace element compositions is comparable to that of an ensimatic island arc origin. Zircons from the plagiogranitic rocks associated with this ophiolite was dated to 493 +7/-4 Ma (Dunning & Pedersen, 1988). An assembly of intrusions of trondhjemitic, tonalitic and doleritic compositions later intruded these rocks and revealed a U/Pb zircon age of 485 ±

2 Ma (Sauøy Diorite). The second spreading event is recorded in the swarm of boninitic dykes that intrude the aforementioned rocks. These younger dyke swarms are classified into three groups; Duøy, Helganes and Laksodden Dyke Swarms established by orientations and cross-cutting relationships.

The whole complex is overlain by the Torvastad Group comprising volcaniclastic rocks, basaltic pillow lavas, cherts and shales. The lowermost part of the group comprises of pyroclastic deposits that suggests deposition subsequent to the second spreading event (Dunning & Pedersen, 1988). Torvastad Group can be subdivided into four major formations. The Midtøy Formation displays intermediate pyroclastic flow deposits, various crystal tuffs and basaltic lava flows. The Velle Formation comprises volcaniclastic and pyroclastic deposits similar to the Feøy Gabbro, the Vikingstad Formation is a pillowed greenstone unit with locally interbedded cherts and phyllites. Lastly, the Håland Formation consists of phyllites and cherts (e.g. Pedersen & Hertogen, 1990). The Langevåg Group on Bømlo show similarities with the Torvastad Group and have been correlated due to their similar deposits and geochemical characteristics (Pedersen & Dunning, 1997)

In the Late Ordovician, the Skudeneset Group was deposited unconformably on top of the ophiolite and the West Karmøy Igneous Complex after a period of uplift and erosion processes (e.g. Pedersen & Hertogen, 1990). The Skudeneset Group is the youngest sequence on Karmøy.

Geology of the study area: Lykling Ophiolite Complex and associated volcano-sedimentary sequences

The Lykling ophiolite belongs to the Upper Allochthon of the Caledonides and is located on various islands in and around the area of Bømlo in SW Norway. Brekke et al. (1984) divided the ophiolite and associated sequences into five lithostratigraphic units; the Lykling Ophiolite, the Geitung Unit, the Langevåg Group, the Siggjo Complex and the Vikafjord Group. These units represent a geological section through a convergent plate margin from the stratigraphically old oceanic crust through overlying island arc sequences and marginal basin deposits (Brekke et al., 1984).

The lowermost unit of the complex is the Lykling ophiolite. This ophiolite is regarded as having an almost complete pseudostratigraphy and is therefore divided into a lower igneous zone (LOC), the overlying mixed extrusive/sedimentary zone (Geitung Unit) and an upper

sedimentary sequence (Figure 2.2) (Nordås et al., 1985). Serpentinites overlain by saussuritized gabbro are in parts layered, and generally the gabbro is described as homogenous or pegmatitic and microgabbroic. Trondhjemites have intruded both the plutonic and the volcanic parts of the ophiolite complex (Nordås et al., 1985).

The Geitung Unit represent a mixed extrusive/sedimentary zone that is made up of metabasalts, quartz-keratophyres and volcaniclastic breccias interbedded with sedimentary layers of chert, sandstones and minor conglomerates (Brekke et al., 1984; Nordås et al., 1984; Amaliksen, 1983). Trace element patterns is similar to that of modern immature island arc tholeiitic volcanics (Brekke et al., 1984) with the characteristic negative Nb- and Ta anomalies (Pedersen & Dunning, 1997). A basaltic-andesite of the Geitung Unit yielded a U/Pb zircon age of 494 ± 2 Ma (Pedersen & Dunning, 1997). This age conforms to the age from the tholeiitic axis sequence rocks (KAS) of the Karmøy ophiolite suggesting a cogenetic history between the two complexes. Both the LOC (Lykling ophiolite) and the extrusive/sedimentary sequence (Geitung Unit) is intruded by large bodies of tonalite and trondhjemite (Nordås et al., 1985). These plagiogranites comprises approximately 6 percent of the LOC (Nordås et al., 1985). They occur as voluminous intrusions and subordinate dykes within the gabbro of the ophiolite complex and the mixed extrusive/sedimentary zone (Amaliksen, 1983). Unconformably over the Geitung Unit and the Lykling ophiolite lies brecciated sediments derived from local substrate (Brekke et al., 1984).

The overlying Langevåg Group represent a transition from subaerial deposits to submarine conditions. The lower part comprises subaerial volcanics such as tuff-breccias and aa-lavas that are covered in an upward fining submarine deposit of subaqueous debris flows, radiolarian cherts, volcaniclastic turbidites and waterlain tuffs (Brekke et al., 1984). The top of the Langevåg Group is dominated by volcaniclastics of tholeiitic to alkaline affinity (Nordås et al., 1985). The Langevåg Group have been correlated with the Torvastad Group on Karmøy due to their similar geochemical characteristics and lithostratigraphy. (Pedersen & Dunning, 1997; Sivertsen, 1992) Both these groups represent Lower to Middle Ordovician strata that have formed, and progressively deepened a marine basin in a back-arc setting (Pedersen & Dunning, 1997).

The Siggjo Complex overlies both the Lykling ophiolite and the Geitung Unit unconformably. The unit is regarded as a part of the mixed extrusive/sedimentary cover (Nordås et al., 1985).

Subaerial volcanics mixed with intercalations of sedimentary rocks make up the complex (Brekke et al., 1984). Compositions of the Siggjo volcanics range from basaltic to rhyolitic and are characterized by relatively high K_2O contents (Furnes et al., 1986). An andesite sample from Siggjo revealed U/Pb ages of 473 ± 2 Ma and this age is comparable to the high-K calc-alkaline volcanics of the Feøy gabbro found in the Karmøy Ophiolite Complex (Pedersen & Dunning, 1997). The complex has close affinity to continental arc volcanics (Brekke et al., 1984; Dunning & Pedersen, 1988). The Kattnakken volcanics is a lateral continuation of the Siggjo Complex on the island of Stord and was formed from the same processes. The Kattnakken volcanics yielded a zircon U/Pb age of 476 ± 4 Ma (Pedersen & Dunning, 1997).

The Siggjo Complex is overlain by the Vikafjord Group dominated by sedimentary rocks with volcanics in the very upper parts. Limestones in the outer Hardangerfjord area have been correlated with the Vikafjord Group on Bømlo revealing a deposition age of 445 – 460 Ma Stubseid (2017). Alluvial debris flow deposits make up the lower part of the sequence and limestone and calcareous phyllites are present. A coarsening upwards sequence with turbiditic greywackes and sandstones represent a prograding delta. The fine-grained phyllites, cherts and non-fossiliferous limestones of the overlying Sagvatn Formation represent a second transgression and are overlain by coarse sandstones and conglomerates that represent an ancient fan-delta. At the very top of the Vikafjord Group subaerial, mafic lavas protrude. These extrusive volcanics consists of pahoehoe lavas, subordinate massive lavas and tuffs (Brekke et al., 1984).

The youngest group on Bømlo is the Utslettefjell Conglomerate. This group lies unconformably above the Vikafjord Group and are of Lower Silurian age. Schematic illustrations of the Lykling- and Karmøy Ophiolite Complexes can be found in figure 2.3.

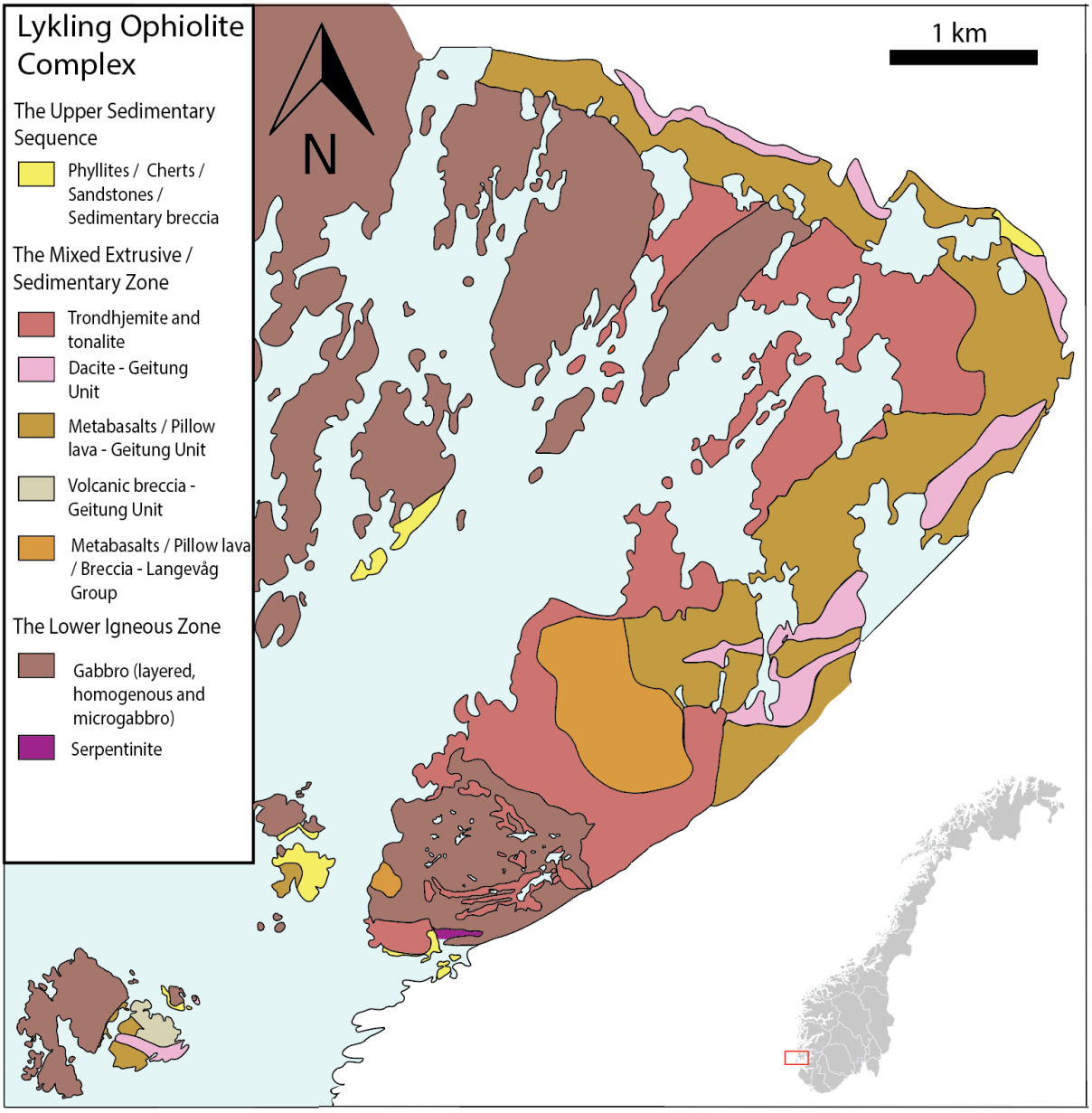

Figure 2.2. Geological map of the study area. Encompasses the Lykling Ophiolite Complex in the Lykling region on Bømlo (Modified from Nordås et al., 1985.)

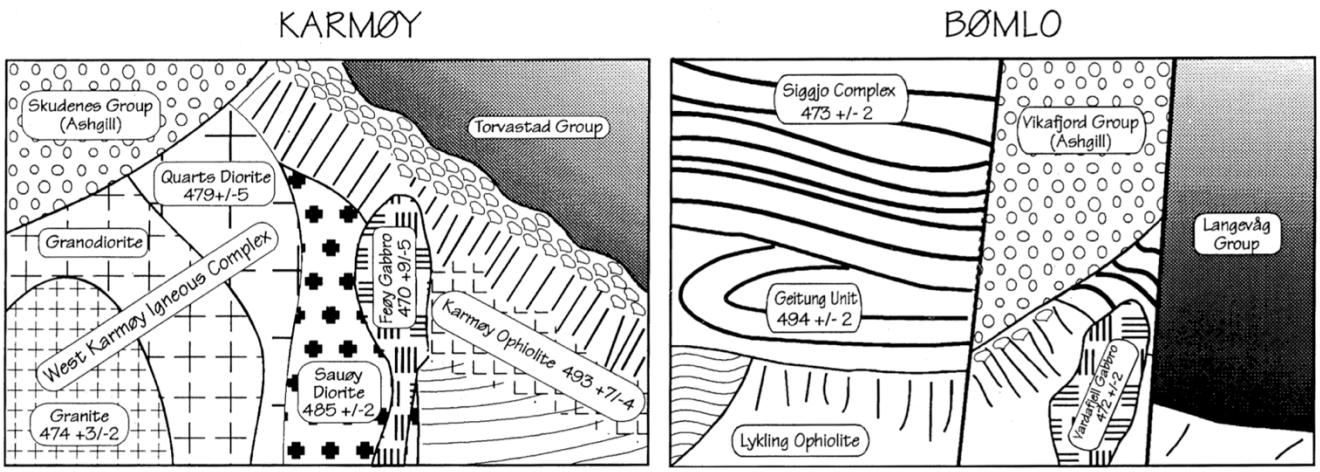

Figure 2.3. Schematic illustrations of the geology of the outboard terranes on Karmøy and Bømlo. From Pedersen & Dunning (1997).

Upper Ordovician to Lower Silurian Ophiolite complexes

Upper Ordovician ophiolites have been recognized in the Caledonian allochthons. These are regarded as the youngest ophiolite complexes of the orogen and represents a short-lived marginal basin during the final stages of the Iapetus Ocean (Dunning & Pedersen, 1988). A pegmatitic diorite in the Solund-Stavfjord Ophiolite Complex revealed U/Pb ages of 443 ± 3 Ma putting the formation of the complex in Late Ordovician time, and 40 – 50 Ma younger than the older generation of Caledonian ophiolites (Dunning & Pedersen, 1988). The overlying Staveneset Group show evidence of mixed metavolcanics as well as continentally derived metasediments further supporting a marginal basin formation close to a continental margin (Furnes et al., 1990).

2.3 The Sunnhordland Batholith and West Karmøy Igneous Complex

The Sunnhordland Batholith and the West Karmøy Igneous Complex are two plutonic complexes that intruded their respective ophiolite complexes and their associated island arc sequences in Middle/Late Ordovician to Early Silurian times. The Sunnhordland Batholith is exposed south of Bergen on the islands of Bømlo, Stord, Tysnes and Austevoll and occupies an approximate area of 1000 km^2 (Andersen & Jansen, 1987). This batholith is subdivided into three distinct units ranging from gabbroic to granodioritic and granitic compositions. The Vardafjell Gabbro that represent the oldest part of the batholith is dated from magmatic zircons to 472 ± 2 Ma (Pedersen & Dunning, 1997). Two granitic plutons (Rolvsneset and Korsneset granites) that represent the late evolution of the batholith are dated to 466 ± 2 Ma and 468 ± 1 Ma respectively (Schreiber et.al., 2016; R.B. Pedersen, unpublished data).

The West Karmøy Igneous Complex (WKIC) intrudes the Karmøy Ophiolite Complex and associated dyke swarms. The WKIC is mainly composed of quartz-diorite in its outer parts while the central parts are dominated by granites and granodiorites (e.g. Pedersen & Dunning, 1997). A quartz-diorite that define the outer rim of the complex is dated to 479 ± 5 Ma, and S-type granites that represent the youngest part of the complex yielded an age of 474 +3/-2 Ma (Pedersen & Dunning, 1997). Inherited zircons of Proterozoic age (1868 – 2170 Ma) are abundant in the younger plutons of this complex, and probably reflects the melting of continental margin sediments during the arc-continent collision (Pedersen & Dunning, 1997).

2.4 Magmatic and tectonic evolution of the outboard terranes

An evolution of the formation and subsequent accretion of the ophiolites and arc complexes of the Caledonides of SW Norway can be summarized based on the extensive research on field relationships, geochemistry and geochronology (e.g. Sturt & Thon, 1978; Furnes, 1980; Brekke et al., 1984; Furnes et al., 1986; Nordås et al., 1985; Dunning & Pedersen, 1988; Pedersen & Hertogen, 1990, Pedersen et al., 1992; Pedersen & Dunning, 1997; Fonneland, 2002; Viken, 2017; Stubseid, 2017). It has been well documented that the ophiolite complexes in SW Norway are closely related in time, thus suggesting a common geologic history (e.g. Dunning & Pedersen, 1988; Pedersen et al., 1992). The ophiolitic terrain was subjected to a continuous supra-subduction magmatism for at least 25 My. An immature island arc volcanism was starting to build 494 ± 2 Ma on top of older oceanic crust, but ophiolitic volcanism continued for 10 million years (My) concurrent with the immature island arc build up. Arc volcanism continued for 20 My evolving from immature to mature island arc volcanism and geochemically evolved from a tholeiitic arc magma to a high-K calc-alkaline magma signature. During the 20 My transition, dyke swarms of boninitic and IAT (island arc tholeiites) magmas intruded the complex (485 ± 2 Ma and 479 ± 5 Ma). The base of the arc crust was intruded by quartz-dioritic, tonalitic and granitic rocks between 485 ± 2 Ma and 474 +3/-2 Ma. These plutons contained inherited Precambrian zircons suggesting these magmas was partly formed from subducted continental material of Laurentian affinity and further supports a supra-subduction zone (Pedersen & Dunning, 1997).

An attempt at reconstructing the tectonic evolution was put forth by Pedersen et al. (1992). In this study, Ordovician faunal data was compared with new geochemical data as well as U/Pb radiometric dating data, to propose an origin closer to the Laurentian margin. Contemporaneous magma revealed inherited zircons of Archaen age that points to a Laurentian rather than Baltic origin. This data suggests that the ophiolite and arc complexes developed within a subduction system along the Laurentian side of the Iapetus Ocean, and in contrast to former assumptions (e.g. Brekke et al., 1984) that the ophiolitic terrane developed adjacent to the Baltic margin. Pedersen et al. (1992) constructed an evolutionary model in six steps of the early Ordovician island arc and ophiolite sequences (Figure 2.4).

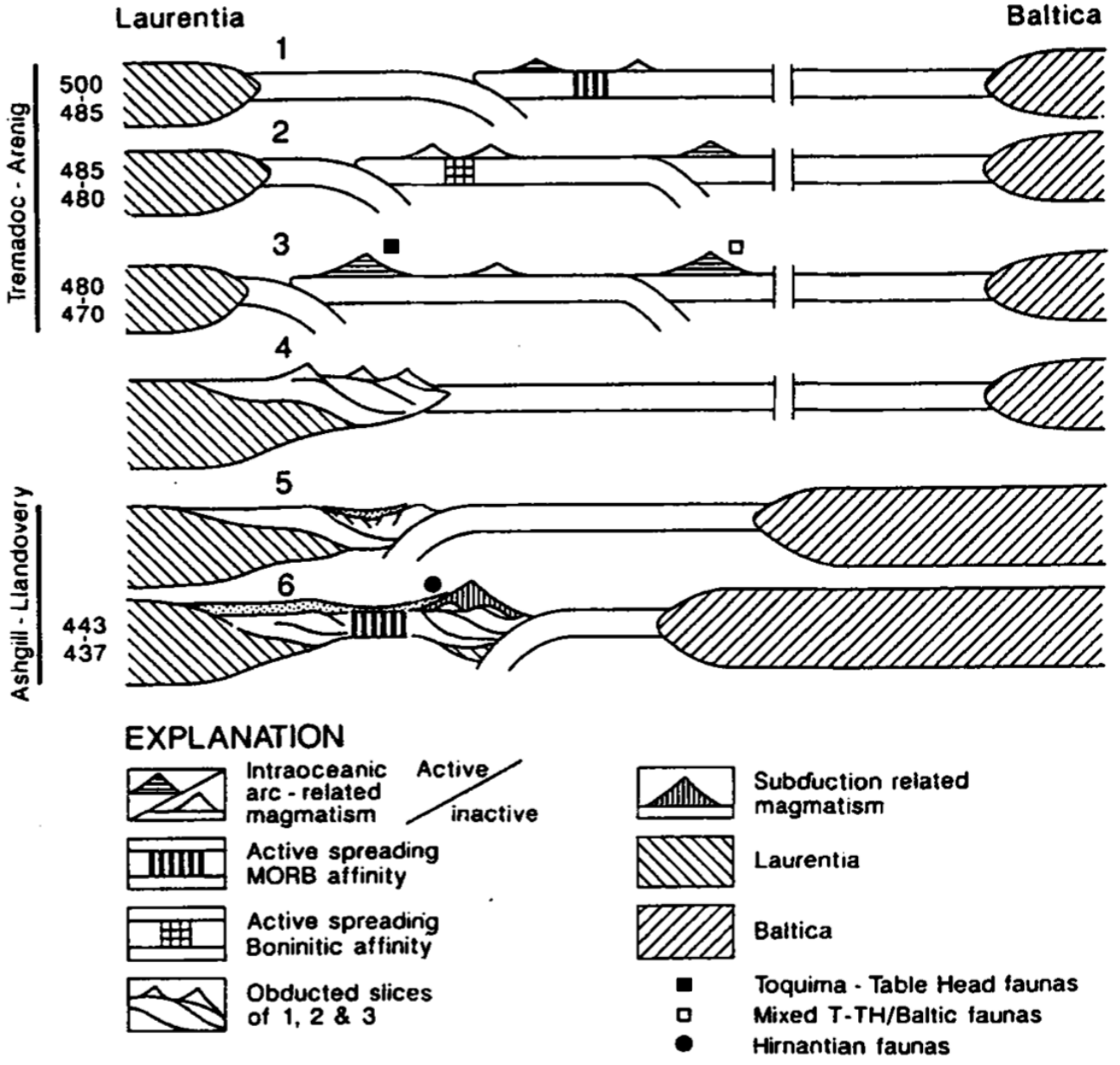

Figure 2.4. Tectonic evolution model from Pedersen et al. (1992). **1-2:** Initiation of subduction and development of immature island arcs (Geitung Unit). **3:** Build-up of mature island arcs (Siggjo Complex). **4**: Accretion of island arcs onto the Laurentian margin. **5-6**: Further subduction of the oceanic crust beneath the Iapetus Ocean and rifting of active continental margin and subsequent formation of late Ordovician to early Silurian marginal basins (Solund-Stavfjord Ophiolite Complex).

3. Analytical methods

3.1 Fieldwork and sampling

The fieldwork that is the basis for this study was conducted in 21 days during two intervals in June and August of 2020. The aim of the fieldwork was to establish field relationships and to carry out sampling. In total 64 representative samples were collected from four different lithologies spanning parts of the Bømlo peninsula from Bremnes in the north to Barbuneset on Lykling in the south (Appendix 1 and figure 8.1) These lithologies include granitic intrusive rocks (trondhjemites and tonalites), volcanics of the Geitung Unit, gabbros of the Lykling Ophiolite Complex and associated basaltic dikes. Out of the representative samples 39 samples were selected for geochemical analysis and three trondhjemite samples selected for U/Pb radiometric dating. All the collected samples have been prepared and analyzed at the University of Bergen.

3.2 Single zircon dating of trondhjemite samples

Sample preparation

The three samples that were prepared for zircon dating, were first cut into blocks with a diamond saw. The blocks were then crushed using a jaw crusher, and then pulverized using a Fritsch Pulverizette 13 discmill. The samples were finally sieved and the 315 μm fraction were collected for mineral separation. For each of the three rocks subsamples were collected to be used for geochemical analysis and thin section preparations.

A Holman Wilfley shaking table was used to separate the heavier minerals from the lighter minerals, that were collected in a separate box and dried in a drying cabinet. The heavier minerals were then run through a Frantz magnetic mineral separator to remove magnetic minerals from the sample. Five stages of magnetic removal were used for the samples for optimal removal of magnetic material. Currents were set at 0.3 A, 0.5 A, 0.7 A, 1.0 A and 1.2 A in that order. Forward and sideway tilt was set at 15 degrees during the separation.

Following the magnetic separation heavy liquids were utilized to separate minerals of various densities. The samples in this study used the popsicle method with diiodomethane (DIM) which has a density of ± 3.325 g/ml at room temperature. Firstly 30 ml of the heavy liquid was put in

a falcon tube followed by an appropriate amount of sample. When mixing the sample with DIM lighter minerals such as quartz, as well as medium dense minerals such as apatite, floated to the top of the liquid while the heavier zircons (3.9 – 4.7 g/ml) sank to the bottom of the falcon tube. After stirring with a stirring rod to maximize separation the bottom of the falcon tube was submerged in liquid nitrogen for 15 seconds to freeze the zircons in place. Rest of the material was poured out and the frozen zircons were thawed and stored for further preparations.

Samples 20BOM-11 and 20BOM-9A was then used in an acid bath using Aqua Regia (3:1 concentrated HCl + HNO_3) to dissolve the samples of the pyrite present. Sample 20BOM-12A had none to small amounts of pyrite present and was not subjected to acid bath.

At all stages during the preparation extreme caution and care was taken to avoid contamination.

Mount preparation

The material that was left in the samples was put on a petri dish under a microscope and extracted with a pipette. A cluster of 56, 45 and 36 zircons (for 20BOM-9A, 20BOM-11 and 20BOM-12A respectively) that was a representative subset of the total population was extracted. Handpicking individual zircons was refrained from due to personal bias.

The extracted zircons were further mounted in epoxy-filled resin on top of a glass plate and left to dry until hardened. The mounts were then run through a series of polishing processes to remove the epoxy from the grains and to access the core of the zircons. Firstly, the mounts were polished with a 15 μm silicon carbide powder followed by a 6 μm diamond coated paste. Lastly optimal analysis surfaces were obtained by using a 0.05 μm silicon carbide powder to polish uneven surfaces. The mounts were polished in intervals of 30 seconds on each plate before checking under a microscope whether the polish was sufficient enough for the next step. Images of each mount were taken with a mobile camera through the lens of the microscope after each polish.

Cathodoluminescence and backscatter imaging

Cathodoluminescence (CL) and backscatter imaging were used on the grains to view the internal structures of the zircons. These two imaging processes help towards selecting which grains to analyze, and where to point the laser during analysis. The mounts with zircons were

coated with carbon and put on a sample block with carbon tape. A Zeiss Supra 55 VP Scanning electron microscope equipped with a CENTAURUS CL detector and backscatter detector was used. Backscatter imaging was used to reveal inclusions and deformation within the zircons as well as other minerals that may have been selected by mistake when preparing the mounts. CL imaging was used to see zonation within the zircons and if the grains have any defects that may affect the analysis.

In situ U/Pb, REE, and trace element analysis of zircon using Laser ablation inductively coupled plasma mass spectrometer (LA-ICP-MS)

Before laser ablation the mounts were cleaned with de-ionized water and diluted HNO_3 (2%) to remove surface contaminations. The analysis was carried out using a Resonetics 193 mm ArF Excimer laser connected to a Nu ATTOM single collector ICP-MS. The laser was fired with a spot size of 26 μm, frequency of 5 Hz, and fluence of 2.2 – 2.5 J/cm^2, with all analysis parameters found in Appendix 3 – LA-ICP-MS. However, for the REE analyses the masses ^{139}La, ^{140}Ce, ^{141}Pr, ^{146}Nd, ^{147}Sm, ^{153}Eu, ^{157}Gd, ^{159}Tb, ^{163}Dy, ^{165}Ho, ^{166}Er, ^{169}Tm, ^{172}Yb, ^{176Lu}, and ^{179}Hf was analyzed with deflector peak jumping using 200 μs dwell time, while for the trace element analyses the masses ^{89}Y, ^{91}Zr, ^{139}La, ^{140}Ce, ^{141}Pr, ^{146}Nd, ^{152}Sm, ^{153}Eu, ^{157}Gd, ^{159}Tb, ^{164}Dy, ^{165}Ho, ^{166}Er, ^{169}Tm, ^{174}Yb, ^{175}Lu, ^{177}Hf, ^{181}Ta, ^{232}Th, and ^{238}U used link scan mode.

Four standard zircon grains were analyzed together with the sample from this study. These include the primary reference 91500, while Plesovice, GJ-1 and Mud Tank were used as secondary standards. The 91500 standard zircon is 1065 Ma and varies in grain size (Wiedenbeck et al., 1995). The Plesovice standard zircon has a grain size of 1 – 6 mm and an age of 337.1 Ma (Slama et al., 2008). The GJ-1 standard is a larger sized zircon at approximately 1 cm with an age of 609 Ma (Jackson et al., 2004). The Mud Tank standard is dated to 734.4 ± 1 Ma (Horstwood et al., 2016). Analysis are carried out with standard-sample bracketing to monitor analytical performance and correct for instrument drift during the analysis run.

Iolite 4 (v. 4.4.5, Paton et al., 2011) was used to process the raw data, with the "VizualAge UComPbine" data reduction scheme (Chew et al., 2014) for U/Pb data, while REE and trace element data used the "Trace Element" data reduction scheme (Paton et al., 2011). For the trace element data, ^{91}Zr was used as an internal standard. Data reduction includes instrumental mass bias compensation, element fractionation, and gas blanks correction. Down-hole element fractionation was corrected using an exponential or exponential + linear function. For U/Pb

analysis common Pb were monitored, but no common-Pb correction were applied to the data. Zircons with excess amounts of common Pb was excluded.

Isoplot (9.0) was used to present the U/Pb data acquired. IsoplotR allows for concordia, probability density and weighted mean plots (Vermeesch, 2018). All U/Pb ages below are presented as $^{206}Pb/^{238}U$ ages as this is the most precise age for zircons younger than 1000 Ma.

3.3 Major- and trace element analyses

Sample preparation for geochemical analyses were firstly done by cutting each sample into slices with a diamond saw to remove weathering surfaces. Furthermore, the samples were crushed down to small pebbles by hand using a hammer on a steel plate mounted on a stump. Lastly the samples were crushed to fine powder using a vibratory disc mill of agate. Loss on ignition (LOI) was measured on all samples. Two to four grams of the sample were heated to 1000 °C for two hours in a lab furnace, and accurately weighed before and after heat loss. This process removes all the volatiles and organic material present in the sample.

X-ray fluorescence (XRF)

For x-ray fluorescence analysis, the rock powder was melted and poured into collectors to form glass tablets. For this, 0.9600 ± 0.0002 g of rock powder were mixed with 6.7200 ± 0.0002 g of dried flux (Spectromelt A-10, lithium tetraborate). The sample was further placed in a gold-palladium crucible, mounted in a furnace and heated to above 1000 °C where the sample melted and was eventually poured into the collector. In total 39 glass tablets were produced. When analyzing the concentration of the different major elements (Al, Ca, Fe, K, Mg, Na, Mn, P, Si, Ti) a Bruker S4 PIONEER X-ray fluorescence spectrometer was used. Quantification was based on several USGS CRMs, while quality control was done by analyzing USGS CRM BCR2 (Columbia river basalt).

Inductively coupled plasma mass spectrometer (ICP-MS) and inductively coupled plasma atomic emission spectrometer (ICP-AES)

Samples weighing approximately 100 mg each was accurately weighed into a 25 ml PFA Savillex beaker and digested in 3 ml concentrated hydrofluoric acid (HF) on a heating plate at 135 °C for 48 hours. The residual fluoride was further hydrolyzed in a weak solution of nitric acid (HNO_3) under sub-boiling point conditions to ensure evaporation to dryness. This process

was necessary for unsolvable fluorides to transform to solvable nitrates. The remaining sample was dissolved and diluted in volumetric flasks to 50 ml by adding 2% HNO_3.

When analyzing the concentration of the different trace elements (Li, Sc, Ti, V, Cr, Mn, Co, Ni, Cu, Zn, Rb, Sr, Y, Zr, Nb, Cs, Ba, Hf, Ta, Pb, Th and U) a Thermo Scientific Element XR High-Resolution Inductively Coupled Plasma Mass Spectrometer (HR-ICP-MS) was used. Before instrumental analysis the samples were diluted with 2% HNO_3. Indium (In) was used as the internal standard, and both USGS CRM BCR2 (Columbia river basalt) and CRM SPS-SW2 (synthetic water) standards were repeatedly run throughout the analysis.
Most major- and some trace elements (Al, B, Ba, Ca, Co, Cr, Cu, Fe, K, Li, Mg, Na, Mn, Ni, P, Pb, S, Sr, Ti, V, Y, Zn, Zr and REE, *optional Ga, Ge, Mo and others*) was analyzed using an ICP Atomic Emission Spectrometer (ICP-AES) (Thermo Scientific ICap 7600). Pre-analysis the samples were diluted with 2% HNO_3. Scandium (Sc) was used as an internal standard. USGS CRM BCR-2 was used for quality control.

4. Results

The results presented in this study is largely focused on comparisons between trondhjemite and the Geitung Unit volcanics as they provide key information into the early evolution of the island arc system. Samples were collected from four different lithological units within or in association with the Lykling Ophiolite Complex. These four lithologies include granitic intrusions (tonalites and trondhjemites), dacitic and rhyolitic volcanic rocks that are present within the Geitung Unit, ophiolitic gabbros, and basaltic dikes that intrude these gabbros. A total of 39 samples were analyzed with respect to major- and trace element compositions and three samples were dated by zircon geochronology. Trondhjemite intrusions are common in the Lykling area (Figure 4.1), and 15 samples were collected of trondhjemites and tonalites to ensure that the geochemical spectrum of the area was well covered. From the Geitung Unit, 11 samples of dacites, andesites and rhyolites were collected. In addition, five samples were collected from the ophiolitic gabbro, as well as one gabbro from the Vardafjell Gabbro (Sunnhordland Batholith). Seven samples were collected of basaltic dikes within the study area. In addition to a report on the field observations, the geochemical characteristics of the various lithologies and geochronology are also provided in this section.

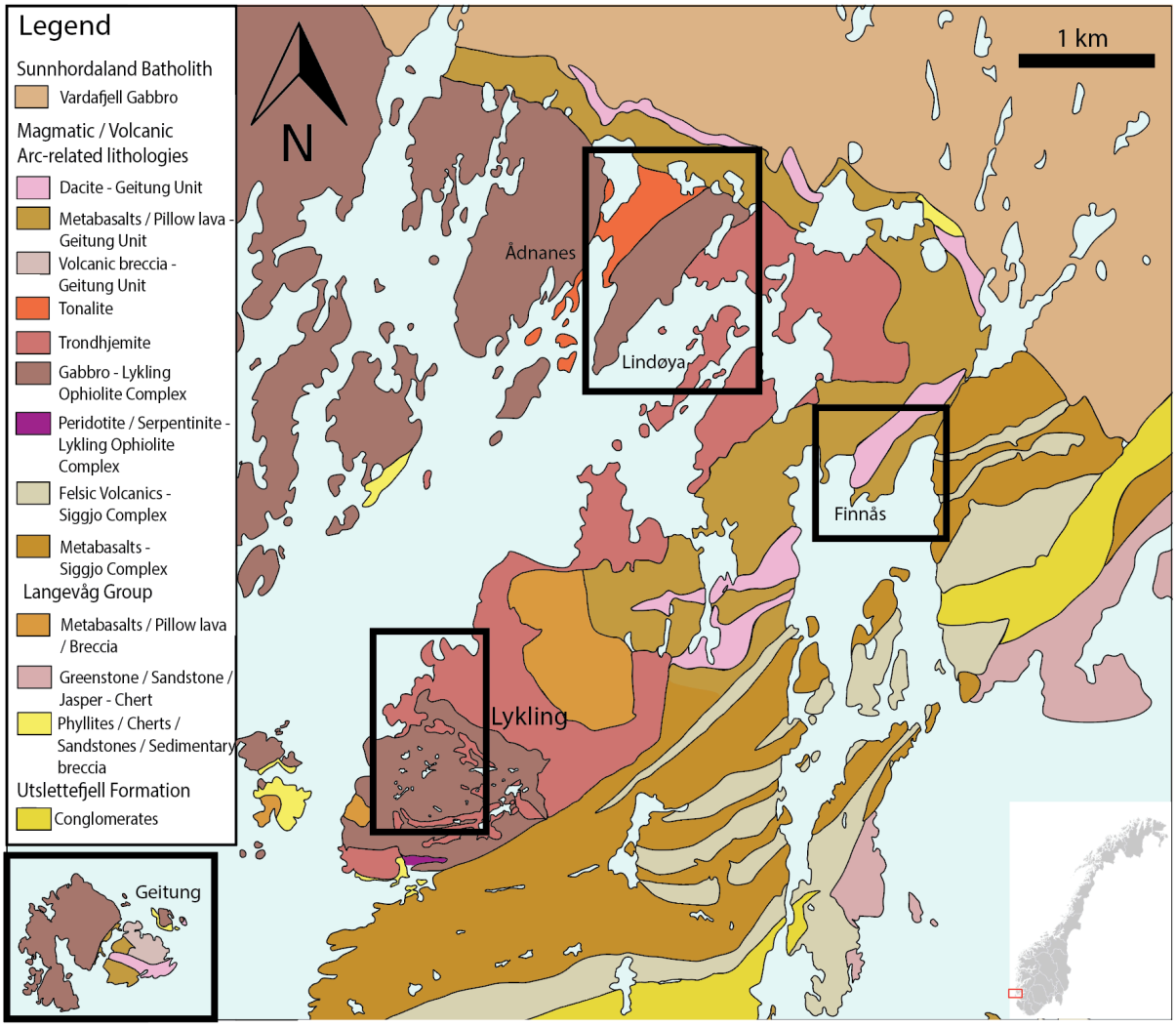

Figure 4.1. Geological map of the study area in the Lykling region on central Bømlo. Key sample locality areas are marked in black square boxes. Drawing based on NGU 2021 (https://geo.ngu.no/kart/berggrunn_mobil/).

4.1 Key localities and field relationships

The following chapter is a list of the six key localities and a brief description of them. These localities cover the areas where most of the samples were collected, and where key field relationships were determined. A full list of all samples collected can be found in table 4.1. A detailed description of each sample locality can be found in Appendix 1.

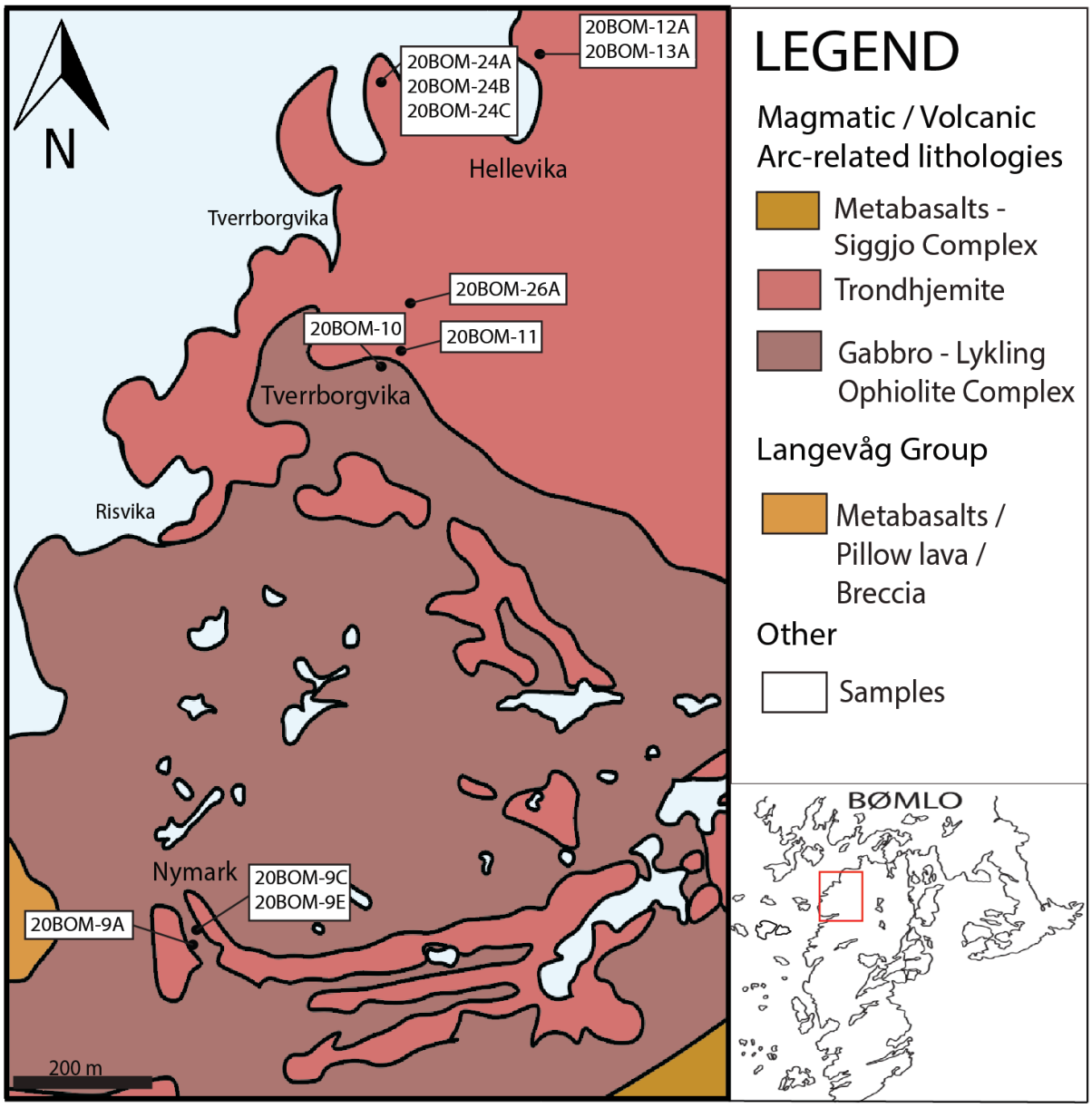

Figure 4.2. Geological map of the Lykling area on Bømlo showing the geology of the three main localities (Nymark, Øvre Tverrborgvika and Hellevika) and the sample locations. Drawing based on NGU 2021 (https://geo.ngu.no/kart/berggrunn_mobil/)

The Nymark locality

Located in southern Lykling (Figure 4.2) this locality clearly visualizes the intrusive contact between the trondhjemites and the ophiolitic gabbro that predates these granitic rocks (Figure 4.3A & B). Whereas trondhjemites dominate in the southern part of the area, tonalite is present in the northern part at the Ådnanes locality. The trondhjemites can be distinguished from the homogenous gabbros by the presence of quartz, and from the tonalites by their lighter color which is due to their lower contents of mafic minerals. The contact on this locality is sharp with massive granite on one side and schistose gabbro on the other side. The schistosity decrease further away from the contact and is regarded a contact feature caused by rheological contrasts. The gabbro is also more fine-grained towards the contact and is considered a microgabbro. The trondhjemite displays high concentrations of quartz and is darkly colored with no apparent K-feldspar present. Plagioclase is also abundant (Figure 4.4B). The dark color is proposed to be influenced by the mafic minerals within the rock. At this locality, a sample of trondhjemite (20BOM-9A) was collected a few meters away from the intrusive contact (Figure 4.4A), and samples of trondhjemite and gabbro (20BOM-9C and 20BOM-9E respectively) were collected close to the contact.

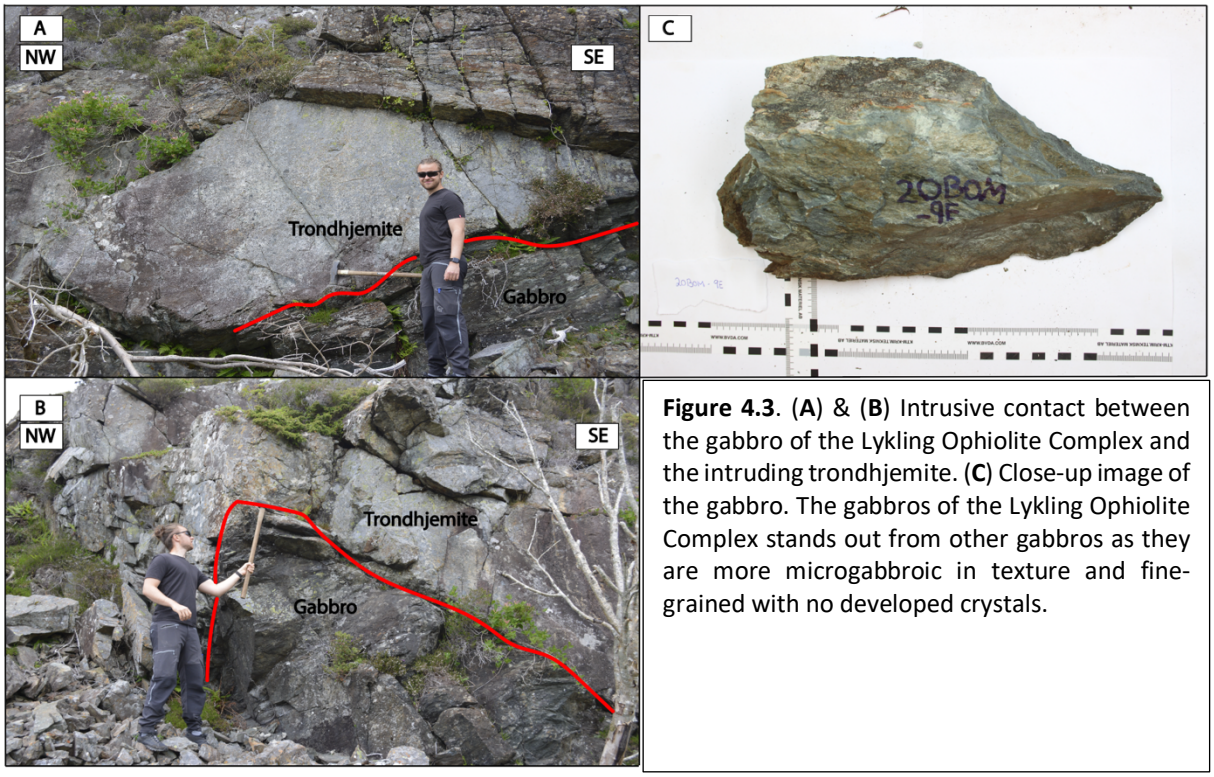

Figure 4.3. (**A**) & (**B**) Intrusive contact between the gabbro of the Lykling Ophiolite Complex and the intruding trondhjemite. (**C**) Close-up image of the gabbro. The gabbros of the Lykling Ophiolite Complex stands out from other gabbros as they are more microgabbroic in texture and fine-grained with no developed crystals.

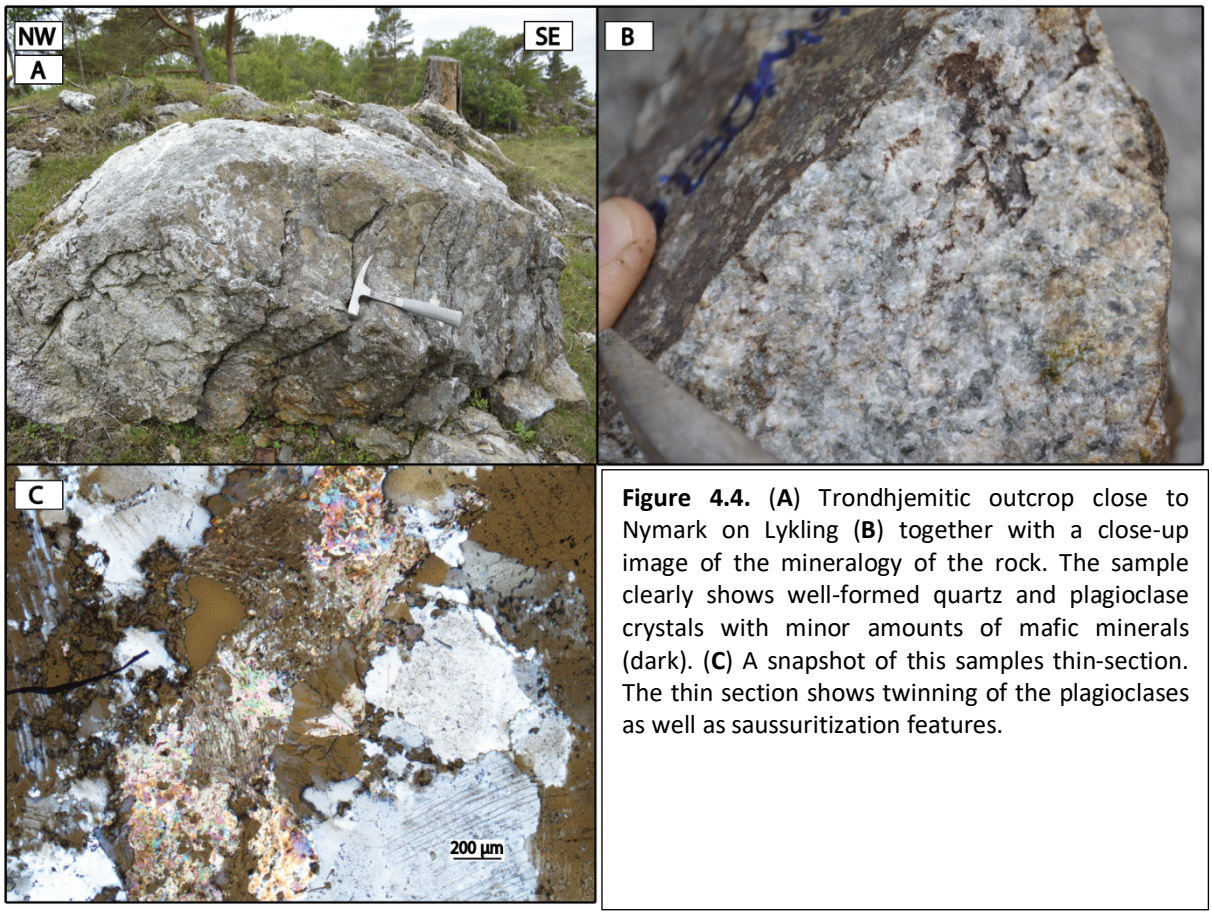

Figure 4.4. (**A**) Trondhjemitic outcrop close to Nymark on Lykling (**B**) together with a close-up image of the mineralogy of the rock. The sample clearly shows well-formed quartz and plagioclase crystals with minor amounts of mafic minerals (dark). (**C**) A snapshot of this samples thin-section. The thin section shows twinning of the plagioclases as well as saussuritization features.

The Øvre Tverrborgvika locality

Øvre Tverrborgvika is located in the central parts of Lykling close to the coastline (Figure 4.2). The outcrop is a road cut where a dark granite is exposed (Figure 4.5A). This lies in close contact with the homogenous gabbro of the ophiolite complex and has a sharp boundary indicating an intrusive contact where deformation is visible (Figure 4.5B). The gabbro that lies in contact with the trondhjemite is also here schistous. A sample of trondhjemite (20BOM-11) was taken from this outcrop for geochronological and geochemical studies (Figure 4.5C). In hand specimen, the sample is coarse grained and comprises predominantly quartz with some visible plagioclase. The quartz distribution is not uniform throughout the whole rock and can some places act as veins or clusters/lenses of quartz in a darker fine-grained matrix. This locality represents one of the most mafic trondhjemites found in the Lykling area.

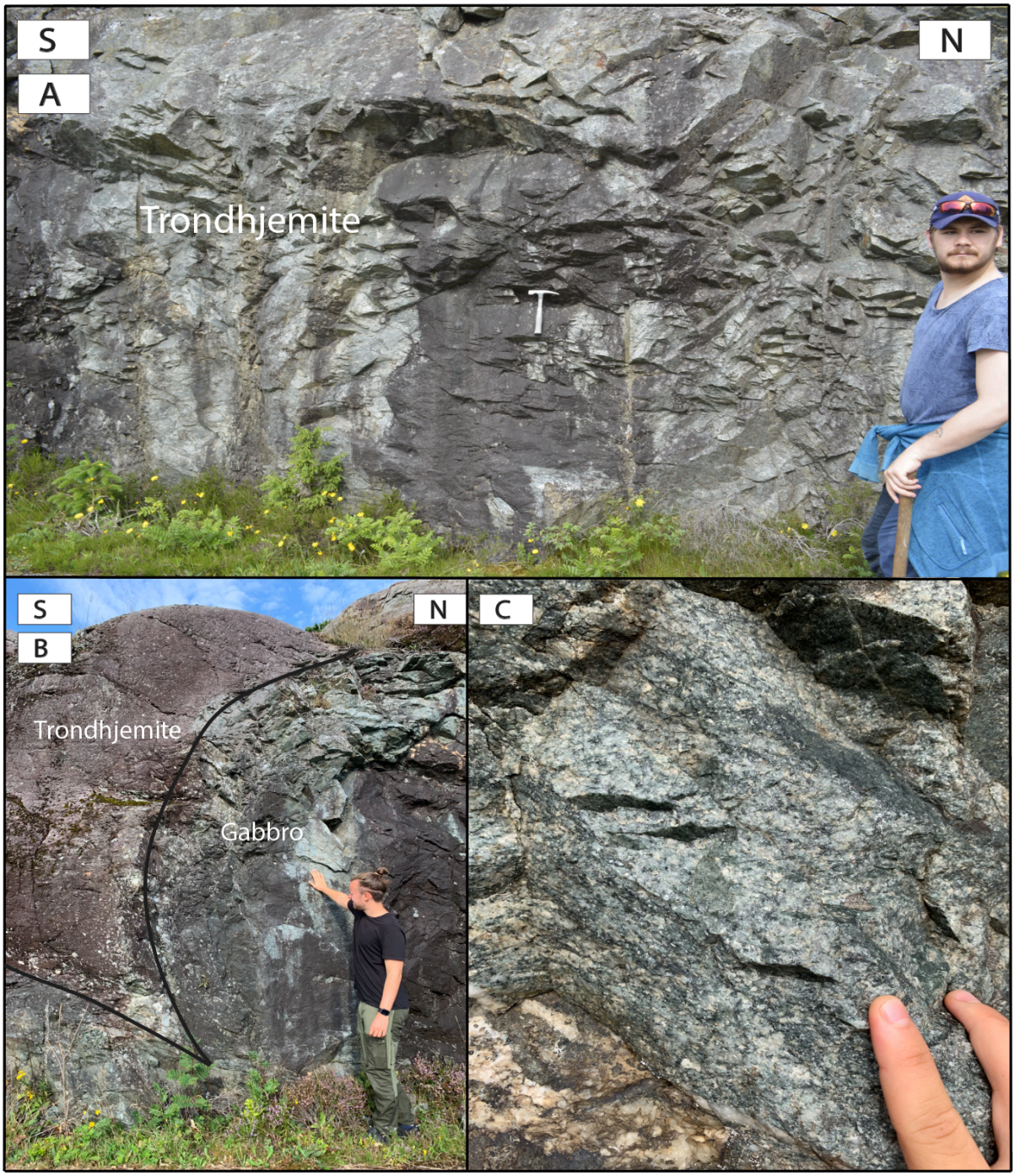

Figure 4.5. (**A**) Outcrop where the relative mafic trondhjemite was collected (20BOM-11). (**B**) Weathered trondhjemite intrusion in contact with homogenous ophiolite gabbro. The gabbro is slightly tectonized close to the contact. (**C**) Close-up photo of the dark trondhjemite. Photos by M. Slotnes.

The Hellevika locality

Hellevika is an inlet in the northern parts of the Lykling area (Figure 4.2). Basaltic dikes that trend in different directions are particularly common in this area. One trondhjemite sample (20BOM-12A) was collected from this location. On closer inspection, this rock is massive/featureless and coarse grained. Visible minerals are predominantly quartz and plagioclase, where the quartz crystals are more developed. Darker, smaller minerals are present, but indistinguishable. This trondhjemite has a more felsic appearance than the samples from Øvre Tverrborgvika and Nymark.

Numerous basaltic dikes of different generations are present in this area. One of the larger dikes (20BOM-13A) was sampled close to the trondhjemite sample (20BOM-12A) that was collected from this area (Figure 4.6C & D). The large dikes are oriented towards NW-SE while a generation of more deformed and smaller dikes are oriented E-W.

Several basaltic dikes (20BOM-24A, 20BOM-24B and 20BOM-24C) were sampled on the other side of the inlet (Figure 4.2). At this locality one can clearly see field relations between the different basalt dikes (Figure 4.6A & B). The larger dike (sample 20BOM-24B) cross-cuts the older, smaller dikes and has a different orientation (NNE-SSW). The smaller dikes trend in an E-W/NW-SE direction. The older dikes are more metamorphosed and deformed and their intrusive contacts with the surrounding granitic pluton are less well preserved. The younger and larger dike exhibit clear intrusive contacts. Sample 24B (young generation) displays quartz veins within the dike, but no sulfide mineralizations. 24C (older generation) displays no quartz veins, but some mineralizations. Several other cross-cutting dikes are located within the area, and they all display the same features as mentioned above. A third-generation dike that is oriented towards NNE-SSW was also observed. This dike, which is cross-cut by quartz veins, may be one of the Permian-Triassic dikes that also sporadically occur in the area.

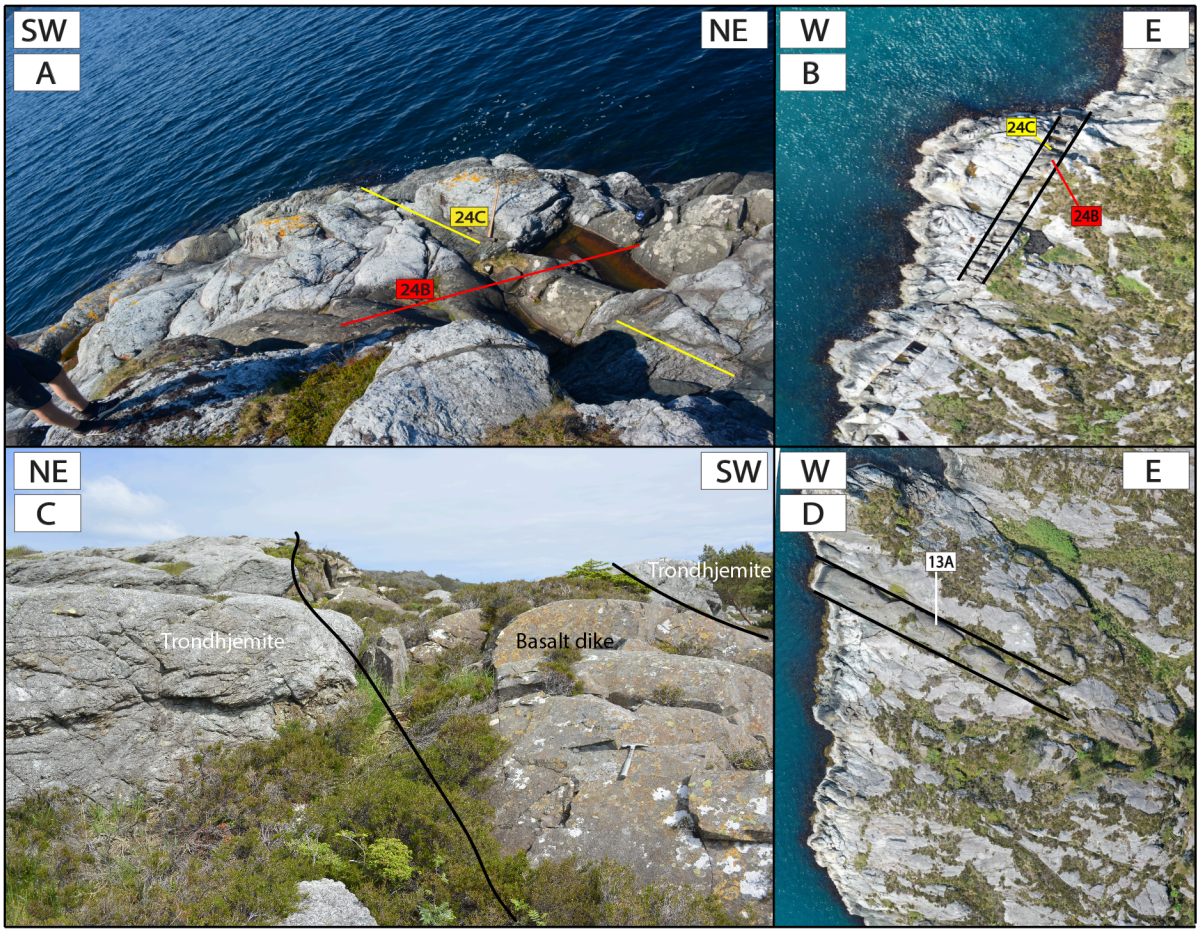

Figure 4.6. (**A**) South Hellevika sample location where cross-cutting relations can be determined in-field. Sample 20BOM-24B and 24C and what dike they belong to are marked. (**B**) Aerial mosaic photo of sample location south of Hellevika. (**C**) North Hellevika sample location of a large dike intruding into trondhjemite. (**D**) Aerial mosaic photo of sample location north of Hellevika.

The Ådnanes and Lindøya localities

This is the only place within the study area where tonalite was observed and collected. The intrusive field relationships are here also well displayed. The intrusive contact between the tonalite and the massive gabbro of the ophiolite is well exposed (Figure 4.8B), and the presence of gabbroic xenoliths within the tonalitic rock shows the relative age and that the tonalite represent the intruding body (Figure 4.8C). The tonalite occurs also as dikes and veins within the gabbro and the two lithologies alternate along the outcrop (Figure 4.8A).

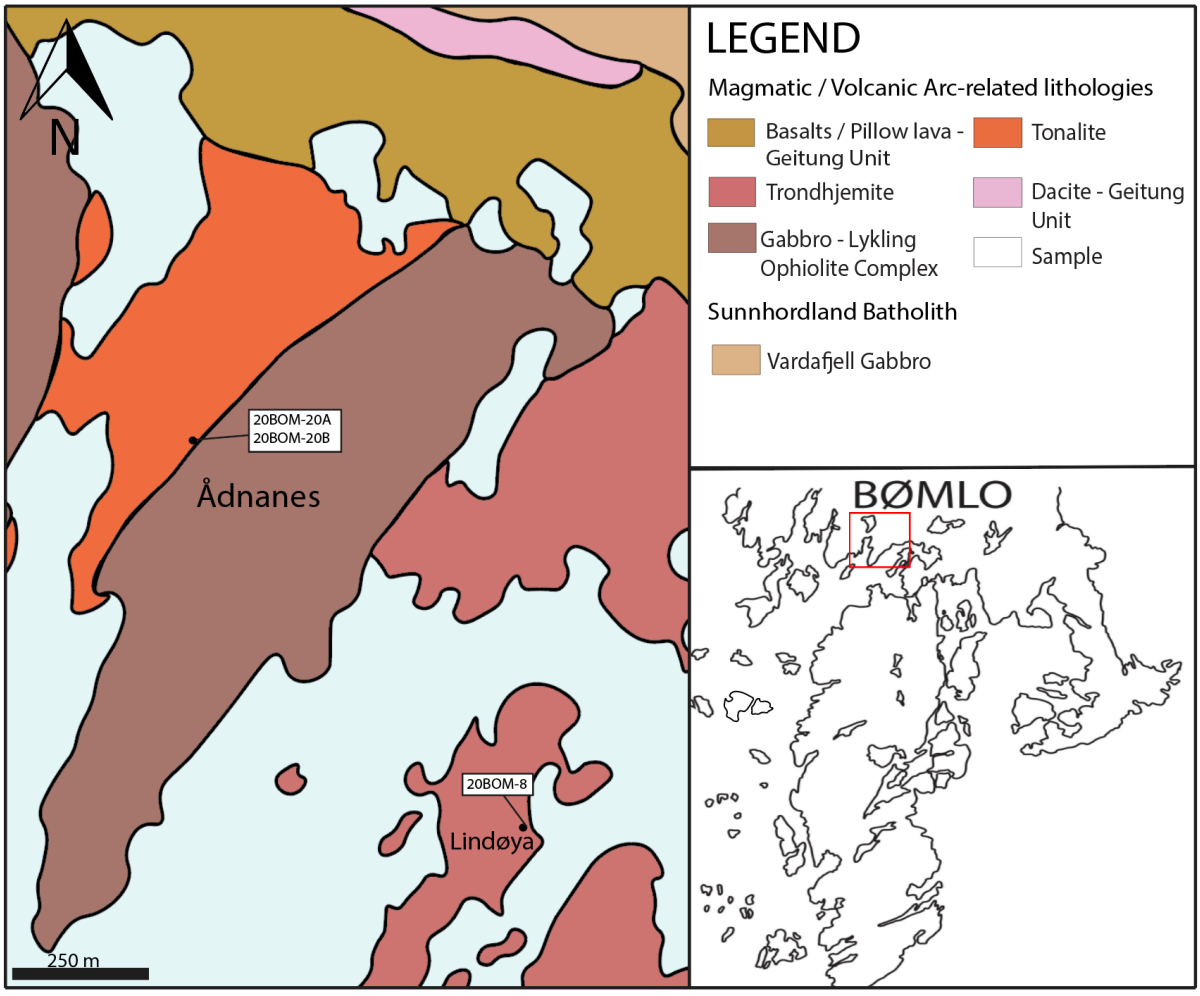

Figure 4.7. Geological map of the Ådnanes locality and Lindøya where three samples were collected. Drawing based on NGU, 2021 (https://geo.ngu.no/kart/berggrunn_mobil/).

Sample 20BOM-20A was collected from the tonalite in this outcrop (Figure 4.8A). The rock is coarse grained dominated by quartz and plagioclase with a considerable amount of biotite. Texturally this rock is different than the trondhjemites found further south on Lykling and it has a more felsic appearance. This may be due to the high abundance of plagioclase in the tonalite which is reflected in the geochemistry of the rock (see geochemistry in Table 4.2). Outcrops where tonalite and trondhjemite are in close proximity were not found. The gabbros

of the Lykling Ophiolite are here significantly more coarse-grained and differ from the microgabbros that dominates at the Nymark and Øvre Tverrborgvika localities. In this coarse-grained gabbro, visible plagioclase is present in the form of well-developed crystals and give the rock a lighter appearance.

Lindøya is an island located north of Lykling (Figure 4.7). There are not many outcrops on the island as most parts are covered with grass, but through the middle of the island a large basaltic dike cut through. The surrounding trondhjemite is dark with glassy texture with next to no minerals visible. The rock has similar textural traits as the dacites of the Geitung Unit (see Finnås and Geitung localities). Sample 20BOM-8 was collected and classified as trondhjemite.

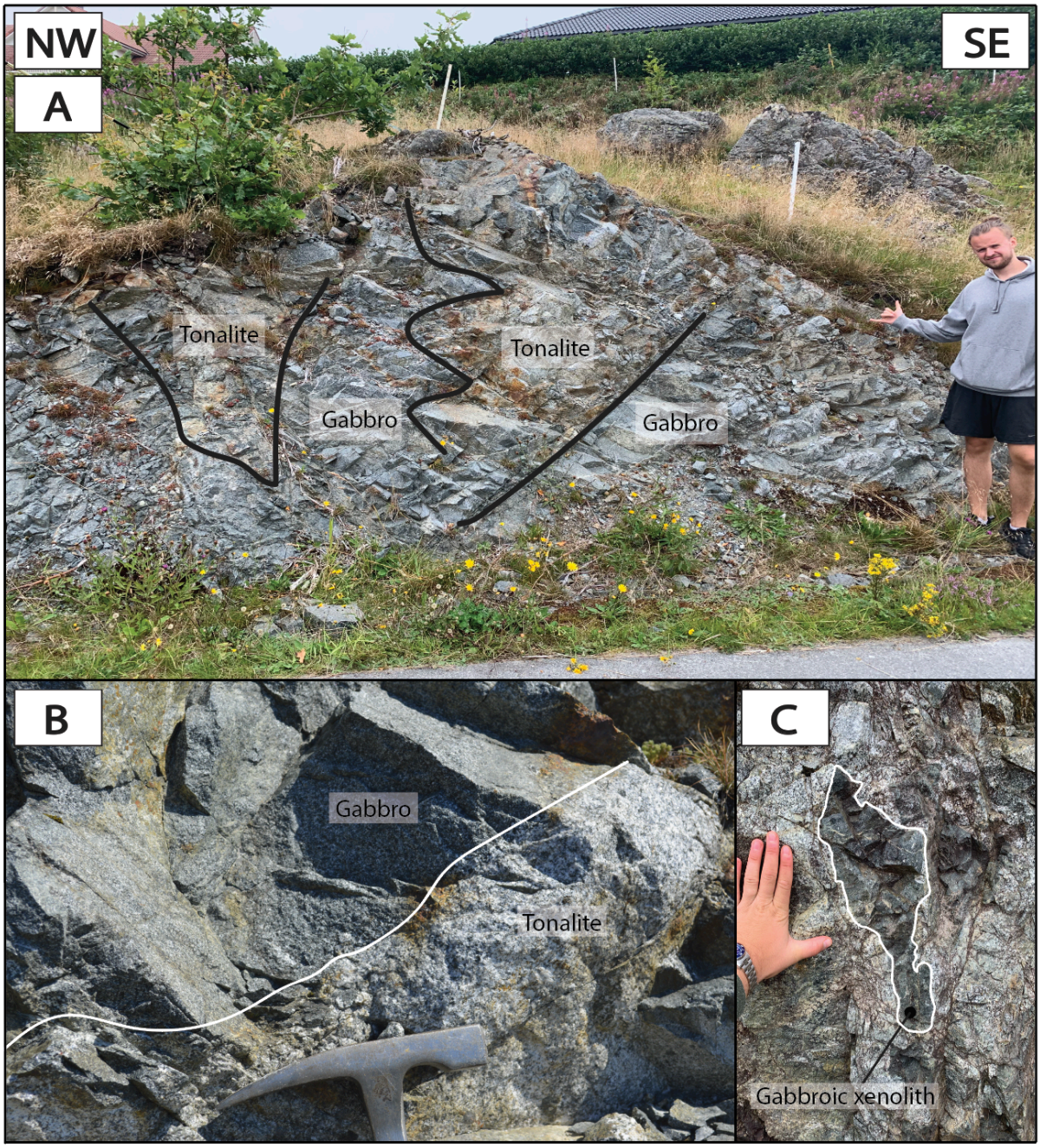

Figure 4.8. (**A**) Outcrop of alternating tonalite and gabbro. Sample 20BOM-20A was sampled from this tonalite. (**B**) Intrusive contact between tonalite and gabbro. (**C**) Gabbroic xenolith within the tonalite.

The Finnås locality

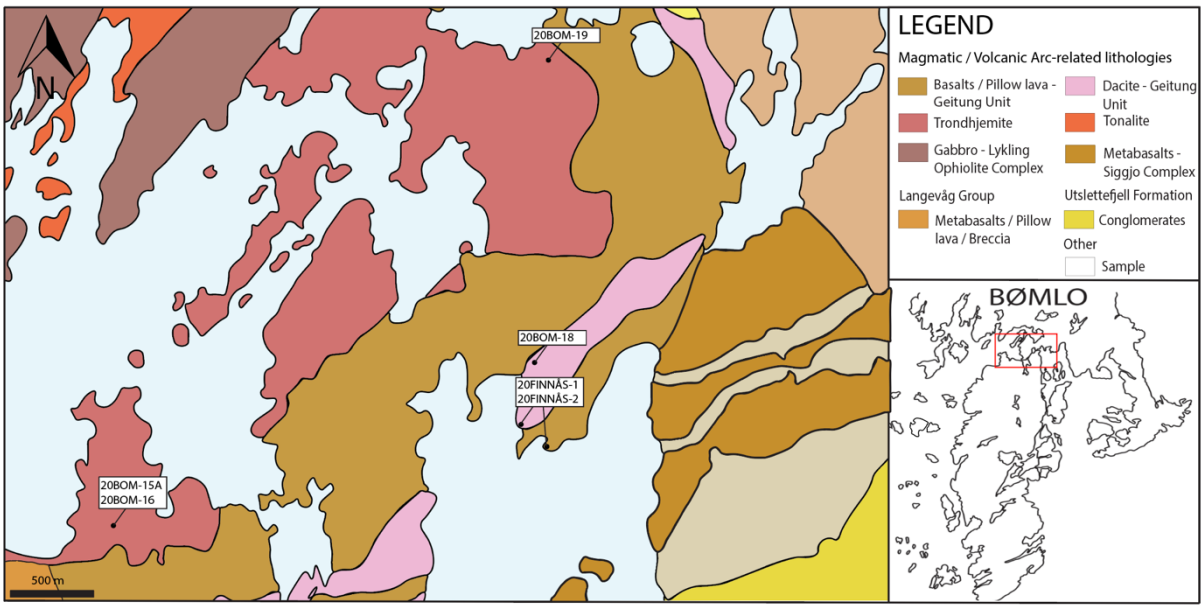

Figure 4.9. Geological map of the Finnås locality and northernmost Lykling. Sampling localities are marked on the map. Drawing based on NGU, 2021 (https://geo.ngu.no/kart/berggrunn_mobil/)).

Finnås is a small peninsula that stretches out into Finnåsvika east of Lykling (Figure 4.9). The area is dominated by the volcanic lithologies of the Geitung Unit. Three fine-grained felsic samples (20FINNÅS-1, 20FINNÅS-2, 20BOM-18) were collected from this area. On outcrop scale and in hand specimen these rocks exhibit extrusive characteristics. They are very fine grained with glassy textures and show "flakes" of quartz. There are no distinct crystal structures and has the appearance of pure quartz. 20BOM-18 is mildly different texturally than the samples collected by the shore. This specimen exhibits fine-grained crystal, and has not the same glassy texture as the samples from Finnås. Larger crystals of plagioclase are visibly clustered together with some parts of the rock exhibiting glassy textures. Another sample with similar mineralogy and texture is sample 20BOM-19. This particular sample was extracted north of Finnås in an area mapped as trondhjemite by NGU. However, distinguishing this rock from the Geitung Unit dacites and the trondhjemites is difficult. Texturally, this sample resemble a slightly coarser variant of dacite, while geochemically exhibiting traits that are similar to the trondhjemites.

The Geitung locality

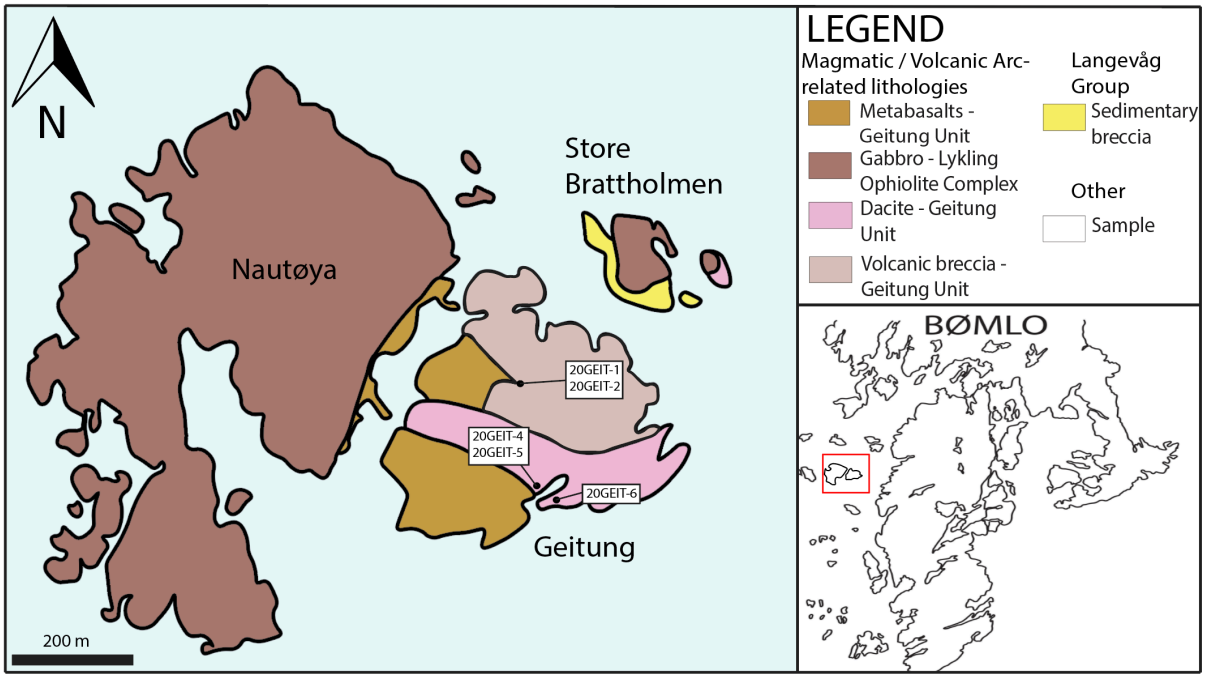

Figure 4.10. Geological map of the island of Geitung west of Lykling on Bømlo. Sample locations marked on the map. Drawing based on NGU, 2021 (https://geo.ngu.no/kart/berggrunn_mobil/).

Geitung is a small island located just off the coast west of Lykling and is primarily dominated by lithologies from the Geitung Unit (Figure 4.10). The small island contains several extrusive lithologies ranging from dacites and volcanic breccias to fine grained layers that may represent ash (Figure 4.12 and 4.13). Flow banding is observed within a few of the outcrops (Figure 4.13). Sample 20Geit-1, 20Geit-2, 20Geit-4, 20Geit-5 and 20Geit-6 were all collected on this island. Similar to Finnås, the rocks on Geitung are very fine grained with glassy textures clearly indicating extrusive deposits. Although the dacites are texturally different from the trondhjemites the same minerals seem to be present in these two lithologies, indicating that they are intrusive and extrusive parts of the same magmatic event. Both are quartz dominated and poor in K-feldspar.

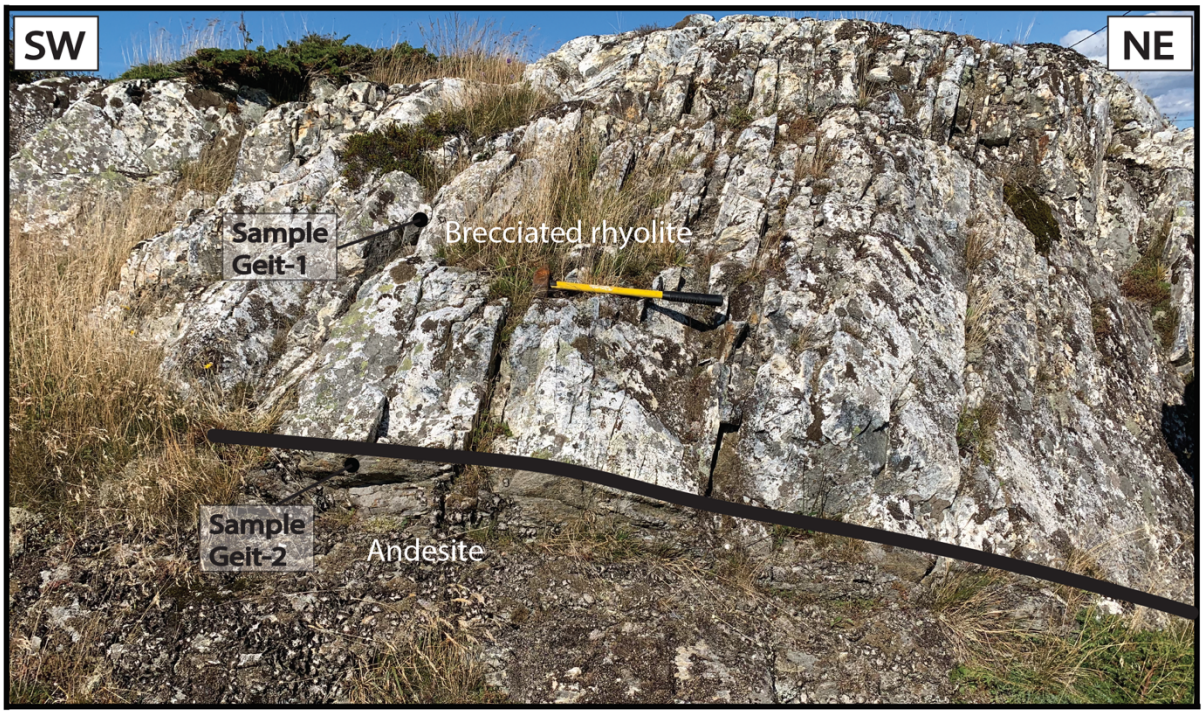

Figure 4.11. Outcrop on where the samples 20Geit-1 and 20Geit-2 was collected. This outcrop represents the contact between the extrusive deposits of the Geitung Unit.

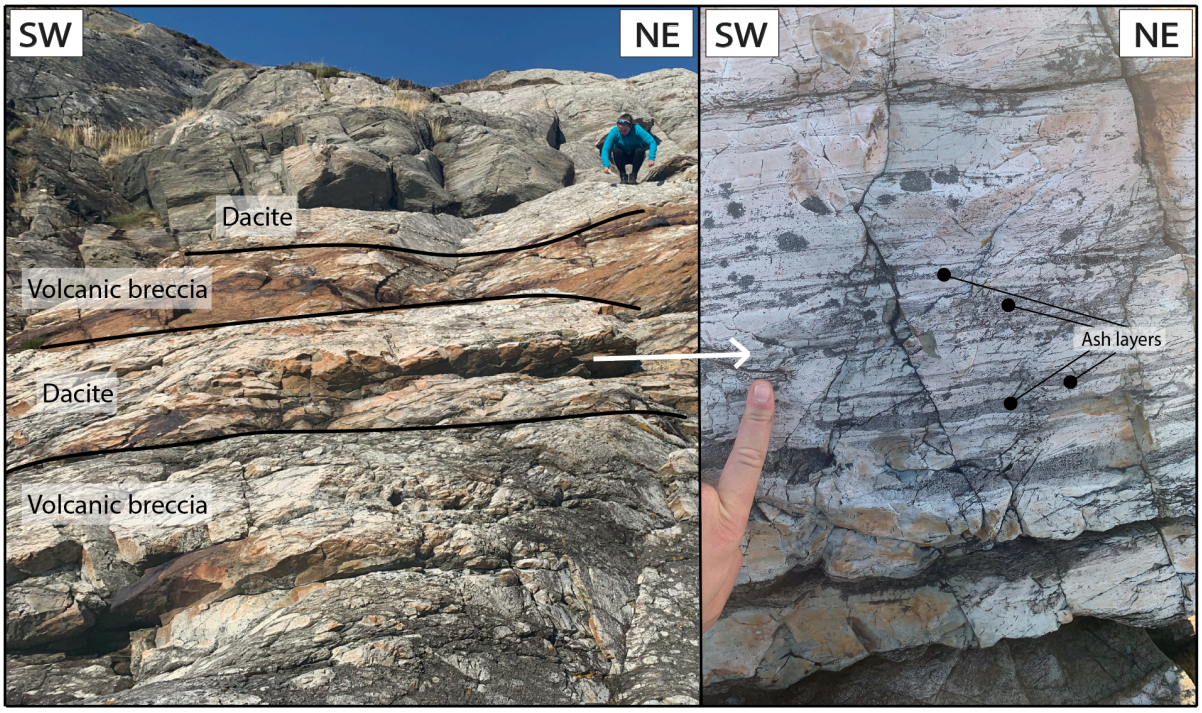

Figure 4.12. Alternating volcanic breccia and more massive layers within the outcrop.

Figure 4.13. Volcanic breccia with flow banding features.

Sample	Locality	Coordinates	Lithostratigraphic Unit	Lithology	Analysis
20BOM-1	Lykling (Figure 4.2)	59° 42' 6.81" N 005° 10' 30.21" E	Granitic intrusion	Trondhjemite	Major- and trace element analyses
20BOM-2		59° 42' 6.81" N 005° 10' 30.21" E	Granitic intrusion	Trondhjemite	
20BOM-4		59° 43' 1.05" N 005° 10' 24.79" E	Granitic intrusion	Trondhjemite	
20BOM-6		59° 43' 4.84" N 005° 10' 15.61" E	Granitic intrusion	Trondhjemite	
20BOM-7		59° 43' 12.37" N 005° 11' 46.39" E	Granitic intrusion	Trondhjemite	
20BOM-15B		59° 44' 11.21" N 005° 12' 33.47" E	Granitic intrusion	Trondhjemite	
20BOM-22A		59° 43' 1.34" N 005° 10' 9.79" E	Dike intrusion	Basalt	
20BOM-22B		59° 43' 0.89" N 005° 10' 8.83" E	Dike intrusion	Basalt	
20BOM-23B		59° 43' 7.86" N 005° 10' 20.96" E	Granitic intrusion	Trondhjemite	
20BOM-27C		59° 42' 14.02" N 005° 09' 51.98" E	Granitic intrusion	Trondhjemite	
20BOM-27D		59° 42' 14.02" N 005° 09' 51.98" E	Lykling Ophiolite Complex	Gabbro	
20BOM-9A	*Nymark (Figure 4.2)*	59° 42' 28.28" N 005° 10' 25.11" E	Granitic intrusion	Trondhjemite	Geochronology and major- and trace element analyses
20BOM-9C		59° 42' 28.28" N 005° 10' 25.11" E	Lykling Ophiolite Complex	Monzodiorite	
20BOM-9E		59° 42' 28.28" N 005° 10' 25.11" E	Lykling Ophiolite Complex	Gabbro	
20BOM-11	*Øvre Tverrborgvika (Figure 4.2)*	59° 43' 8.34" N 005° 10' 39.03" E	Granitic intrusion	Trondhjemite	Geochronology and major- and trace element analyses
20BOM-10		59° 43' 7.39" N 005° 10' 37.08" E	Lykling Ophiolite Complex	Gabbro	
20BOM-26A		59° 43' 13.55" N 005° 10' 49.56" E	Dike intrusion	Basalt	

20BOM-12A	*Hellevika*	59° 43' 37.57 N 005° 11' 1.40" E	Granitic intrusion	Trondhjemite	Major- and trace
20BOM-13A	*(Figure 4.2)*	59° 43' 37.57 N 005° 11' 1.40" E	Dike intrusion	Basalt	element analyses
20BOM-24A		59° 43' 27.40" N 005° 10' 41.49" E	Dike intrusion	Basalt	
20BOM-24B		59° 43' 29.41" N 005° 10' 35.99" E	Dike intrusion	Basalt	
20BOM-24C		59° 43' 29.41" N 005° 10' 35.99" E	Dike intrusion	Basalt	
20BOM-8	Lindøya (Figure 4.9)	59° 45' 17.68" N 005° 13' 28.83" E	Granitic intrusion	Trondhjemite	Major- and trace element analyses
20BOM-19	Gjerdavågen	59° 45' 41.48" N 005° 14' 59.79" E	Geitung Unit (volcanosedimentary unit)	Dacite	Major- and trace element analyses
20BOM-21D		59° 45' 47.56" N 005° 14' 9.20" E	Lykling Ophiolite Complex	Gabbro	
20BOM-21E		59° 45' 47.56" N 005° 14' 9.20" E	Granitic intrusion	Trondhjemite	
20BOM-21F		59° 45' 47.56" N 005° 14' 9.20" E	Granitic intrusion	Trondhjemite	
20BOM-20A	Ådnanes	59° 45' 37.28" N 005° 12' 15.20" E	Granitic intrusion	Tonalite	Major- and trace
20BOM-20B	(Figure 4.9)	59° 45' 37.28" N 005° 12' 15.20" E	Lykling Ophiolite Complex	Gabbro	element analyses
20BOM-25		59° 46' 27.77" N 005° 12' 11.35" E	Vardafjellgabbro (Sunnhordland Batholith)	Gabbro	
20BOM-17A	Finnås (Figure 4.11)	59° 43' 53.90" N 005° 14' 19.10" E	Geitung Unit (volcanosedimentary unit)	Rhyolite	Major- and trace element analysis
20BOM-18		59° 44' 52.08" N 005° 15' 17.28" E	Geitung Unit (volcanosedimentary unit)	Basaltic andesite	
20FINNÅS-1		59° 44' 34.90" N 005° 15' 18.70" E	Geitung Unit (volcanosedimentary unit)	Dacite	
20FINNÅS-2		59° 44' 39.88" N 005° 15' 7.32" E	Geitung Unit (volcanosedimentary unit)	Dacite	
20GEIT-1	Geitung (Figure 4.12)	59° 41' 28.78" N 005° 07' 41.54" E	Geitung Unit (volcanosedimentary unit)	Rhyolite	Major- and trace element analysis
20GEIT-2		59° 41' 28.78" N 005° 07' 41.54" E	Geitung Unit (volcanosedimentary unit)	Andesite	
20GEIT-4		59° 41' 21.27" N 005° 07' 46.48" E	Geitung Unit (volcanosedimentary unit)	Dacite	
20GEIT-5		59° 41' 21.27" N 005° 07' 46.48" E	Geitung Unit (volcanosedimentary unit)	Dacite	
20GEIT-6		59° 41' 21.16" N 005° 07' 51.09" E	Geitung Unit (volcanosedimentary unit)	Dacite	

Table 4.1. A systematic table covering sample locations in this study, their respective lithostratigraphic units, lithology sampled, and analysis work done to the samples.

4.2 Geochemistry

The following chapter presents geochemical data analyzed for all samples. Comments on major- and trace element compositions, rare earth element (REE) patterns, U/Pb dating findings and REE zircon analyses are included in this section. Classification of the rocks follow the scheme from Middlemost (1994) (Figure 4.14).

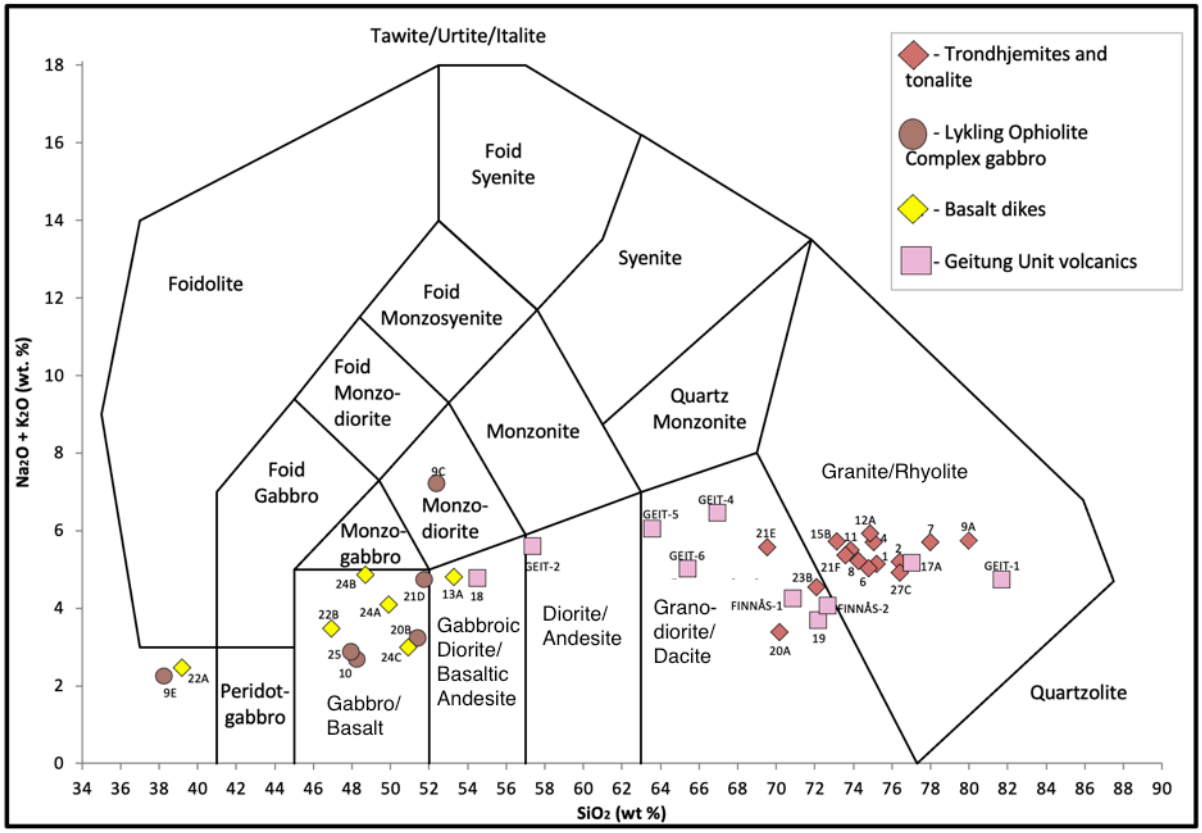

Figure 4.14. Rock classification diagram. SiO_2 vs total alkali diagram for all samples collected and analyzed in this study. Total silica concentrations vary within the trondhjemites and tonalite found on Bømlo, but usually conform to a 73 – 80 wt% SiO_2. The Geitung volcanics classifies as dacites (granodiorite/dacite field) and a few as rhyolites (granite/rhyolite field). Gabbros of the Lykling Ophiolite Complex and the intruding basalt dikes are gabbroic to gabbro dioritic and dioritic in composition. Based on Middlemost (1994).

Trondhjemites and tonalites of the Lykling Ophiolite Complex and the Geitung Unit volcanics

Major element compositions

Trondhjemite and tonalite are subdivisions under the granite umbrella, often referred to as plagiogranite (Amaliksen, 1983). They are a collective noun used when talking about potassium-poor felsic rocks usually associated with oceanic crust formations or ophiolite complexes. Specifically, leucocratic rocks (poor in mafic minerals) differentiated by subalkaline tholeiitic basalts (Coleman & Donato, 1979). Archean TTG suites (tonalite-

trondhjemite-granodiorite) do not go under this terminology. Throughout this thesis, the term plagiogranite will not be further used for the Bømlo trondhjemites and tonalites.

The trondhjemites and tonalites on Bømlo (mainly trondhjemite) can be separated geochemically by their Na_2O and CaO concentrations where the trondhjemites exhibit higher values of Na_2O while tonalite have higher concentrations of CaO (see Table 4.2). This in turn reflects the main feldspar minerals abundant in the two lithologies. Trondhjemites are relatively rich in albite while the tonalites have higher anorthite contents (Figure 4.15). The granitic rocks post-date the gabbro which is evident from the numerous veins of trondhjemite/tonalite that crosscut the gabbros and by the presence of gabbroic xenoliths within these granitic rocks (Figure 4.8C). On Bømlo the trondhjemites are generally medium-grained and phaneritic in texture. In the field the trondhjemites can be distinguished from the homogenous gabbros by the presence of quartz, and from the tonalites by their lighter color which is due to their lower contents of mafic minerals relative to the tonalites. The trondhjemites relatively low CaO values (0.43 – 2.07 wt%) may be linked to the metamorphic nature of feldspar within the rocks. Minor saussuritization of plagioclase can be observed under light microscope and is likely caused by circulating hydrothermal fluids through the rock (Figure 4.3C) (Morad et al., 2010). Rocks of this granitic pluton have high SiO_2 contents ranging from 69.51 wt% to 79.98 wt%, and total alkali from 3.38 wt% to 5.93 wt%. Moderately high aluminum contents (11.02 – 13.31 wt%) show peraluminous characteristics.

Three samples of trondhjemite from three separate locations (Figure 4.2) were selected for geochronology (20BOM-9A, 20BOM-11 and 20BOM-12A).

The geochemical compositions of a representative selection of trondhjemites and dacites are presented in table 4.2. The composition of the remaining trondhjemite, tonalite and dacite samples, as well as the gabbros of the Lykling Ophiolite Complex, the intruding basalt dikes and the rest of the Geitung Volcanics is given in Appendix 2.

The compositional range of the trondhjemitic intrusions and the Geitung Unit volcanics are shown in an alkali vs silica diagram (Figure 4.14). This shows that most of the volcanic samples from the Geitung Unit have dacitic compositions (i.e. they plot within the field of granodiorites/dacites), and how they plot together with the trondhjemitic intrusions that predominantly are slightly more SiO_2 rich and therefore mostly plot within the granitic field. The major element composition of these rocks is also shown in a normative albite, anorthite, orthoclase diagram (O'Connor, 1965). With one exception, this diagram classifies the granitic intrusions of the Lykling Ophiolite Complex as trondhjemites (figure 4.15). The diagram also

displays the similarity between the trondhjemites and the Geitung Unit volcanics, which mostly plot within the trondhjemite field.

Two of the Geitung Unit samples that were collected in the Finnås area plot within the tonalite field (20BOM-18 and 20BOM-19). Texturally 20BOM-19 is coarser grained than the other volcanic samples from Finnås and Geitung, but the sample do still show clear extrusive characteristics. Geochemically this rock contains higher amounts of CaO (as described above as the contributing factor for discriminating tonalite from trondhjemite) and slightly higher aluminum contents. Otherwise the dacites exhibits lower Al_2O_3 contents than the trondhjemites, indicating less plagioclase fractionation and that they are primarily quartz dominated. While having similar geochemical traits as the tonalite on Ådnanes it is however not considered an intrusive tonalite due to the relative fine-grained nature of the rocks texture and poor crystal development. The other sample from the Finnås area (20BOM-18) plots in the silica vs alkali diagram as a gabbroic diorite (intrusive equivalent for basaltic andesite). and is therefore from the metabasalt sequences of the Geitung Unit. Sample 20Geit-2 plots as granite in the feldspar triangle, but this is an andesite (57.39 wt% SiO_2) and is also therefore not a granitic rock and eligible for this type of classification.

The trondhjemites/tonalite samples exhibit low-K values (0.09 – 0.96 wt%) and belong accordingly to a low-K magmatic series (Figure 4.16). The Geitung extrusives from the Finnås area are also plotting as a low-K magmatic series, but the samples from the island of Geitung are more potassium-rich and follow the calc-alkaline series. This is also reflected in figure 4.15 where the Geitung Unit volcanics that plot within the trondhjemitic field define two distinct groups. Geitung Unit samples with >68 wt% SiO_2 classify as dacites in the diagram of Middlemost (1994) but classify as rhyolites according to classification scheme of Ewart (1982) (Figure 4.16). These samples have also low-K values similar to the trondhjemites. Dacites with <68 wt% SiO_2 have higher K values and plot in the calc-alkaline series. The andesite sample 20Geit-2 plot as banakite in the alkaline series anomalous from the rest of the samples, and may represent a younger intrusion.

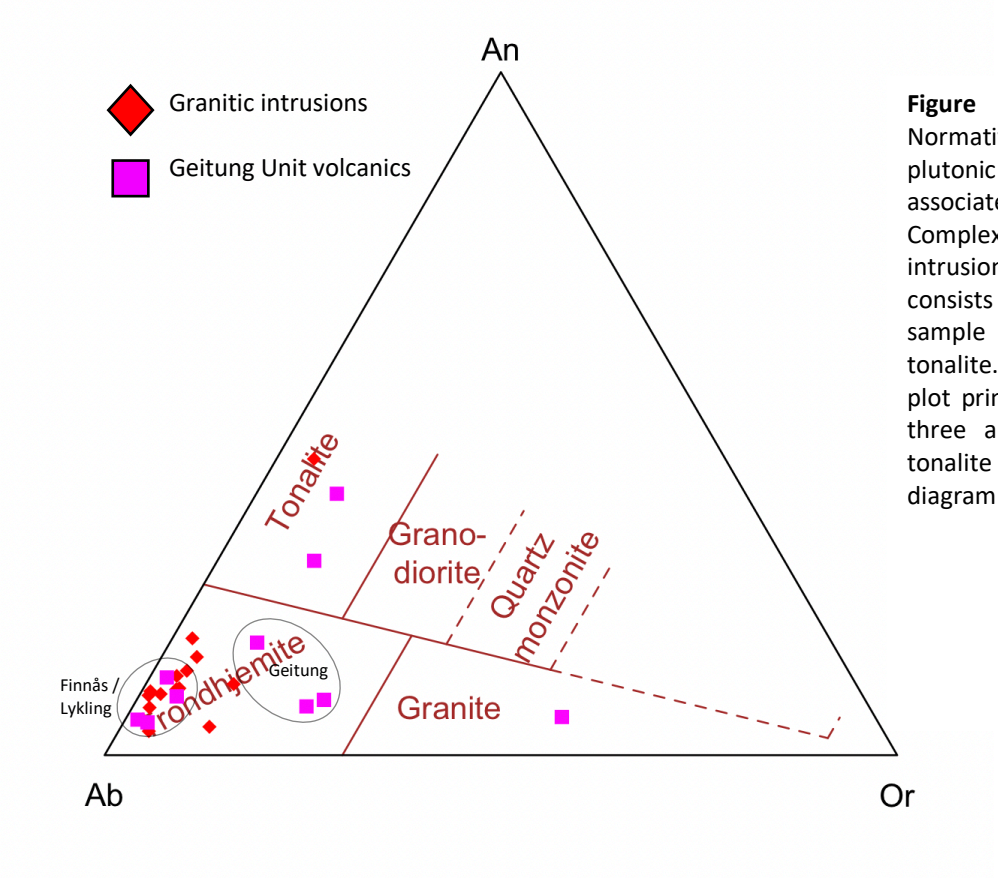

Figure 4.15. Feldspar triangle. Normative feldspar ratios of silicic plutonic and volcanic rocks associated with the Lykling Ophiolite Complex and Geitung Unit. Granitic intrusions on Lykling, Bømlo primarily consists of trondhjemites with one sample plotting in the field for tonalite. The Geitung Unit volcanics plot primarily as trondhjemites, but three anomalous samples plot as tonalite and granite. Classification diagram from O'Connor (1965)

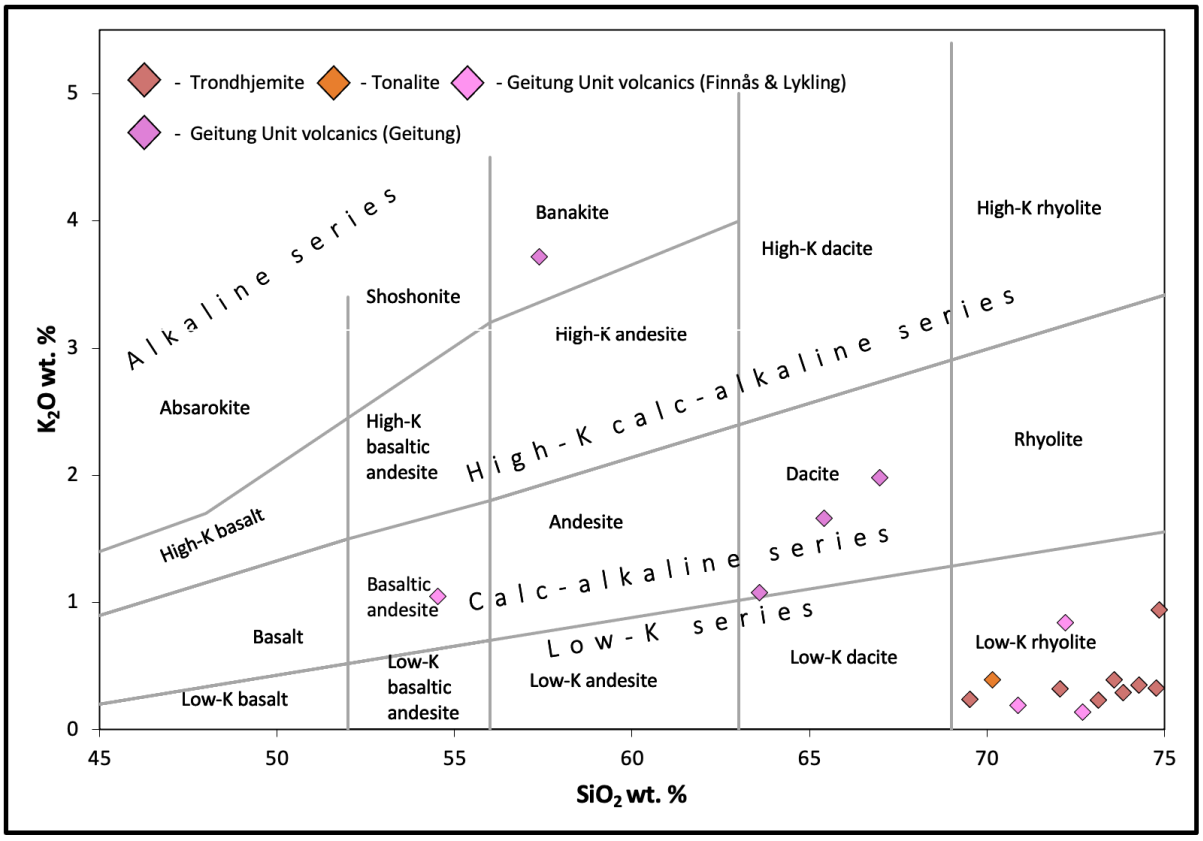

Figure 4.16. SiO2 vs K2O diagram displaying trondhjemite and tonalite samples as well as the Geitung Unit volcanics. Trondhjemites show a low-K (tholeiitic) magma series affinity. Only 9 out of 15 plots in the diagram as 6 of the samples have SiO_2 values >75 wt%. Geitung Unit volcanics have a more separate magmatic origin. Diagram from Ewart (1982).

Trace elements and rare earth element patterns

The trondhjemites on Bømlo have most likely been exposed to slight amounts of metamorphism that may have affected mobile elements, and accordingly any classifications based on mobile elements like potassium. The classification scheme of Hastie et al. (2007) are based on relatively immobile elements like thorium and cobalt (Figure 4.17). In this diagram, the trondhjemites plot in the fields for island arc tholeiite and calc-alkaline magma series, and they show geochemical signatures that span from an immature island arc (tholeiitic) to mature island arc (calc-alkaline). The Geitung Unit volcanics display similar Th-Co systematics in this diagram. The dacites sampled from the island of Geitung show lower Th concentrations and plot as island arc tholeiites. Samples Geit-1 (brecciated rhyolite) and Geit-2 (andesite) plot in the calc-alkaline field together with the dacites from Finnås and Lykling (Figure 4.17). A diagram discriminating the tectonic interpretations of granitic rocks reveal that the trondhjemites were partly formed as ocean ridge granites and partly as volcanic arc granites (Figure 4.19).

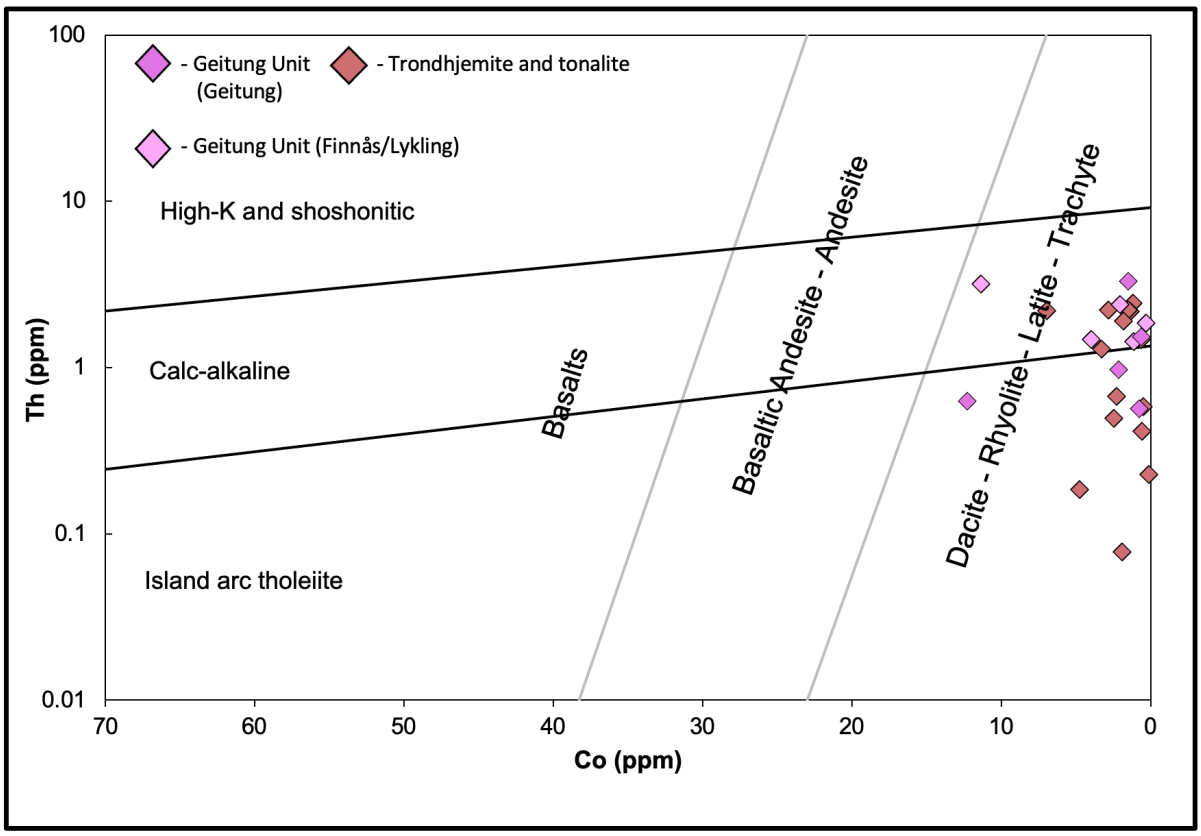

Figure 4.17. Th-Co discrimination diagram from Hastie et al. (2007). The trondhjemite-tonalite instrusions and the Geitung Unit volcanics plot as island arc tholeiite and calc-alkaline magma series rocks.

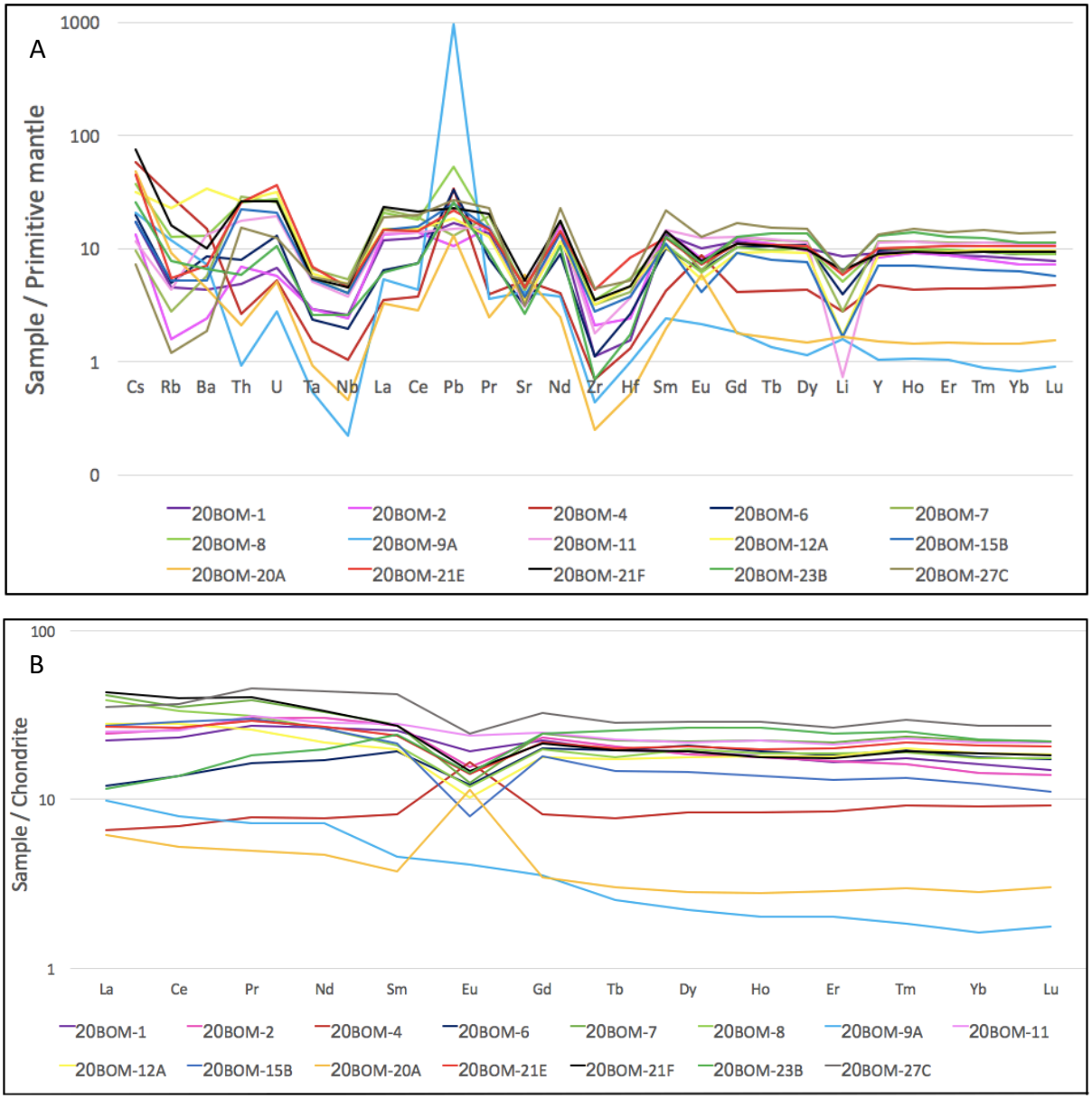

Figure 4.18. (**A**) Trace element and (**B**) rare earth element (REE) patterns for all trondhjemite-tonalite samples. Most of the samples conform to a relatively flat trend at approximately 50 times chondrite with a slight dip towards the HREE. Trace elements normalized against primitive mantle using values from Sun and McDonough (1989) and REE normalized to chondrite.

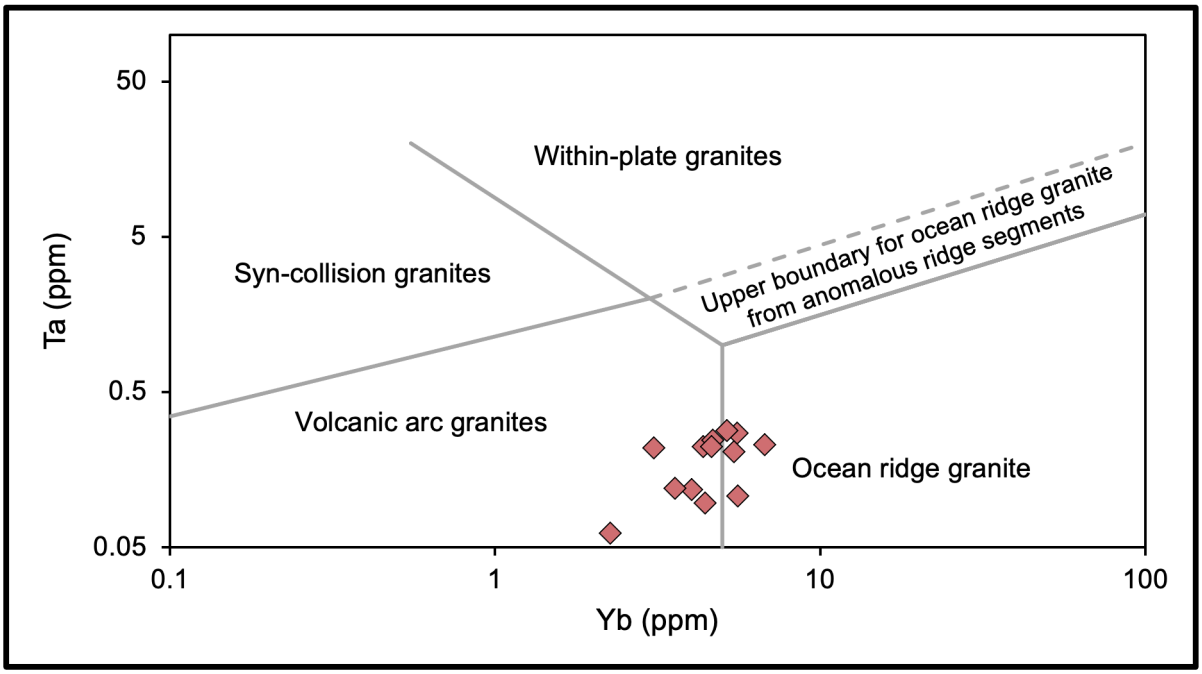

Figure 4.19. Ta-Yb discrimination diagram for the tectonic interpretation of granitic rocks. Diagram from Pearce et al. (1984).

The trace element compositions of the trondhjemite-tonalite intrusions are displayed as primitive mantle normalized values in figure 4.18A. In general, the patterns show a relatively flat trend with some marked anomalies. Nearly all samples have depletions in Rb before enrichment in Th. All samples exhibit negative anomalies for Ta and Nb, positive anomalies in Pb and depleted Zr values. A small negative anomaly is observed in Eu before the curve follows a flat trend, with the exception of a marked negative anomaly for Li. The one sample classified as tonalite (20BOM-20A) has considerably lower values for all elements compared to the trondhjemites and exhibits a positive anomaly for Eu and no anomaly for Li. The positive Eu anomaly suggest accumulation of plagioclase in this rock, which is consistent with the relatively high aluminum content (see Table 4.2). This is supported by the presence of well-developed plagioclase crystals in this sample (see Ådnanes locality). One of the trondhjemite samples (20BOM-4) does also show a positive Eu anomaly, which again suggest that plagioclase locally have accumulated in these plutons.

Overall, the trondhjemites show flat rare earth element (REE) patterns that are dipping slightly towards the heavy rare earth elements (HREE) and that are characterized by marked negative Eu anomalies (Figure 4.18). Two trondhjemite samples (20BOM-6 and 23B) are slightly depleted in light rare earth elements (LREE) relative to the rest and is comparable to the dacite samples from Geitung (Figure 4.20A; GEIT-4, GEIT-5, GEIT-6).

One sample of trondhjemite (20BOM9A) is anomalous to all the other samples as it shows a strong enrichment in LREE relative to HREE. This sample was sampled close to the intrusive contact between the trondhjemite pluton and the ophiolite gabbro and exhibits a relative large uncertainty when dated (488 ± 9 Ma). This sample also have extremely high SiO_2 contents (nearly 80 wt%), which is unusually high compared to the rest of the trondhjemites (70 – 75 wt%). The samples overall values are also significantly lower. Another trondhjemite sample (20BOM-4) and the tonalite sample (20BOM-20A) show flat REE patterns and overall lower values than the other samples, and this is combined with positive Eu anomalies.

The trace element compositions for all Geitung Unit samples are visualized in Figure 4.20. These rocks also show a generally flat trend with a slight enrichment in the incompatible elements. A significant negative anomaly is observed in Ta and Nb, as well as Sr in all samples. Most samples also have negative anomalies for Li. All samples have positive anomalies for Pb. When comparing the various trends to a mean trondhjemite trend most samples follow the same pattern indicating a close relationship between the two lithologies (Figure 4.20). The negative Zr anomaly seen in the trondhjemites is not present in the volcanic samples. This may well be an analytical effect as the Zr in the trondhjemites probably are bound in larger zircons that may be difficult to dissolve completely during sample preparation. Exceptions applied to sample 20BOM-19 which exhibit this anomaly. In the field this sample is texturally coarser grained and might have been misinterpreted as dacite instead of trondhjemite (see Finnås locality).

REE patterns for all the volcanic samples are relatively flat with abundances between 10- and 60-times chondrite, and all have negative Eu anomalies (Figure 4.20). Samples Geit-2, FINNÅS-1 and BOM-18 have higher values (50 times chondrite) than the rest. Both Geit-2 and BOM-18 have andesitic compositions and show clear affinity to each other. Samples FINNÅS-1, FINNÅS-2 and BOM-19 are slightly enriched in LREE compared to HREE. These are the same samples showing coarser textures in hand specimen, and similar to some of the trondhjemites that are plotting as low-K rhyolites. It is uncertain whether these rocks are part of the intrusive trondhjemitic pluton or the extrusive volcanics of the Geitung Unit.

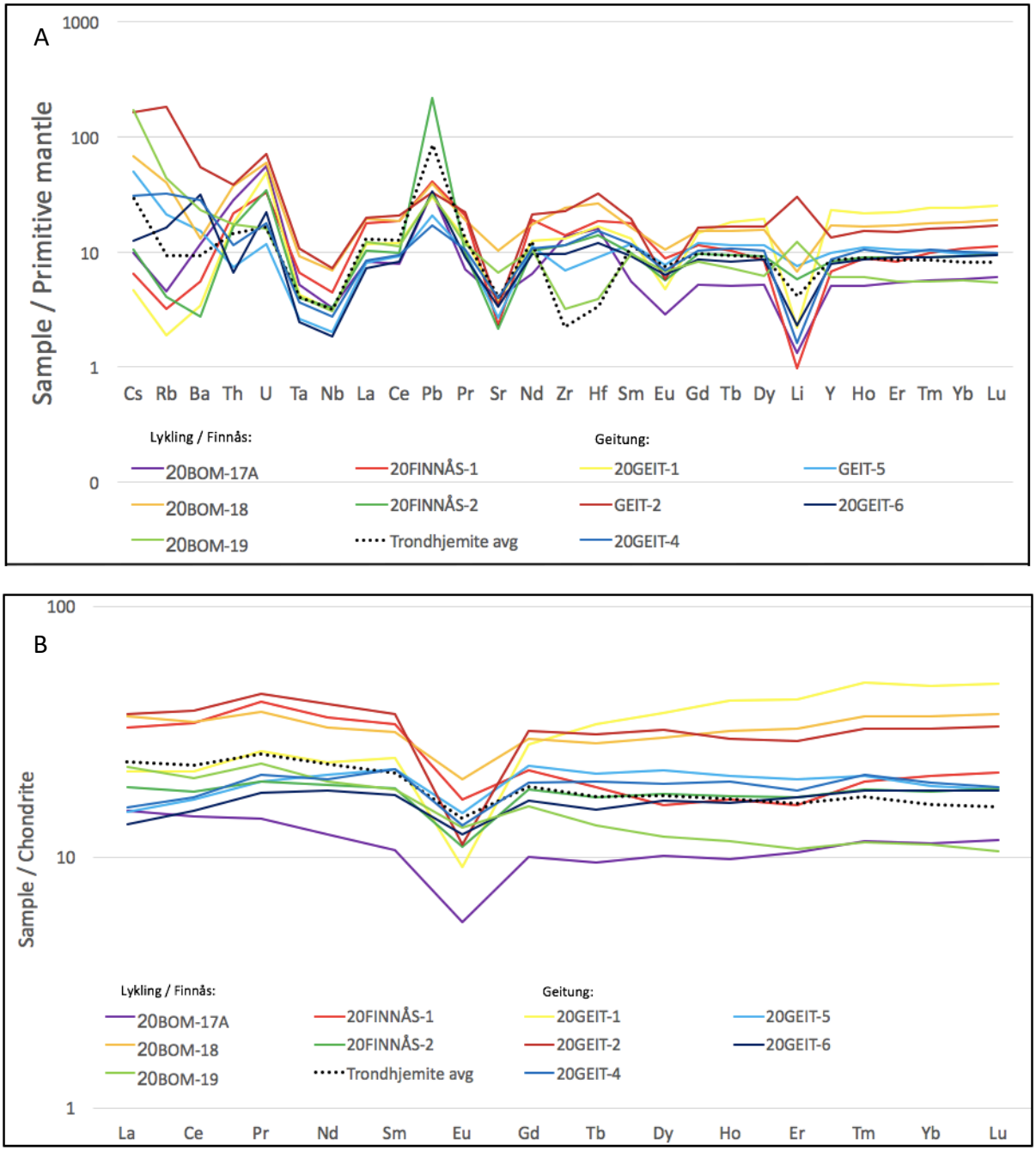

Figure 4.20. (**A**) Trace element compositions and (**B**) rare earth element patterns for the Geitung Unit volcanics with an average trondhjemite pattern added for comparison. Trace elements normalized to primitive mantle values from Sun and McDonough (1989). REE normalized to chondrite

Gabbros of the Lykling Ophiolite Complex and intruding basalt dikes

Major element compositions

The ophiolitic gabbros and its intruding basaltic dikes are also key rocks for clarifying the early development of this arc-complex. Rock classifications of the homogenous gabbros of the ophiolite complex and the intruding basalt dikes are shown in figure 4.14. Total SiO_2 content of the gabbros range from extremely low (38.29 wt%) to near dioritic values (52.43 wt%.) Gabbros of the Nymark locality (20BOM-9C / 9E) show widely different compositions. Sample 9C have relatively high concentrations of SiO_2 (52.43 wt%) and high total alkali (7.20 wt%) while 9E exhibit extremely low SiO_2 values (38.29 wt%) showing compositions of an alkali undersaturated foidolite (Figure 4.14). Considering their close proximity to each other it is assumed that this is related to alterations. In the area of Ådnanes the gabbros exhibits coarse grained textures and they are texturally dissimilar to the microgabbroic rocks of the Lykling study area (see Ådnanes locality, Figure 4.8). However, this sample show compositions that are similar to the rest of the microgabbroic samples (SiO_2 at 51.44 wt% and total alkali at 3.21 wt%). The textural differences do therefore probably only reflect physical differences during crystallization (e.g. degree of under cooling). This sample and others exhibit intermediate MgO values and high CaO/Na_2O contents (Appendix 2).

The basaltic intrusions have SiO_2 contents ranging from 39.17 to 53.30 wt%, however, most have values between 48–50 wt%. Total alkali ranges from 2.39 to 4.86 wt% and show intermediate MgO values similar to the gabbros. Iron contents are slightly higher ranging from 9.29 to 16.75 wt%. The high values in some of the samples may be related to local pyrite mineralizations that occur within some of these intrusions.

Based on geochemical characteristics, the basaltic dikes define two distinct groups; one group that have geochemical signatures with a calc-alkaline to high-K calc-alkaline affinity, and one group fitting neatly into the low-K and lower calc-alkaline magma series (Figure 4.21). These two groups are separated by cross-cut relations in the field, where the calc-alkaline / high-K calc-alkaline basalts are cross-cutting the low-K / calc-alkaline basalts. This give clear indicators that the two groups are separated in time.

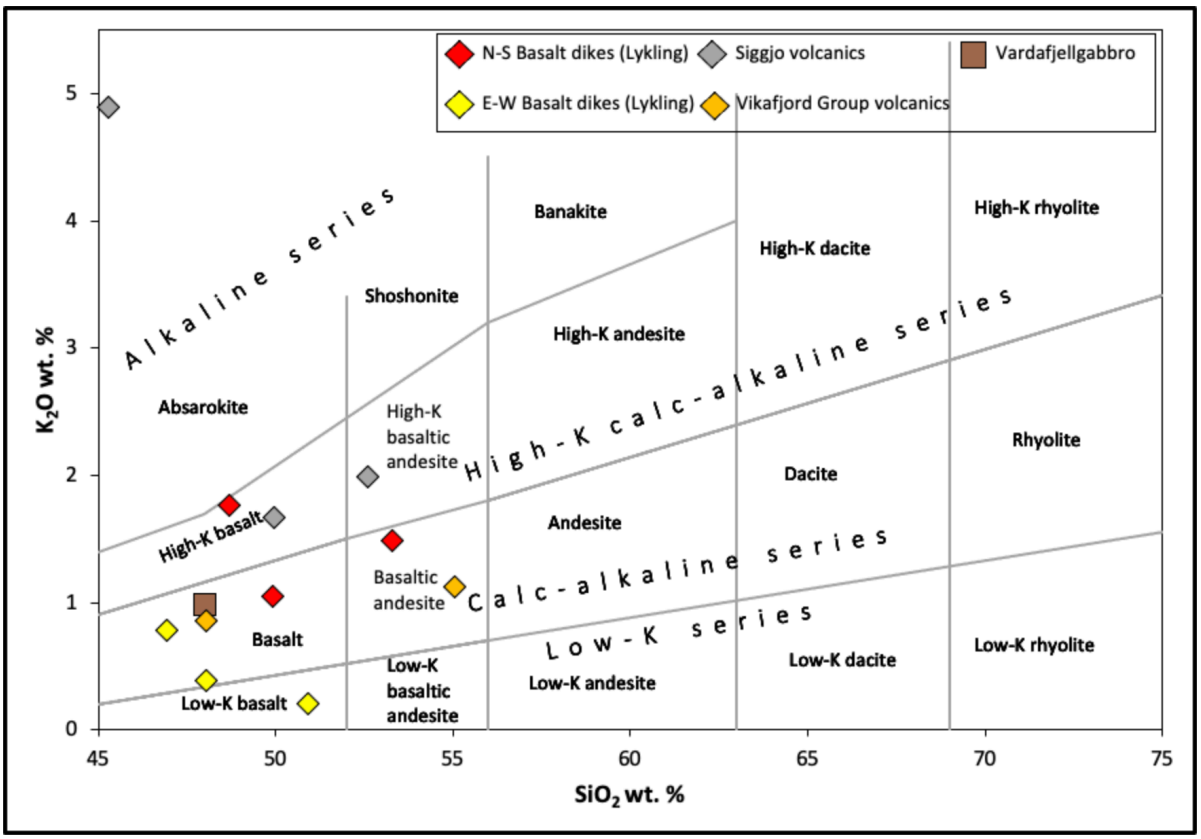

Figure 4.21. SiO_2 Vs. K_2O diagram after Ewart (1982). Basalt samples from this study (red, yellow, brown) and samples from previous studies (grey, orange) (Viken, 2017).

Trace elements and REE patterns

The ophiolitic gabbros on Lykling have low values of the incompatible elements except Cs concentrations which is anomalous for these samples (Figure 4.22). All samples have positive Pb, Sr and Li anomalies. A spider diagram for REE shows that samples 20BOM-9E, 9C, 10, 20B and 27D are depleted in LREE relative to HREE and have immature island arc signatures (Figure 4.22). One sample (20BOM-21D) have a relatively flat pattern with a positive Eu anomaly. Compared to an average pattern for all trondhjemite samples the gabbros are depleted in all incompatible elements relative to the trondhjemites, which exhibits a relatively flat pattern slightly dipping towards HREE.

Samples 9C and 9E have positive Eu anomalies suggesting that these samples represent cumulate gabbros that are enriched in plagioclase relative to the microgabbros. These gabbros that were sampled in the Nymark locality also exhibit different major element geochemistry.

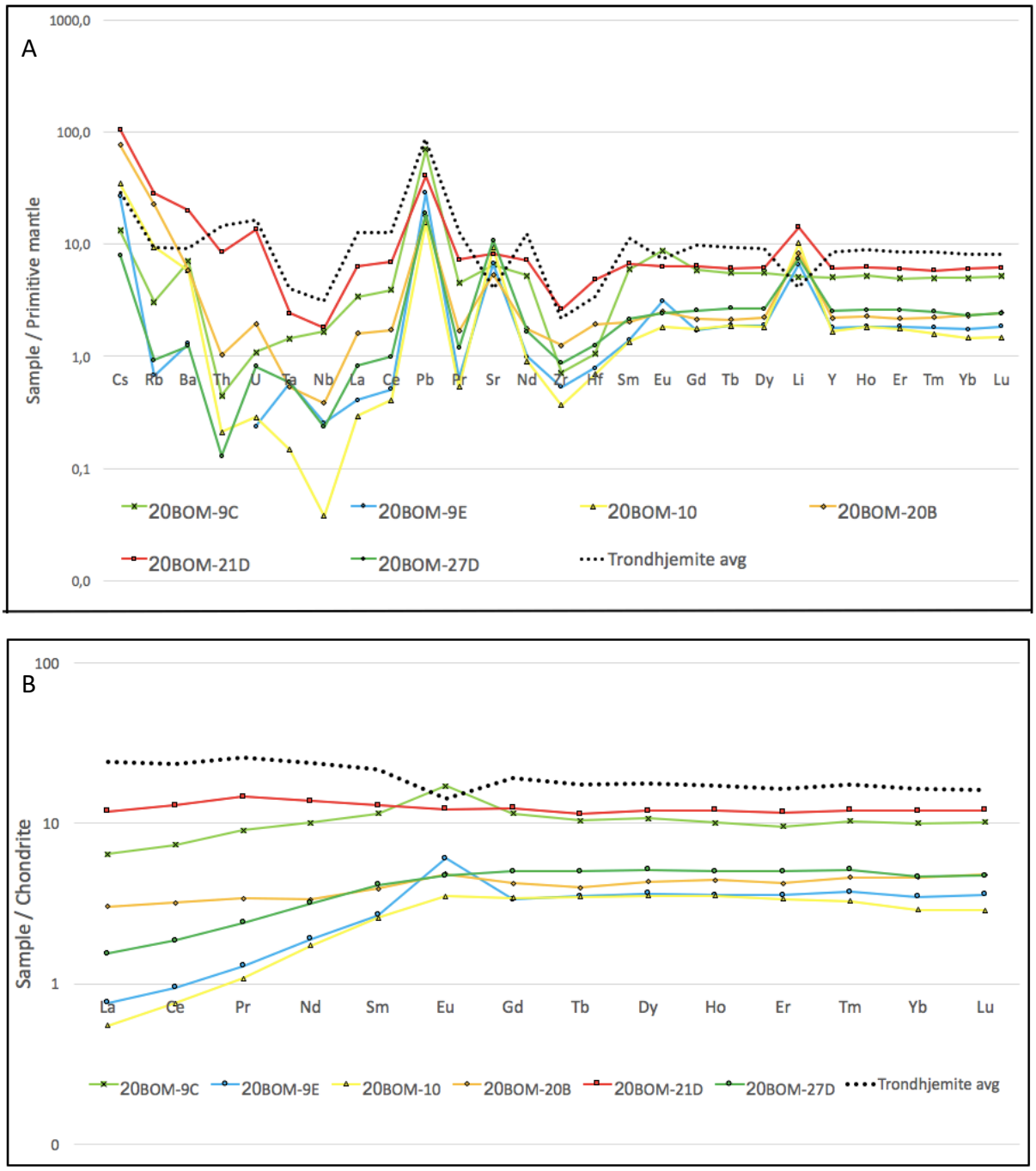

Figure 4.22. (**A**) Trace element spider diagram and (**B**) REE patterns for all gabbros associated with the Lykling Ophiolite Complex. Added is a pattern with average values for all trace elements and REE for all trondhjemite samples. Trace elements normalized to primitive mantle values from Sun & McDonough (1989). REE normalized to chondrite.

The distinction between two separate groups of basaltic intrusions is clearly visible in the extended spider diagram for trace elements where the high-K to calc-alkaline basalts (13A, 24A, 24B) have higher values relative to low-K / calc-alkaline basalts (22A, 22B, 24C, 26A) (Figure 4.24). Both groups are enriched in the incompatible elements with negative Ta and Nb anomalies. The younger high-K to calc-alkaline basalts have a downward trend towards the compatible elements while the older dikes exhibit a flatter trend. The older dikes show some similarities with the gabbros of the ophiolite complex indicating a relation between the two lithologies. General values and patterns of trace elements is similar, and the older dikes have a slight depletion in LREE compared to HREE, exhibiting a shallower positive slope.

Using the trace elements Th/Nb and La/Yb basaltic intrusions can be discriminated by their formation of origin (Hollocher, 2012). The younger dikes (based on field-criteria) have high La/Yb ratios and plot in the field associated with alkaline arcs. The older dikes plot in the field for oceanic arcs (Figure 4.23). This is supported by their respective REE patterns (Figure 4.24). The younger dikes (BOM-13A, 24A, 24B) exhibits enrichment in LREE and have mature island arc signatures while the older dikes (BOM-22A, 22B, 24C, 26A) have slight enrichments in HREE relative to LREE and show more immature island arc signatures.

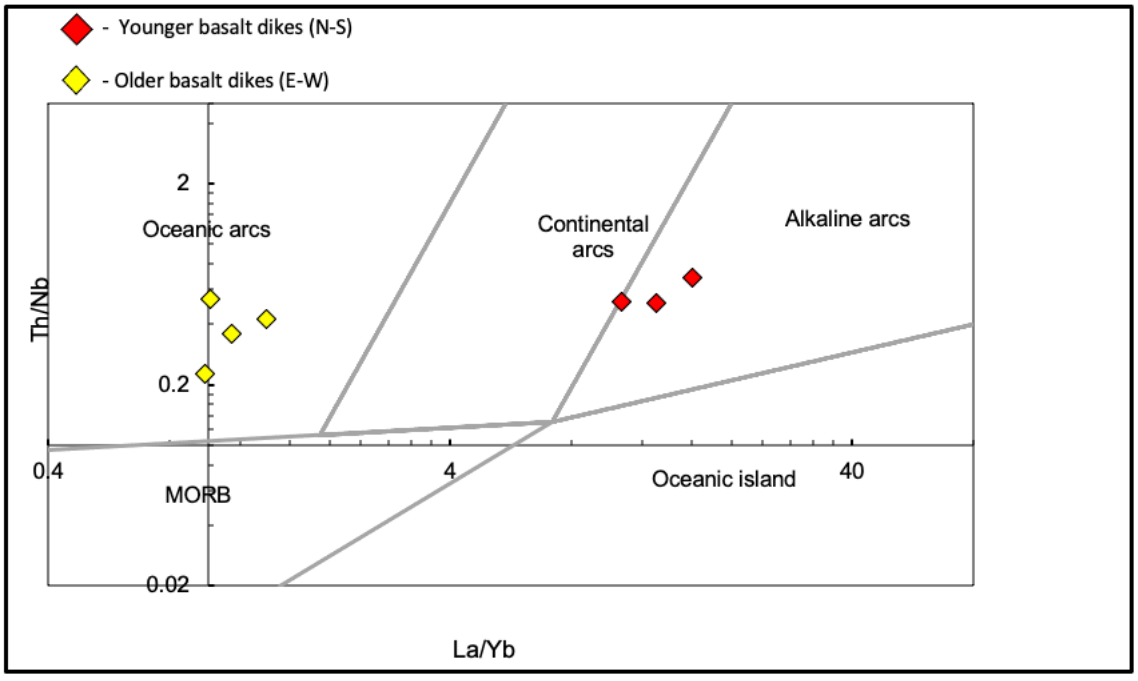

Figure 4.23. Diagram discriminating formation setting of which the basalt dikes were formed. From Hollocher et al. (2012)

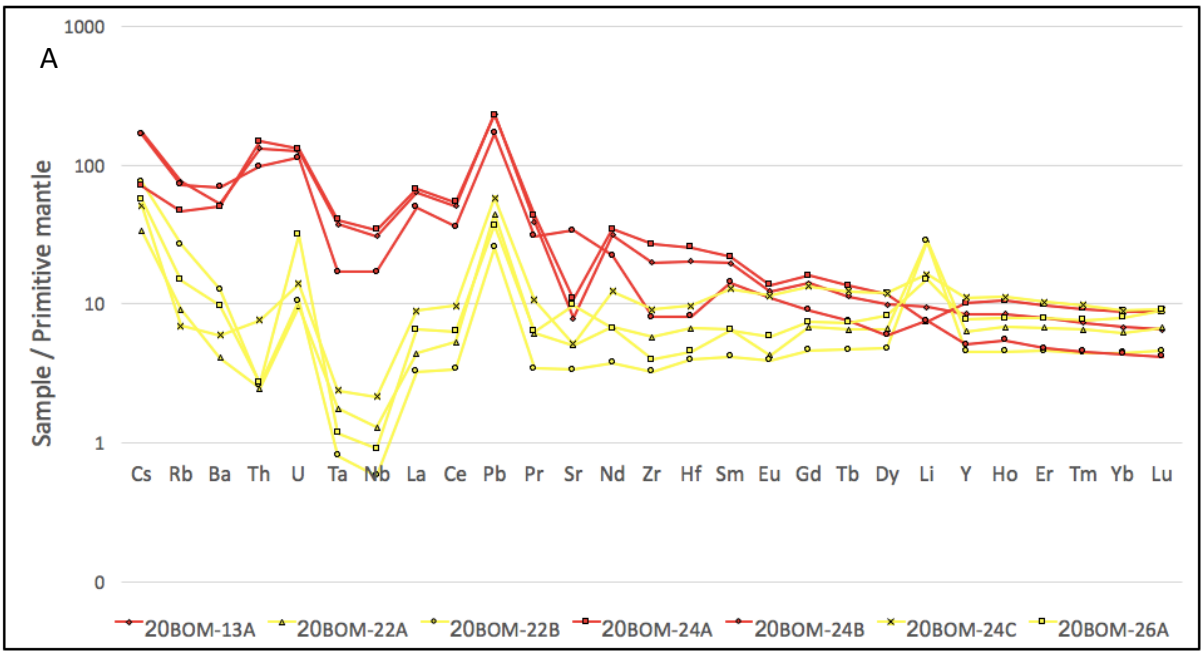

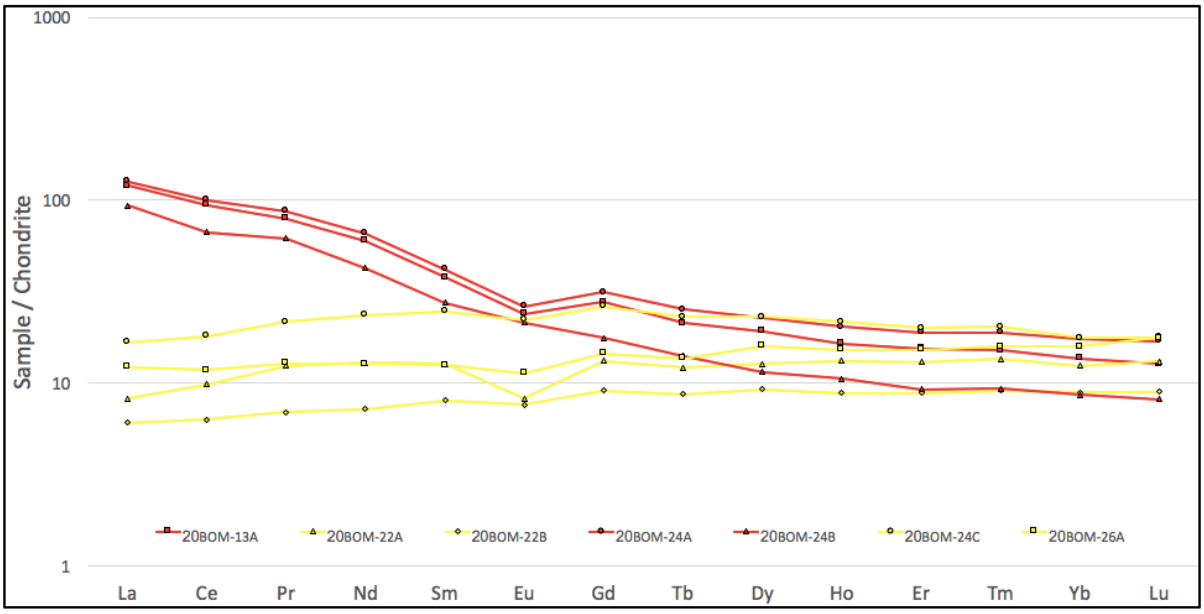

Figure 4.24. (**A**) Trace element compositions and (**B**) REE patterns for basalt intrusions in the Lykling area. Two generations of dikes are clearly visible in this extended spider diagram. Younger, N-S trending basalt dikes (red). Older, E-W trending basalt dikes (yellow). Normalized to primitive mantle values from Sun and McDonough (1989). REE patterns for the younger dikes (red) have a mature island arc signature while the older dikes (yellow) have immature island arc signatures. Normalized to chondrite.

Locality	Lykling								Ådnanes	Sakseid	Finnås		Geitung	
Sample	20BOM-1 (TR)	20BOM-2 (TR)	20BOM-4 (TR)	20BOM-6 (TR)	20BOM-9A (TR)	20BOM-11 (TR)	20BOM-12A (TR)	20BOM-27C (TR)	20BOM-20A (TO)	20BOM-21F (TR)	20BOM-17A (RH)	20FINNÅS-2 (DA)	20GEIT-5 (DA)	20GEIT-6 (DA)
%														
SiO_2	75.22	76.40	75.04	74.78	79.98	73.84	74.85	76.40	70.15	73.59	77.05	72.69	63.59	65.41
Na_2O	4.98	5.11	4.75	4.70	5.42	5.21	4.99	4.83	2.99	4.97	4.79	3.91	4.97	3.35
MgO	0.87	0.91	0.52	0.78	0.48	0.37	0.61	1.03	0.79	0.82	0.79	0.88	2.44	0.53
Al_2O_3	11.84	11.28	12.87	11.62	11.64	11.21	12.35	11.02	13.09	12.78	9.92	9.49	12.86	8.54
P_2O_5	0.06	0.06	0.05	0.08	0.06	0.06	0.07	0.06	0.09	0.09	0.06	0.07	0.17	0.06
K_2O	0.17	0.09	0.96	0.33	0.32	0.29	0.94	0.09	0.39	0.39	0.38	0.14	1.08	1.66
CaO	0.56	0.99	1.14	1.00	0.43	1.29	0.51	0.88	4.76	1.62	0.89	0.97	2.15	1.11
TiO_2	0.24	0.24	0.24	0.27	0.18	0.20	0.24	0.20	0.46	0.31	0.21	0.28	0.88	0.21
MnO	0.10	0.07	0.07	0.08	0.05	0.06	0.06	0.06	0.09	0.08	0.05	0.08	0.11	0.09
Fe_2O_3	4.18	2.58	2.76	2.88	1.23	2.33	2.39	3.38	5.37	3.11	1.13	2.53	8.69	2.72
LOI	1.17	1.47	1.29	0.83	0.45	1.06	0.80	1.16	0.96	0.93	0.86	1.11	1.40	0.77
Total	99.38	99.20	99.69	97.36	100.23	95.92	97.81	99.12	99.14	98.69	96.14	92.16	98.36	84.45
ppm														
Li	13.80	10.19	4.40	6.32	2.53	1.18	2.73	9.74	2.63	10.21	2.12	9.35	12.11	3.67
Sc	6.57	7.00	3.70	9.37	3.82	2.90	6.56	7.87	6.69	7.72	11.60	10.18	21.04	6.35
V	0.27	0.10	0.694	13.17	6.00	2.82	4.56	0.64	28.94	8.81	8.25	0.38	119.90	13.74
Cr	0.31	0.24	0.06	0.79	0.32	0.65	0.52	0.06	0.49	0.94	0.54	0.43	2.70	0.96

Co	0.57	0.50	0.124	2.27	1.93	0.61	1.53	3.29	4.78	2.84	2.07	1.15	12.28	0.76
Ni	0.40	0.22	0.13	0.56	0.29	0.36	0.53	0.13	0.54	0.70	2.43	0.50	3.07	1.32
Cu	3.97	7.03	1.17	3.06	164.90	6.21	2.57	16.78	2.59	3.58	16.68	1.64	4.04	3.46
Zn	24.35	18.92	38.12	59.26	9.77	15.58	18.36	34.93	45.34	36.29	33.66	70.11	75.88	80.17
Rb	2.91	1.01	18.20	3.16	7.45	2.76	14.36	0.765	5.79	10.24	2.90	2.58	13.60	10.45
Sr	74.29	96.49	109.9	66.08	87.17	64.42	72.51	65.53	124.80	108.90	83.51	45.75	57.07	71.27
Zr	12.55	23.34	7.79	12.60	4.87	19.94	35.71	50.00	2.79	38.88	152.50	129.60	77.37	108.90
Nb	1.85	1.72	0.744	1.38	0.16	2.67	3.44	3.51	0.33	3.22	2.35	2.35	1.45	1.31
Cs	0.14	0.11	0.454	0.16	0.16	0.09	0.25	0.06	0.38	0.59	0.08	0.08	0.40	0.10
Ba	30.42	17.04	103.3	59.23	50.91	92.43	235.00	12.94	31.23	70.49	81.55	19.37	105.90	220.40
Hf	0.47	0.74	0.404	0.81	0.31	1.14	1.45	1.61	0.16	1.42	4.88	4.29	2.81	3.69
Ta	0.12	0.12	0.062	0.10	0.02	0.21	0.25	0.23	0.04	0.22	0.21	0.16	0.11	0.10
Pb	1.20	0.74	2.39	2.33	68.13	1.06	1.31	1.92	0.92	1.62	2.32	15.64	1.48	2.38
Th	0.42	0.58	0.227	0.67	0.08	1.48	2.22	1.29	0.18	2.21	2.40	1.43	0.63	0.56
U	0.14	0.12	0.109	0.27	0.06	0.41	0.66	0.26	0.11	0.55	1.16	0.73	0.25	0.47
Y	41.65	37.92	21.54	43.63	4.69	50.85	40.12	59.86	6.89	40.51	23.06	37.14	45.21	36.03
La	8.22	9.06	2.43	4.41	3.64	9.26	10.27	12.96	2.26	15.85	5.65	7.00	5.56	4.96
Ce	22.25	24.67	6.62	13.19	7.60	24.55	26.80	34.92	5.03	37.92	13.92	17.42	15.34	14.65
Pr	3.76	4.19	1.08	2.26	0.99	4.29	3.54	6.22	0.68	5.53	1.96	2.74	2.76	2.47
Nd	18.86	21.70	5.50	12.09	5.13	20.13	15.47	30.98	3.35	23.74	8.79	13.84	15.24	13.13
Sm	5.91	6.35	1.90	4.46	1.06	6.52	4.58	9.73	0.87	6.32	2.46	4.34	5.17	4.07

Eu	1.67	1.36	1.45	1.07	0.36	2.09	0.89	2.15	0.99	1.29	0.48	0.96	1.31	1.07
Gd	6.86	7.16	2.49	6.17	1.09	7.63	5.47	9.96	1.06	6.61	3.08	5.69	7.12	5.15
Tb	1.13	1.20	0.452	1.13	0.15	1.32	1.00	1.66	0.18	1.13	0.55	1.01	1.25	0.90
Dy	7.39	7.05	3.19	7.98	0.84	8.31	6.75	10.92	1.08	7.31	3.86	6.82	8.50	6.40
Ho	1.54	1.51	0.709	1.65	0.17	1.89	1.53	2.45	0.24	1.52	0.84	1.49	1.79	1.40
Er	4.17	4.20	2.12	4.56	0.50	5.24	4.51	6.65	0.71	4.40	2.61	4.33	5.07	4.31
Tm	0.63	0.58	0.331	0.70	0.07	0.83	0.72	1.07	0.11	0.69	0.42	0.67	0.76	0.67
Yb	4.02	3.58	2.26	4.42	0.40	5.43	4.68	6.75	0.71	4.64	2.83	4.52	4.76	4.56
Lu	0.57	0.53	0.352	0.66	0.07	0.82	0.71	1.04	0.12	0.69	0.45	0.71	0.71	0.70

Table 4.2. Geochemistry data for a representative selection of trondhjemites and tonalite samples, as well as dacites from the Geitung Unit. TR = Trondhjemite, TO = Tonalite, DA = Dacite. Both major- and trace element compositions are included in this table. 8 trondhjemite samples from Lykling, 1 tonalite sample from Ådnanes, 1 trondhjemite sample from Sakseid, 2 dacite samples from Finnås and 2 samples from Geitung. A full list of geochemistry data can be found in appendix 2.

4.3 Zircon geochronology of trondhjemites

Three samples were selected for geochronology (20BOM-9A, 20BOM-11, 20BOM-12A). A total of 137 zircons grains were analyzed across the three samples with 56, 45 and 36 grains analyzed respectively. Of these, 11 measurements were rejected from the final data set due to discordance, or due to large analytical uncertainties.

Sample 20BOM-9A:

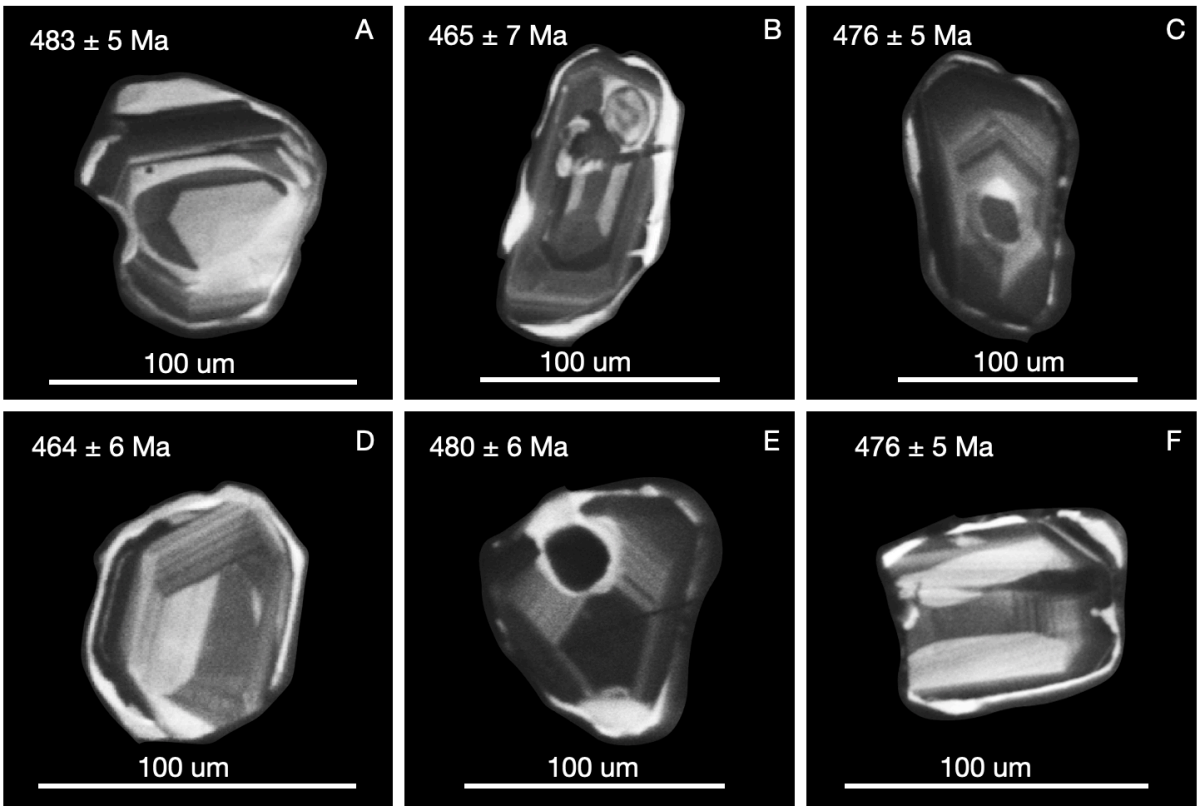

Figure 4.27. A representative selection of zircon grains under cathodoluminescence imaging from sample 20BOM-9A. **A-F** External morphology of zircon grains from this sample. The grains exhibit erosion features and large zonation rims as well as sometimes inclusions of xenocrystic cores.

49 zircon grains were analyzed for this sample with a total of 56 shot positions (several grains were subject to multiple analyses). Of these, 52 analyses were <10% discordant, and two additional grains were filtered from the final data set due to near discordant values of 10% (9.8% and 8.7% discordance). The grains are generally uniformly sized and shaped with lengths at ≈ 100 μm and exhibits subangular to rounded shapes. Internal structures observed within the grains are inclusions of xenocrystic cores and oscillatory zoning (Figure 4.27).

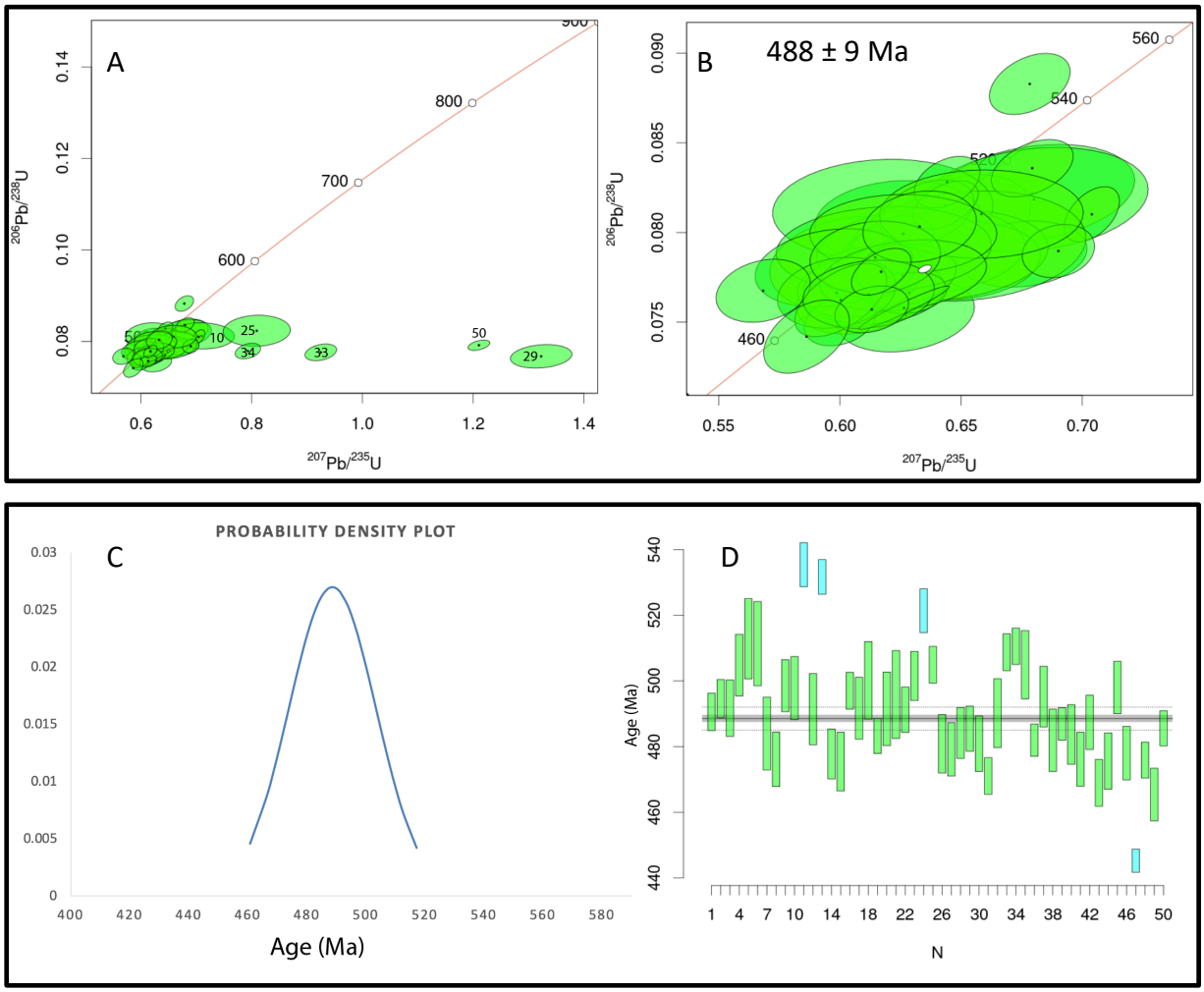

Figure 4.28. **A**) Concordia diagrams before and after **B**) 10% discordance cutoff for trondhjemite sample 20BOM-9A. Shot positions 10, 25, 29, 33, 34 and 50 of discordant grains are marked on the diagram. Concordia age is estimated to 488 ± 9 Ma. **C**) Probability density plot for the trondhjemitic sample 20BOM-9A showing a concentration peak at approximately 489 Ma. **D**) Weighted mean plot for sample 20BOM-9A after discordance cutoff revealing the same age approximation at 489 Ma.

Figure 4.28 visualizes the obtained data from this analysis. Concordia diagrams are presented with all measured data and after 10% discordance cutoff. A weighted mean plot accompanies the concordia diagrams with its respective discordance cutoff profile (Figure 4.28D). The analyzed ages range from 466 Ma to 544 Ma (discordant age). Many of the discordant zircon grains plot below the concordia diagram, which is consistent with Pb loss (Figure 4.28A). Shot positions 10 and 50 detected higher abundance of common Pb within the system due to fractured grains. In addition, shot position 10 were aimed a zircon rim that may have exhibited radiogenic Pb loss due to metamorphic overprint. Shot position 29 aimed a crack within the grain, and radiogenic Pb loss may have occurred. Shot position 33 and 34 are analyses from the same discordant zircon grain. A rather imprecise concordia age of 488 ± 9 Ma is estimated for this sample. A concentration peak at 489 Ma in the data set can be observed in the probability density plot (Figure 4.28C).

Sample 20BOM-11:

A total of 45 grains were analyzed for this sample and 44 grains were >90% concordant. The size of the grains varies in size. Generally, most of the grains are of approximately the same size, but a few stand out as significantly larger than the rest. The grains are subangular and the majority have a more rectangular shape rather than prismatic (Figure 4.29C, E, F). Many grains seem also broken off and eroded. A few grains seem to be fragments of a broken larger grain (Figure 4.29D). The grains exhibit in no expressive way signs of fracturing in more than a few grains. A general description of the zircon grains from this sample is the skewed core to rim ratio. Typically, the grains exhibit large dark U-poor cores with thinner rims (Figure 4.29C, E, F). The rims show oscillatory zoning (Figure 4.29A).

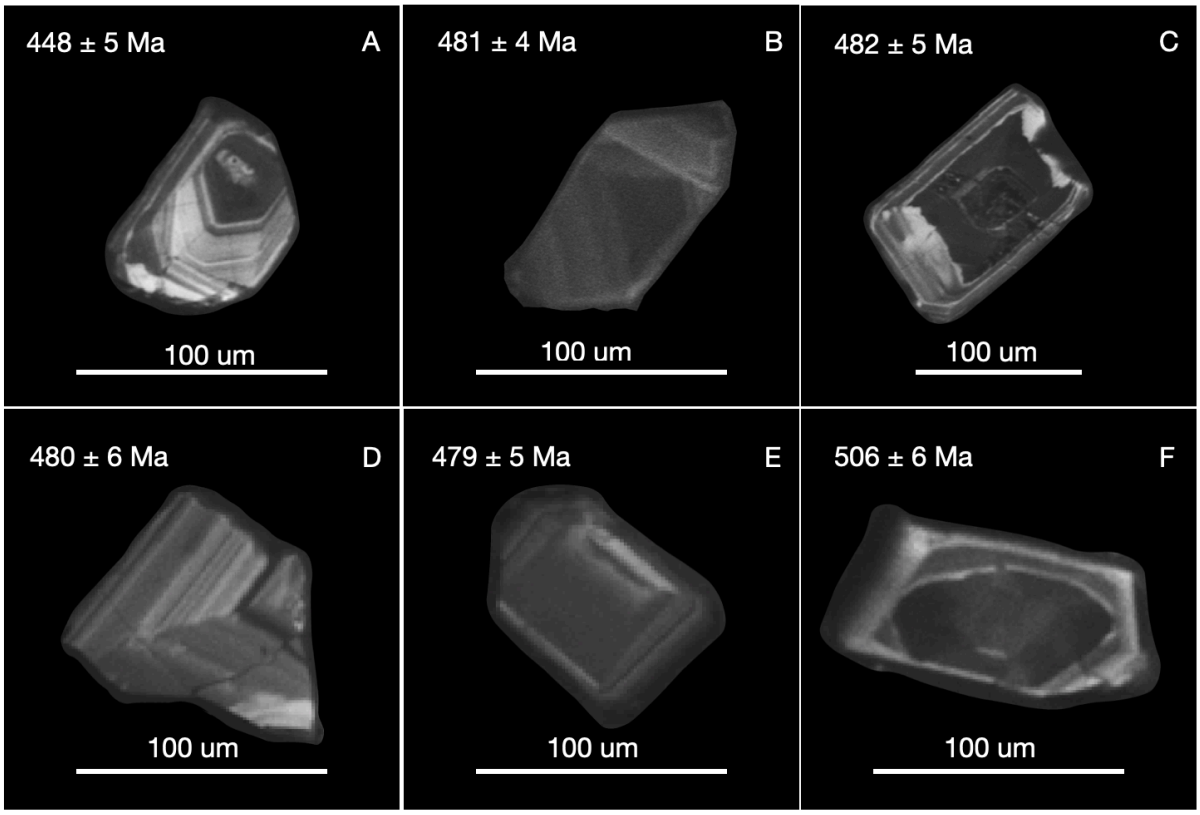

Figure 4.29. A representative selection of zircon grains under cathodoluminescence imaging from the sample 20BOM-11. The grains exhibit various shapes and forms, but generally conforms to a rectangular subangular shape. **A** Grain exhibit a large rim with oscillatory zoning around a smaller core. **B** Zircon with no distinct core or zoning features. **C** Grain with a large core and xenocrystic cores developed inside. Thin rim. **D** Broken off piece of a larger zircon grain. These types of grains are common in this sample. **E-F** Zircon grains with larger cores and thin rims showing oscillatory zoning.

Figure 4.30 represents the combined data obtained from this analysis. Concordia diagrams are given with all measured data, and another concordia diagram shows the filtered data with a <10% discordance cutoff. Weighted mean plot is also shown for the filtered data set (Figure 4.30D). Although most grains were concordant the interval for the spreading of ages (430–564 Ma) are quite significant, but there is no trend visible in the concordia that may signal the presence of inherited zircons. The data is concentrated at a major peak at around 475-480 Ma in the probability density plot (Figure 4.30C). Based on these data a concordia age of 479 ± 5 Ma is estimated for this sample.

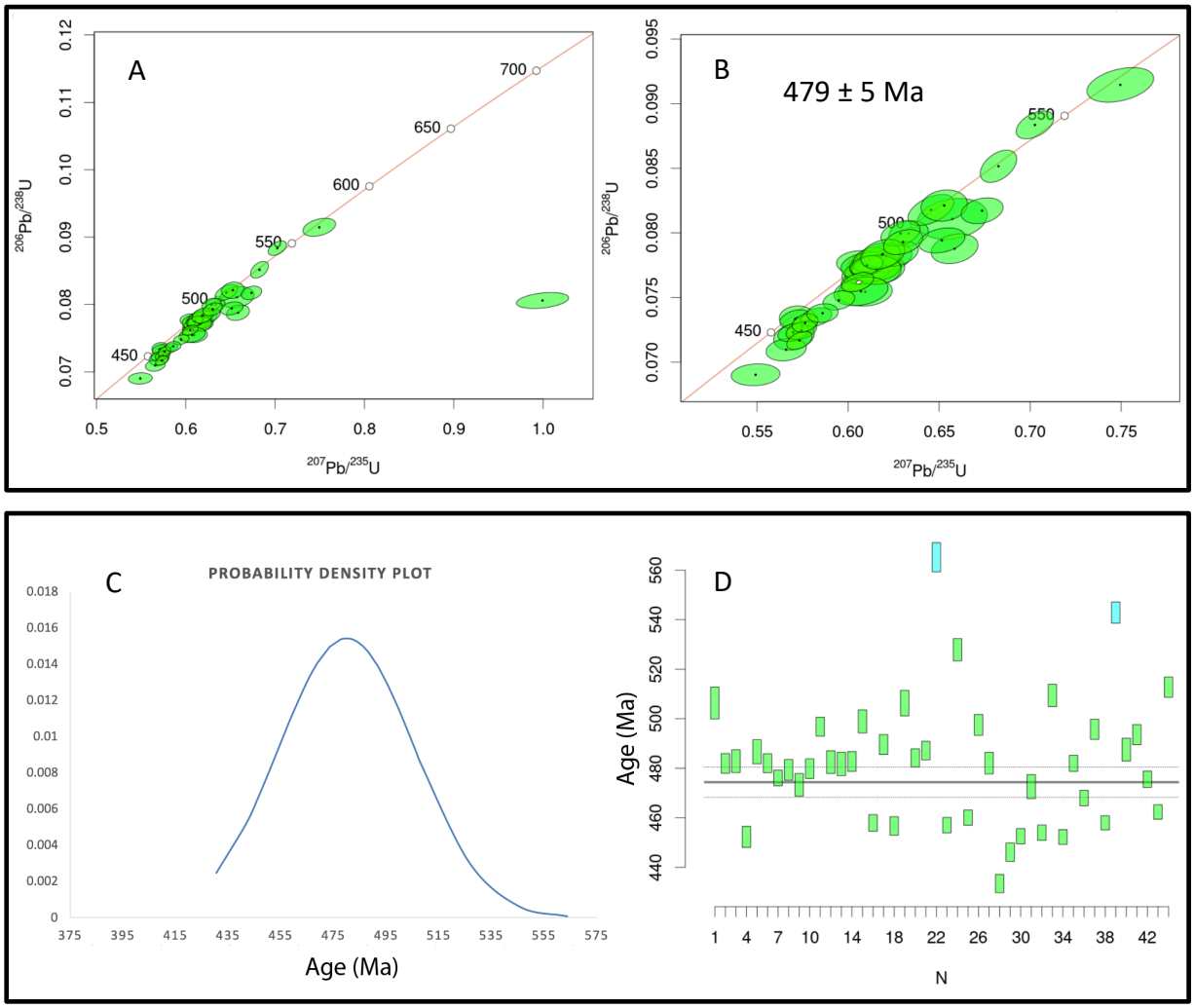

Figure 4.30. **A**) Concordia diagrams from sample 20BOM-11 showing concordia line and age before discordance cutoff, and **B**) after 10% discordance cutoff. Concordia age is estimated to be 479 ± 5 Ma. **C**) Probability density plot revealing a concentration peak at 480 Ma. **D**) Weighted mean plot showing a younger mean age of ≈ 474 Ma.

Sample 20BOM-12A: A total of 36 grains were analyzed from this sample where 33 grains are >90% concordant. Sizes of the grains varies from 80–100 μm with a few smaller grains present. The grains are subangular and the majority have rectangular shapes similar to the grains from sample 20BOM-11 (Figure 4.31). The zircons have for the most part contained their original shape, and dissolution features and broken off pieces are not common in this sample. Only one grain exhibit fracturing (Figure 4.31C). The more pristine shaped zircons are equant in shape (Figure 4.31A) but stubby forms are also present (Figure 4.31C). This sample show more grains with thicker rims compared to 20BOM-11, and the rims exhibit oscillatory zoning (Figure 4.31A, C, D, E). Some grains have xenocrystic cores appearing as either subrounded grains enclosed within the zircon (Figure 4.31A) or as bubble structures (Figure 4.31D-E).

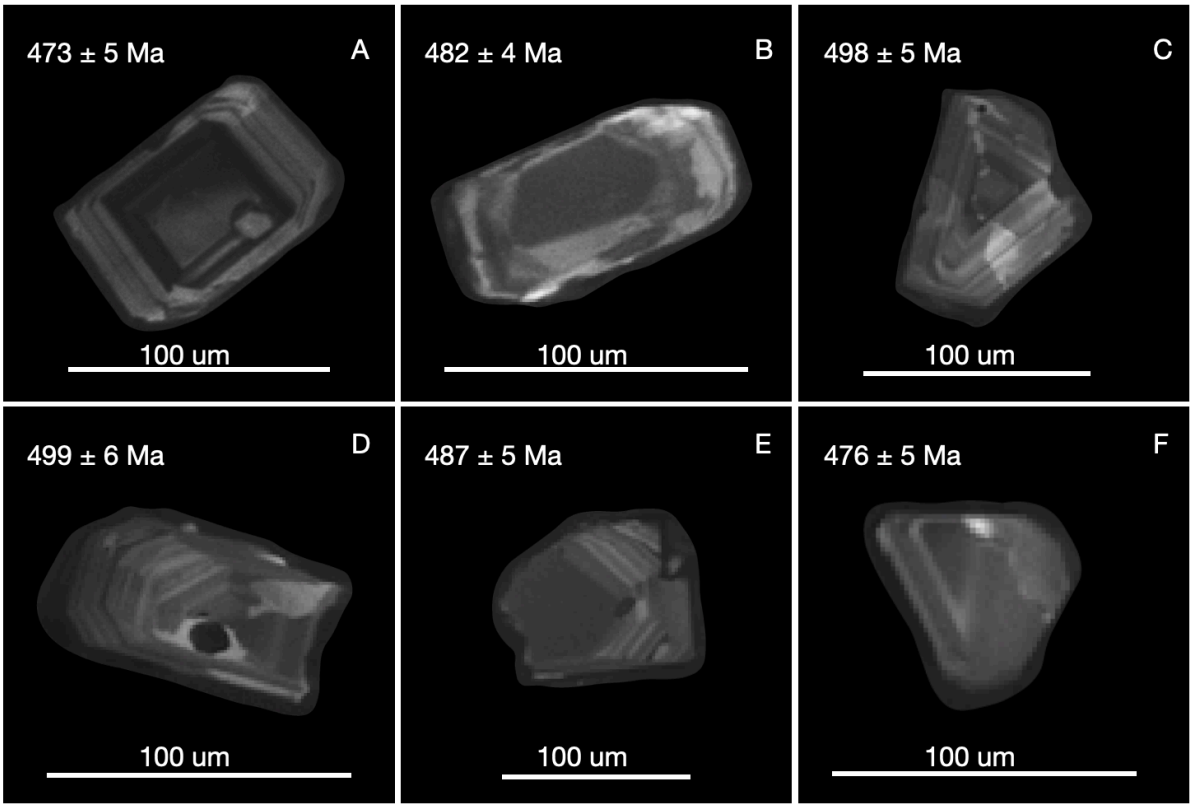

Figure 4.31. A representative selection of zircon grains under cathodoluminescence imaging from sample 20BOM-12A. **A** Equant shaped zircon grain with a xenocrystic core inclusion. **B** Zircon with no apparent core-rim boundary. **C** Grain with small core and large zonation rims. The grain exhibits fracture features. **D** Zircon grain with xenocrystic core appearing as a bubble. Irregular zoning. Broken off/eroded on one side. **E** Grain with large core and oscillatory zoning. A Small xenocryst appear as a bubble. **F** Near featureless zircon grain with no distinct core or rims.

In figure 4.32 the collective data set for this sample is presented in concordia diagrams and as a weighted mean plot. The ages of individual data points range from 412 Ma to 546 Ma. With a 10% discordance cutoff, the age range is reduced to 451-512 Ma.

For some of the discordant grains the discordancy can be explained by the position of the analyses and imperfections in the grains. A concordia age of 482 ± 5 Ma is calculated for this sample. A major peak in the probability density plot is concentrated at around 485 Ma (Figure 4.32C).

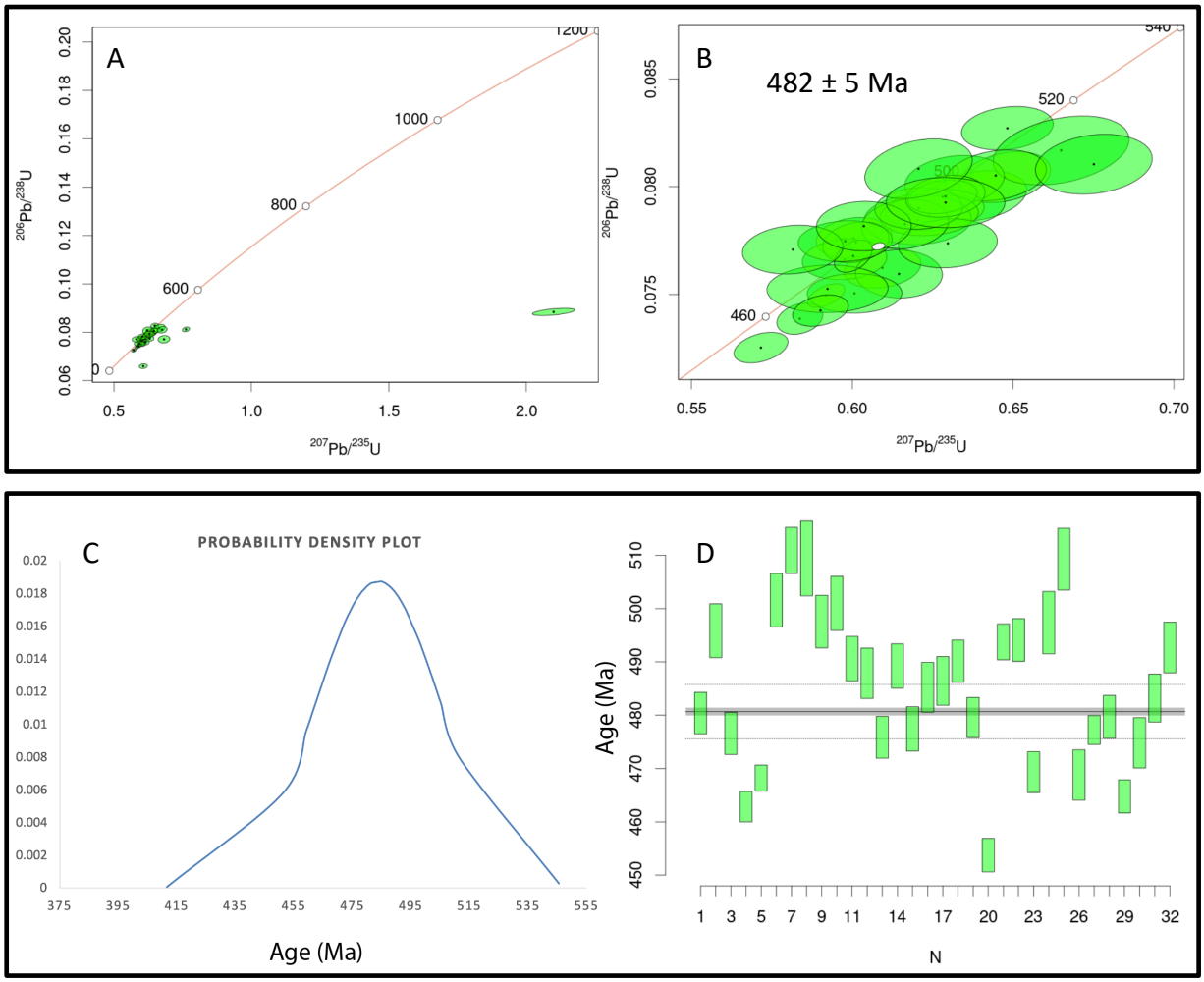

Figure 4.32. **A**) Concordia diagrams of sample 20BOM-12A before and **B**) after 10% discordance filtering. Concordia age is calculated to 482 ± 5 Ma. **C**) Probability density plot for sample 20BOM-12A. Concentration peak at 485 Ma. **D**) Weighted mean plot with discordance cutoff reveals a mean age of 480 Ma.

4.4 Geochemistry of zircons

REE analysis was conducted on zircon grains of one of the trondhjemite samples (20BOM-11) to support petrogenesis of the trondhjemites and radiometric age that was revealed through U/Pb dating. Analysis of detrital zircon grains from a siltstone that is interlayered with the volcanic sequence on Geitung was also carried out. The zircons of this siltstone yield the same age as the Geitung Unit volcanics (Viken, 2017) and they are therefore probably derived from the volcanic sequence.

The REE analysis on both samples were performed on concordant grains with no sign of inheritance. The REE pattern of the zircons of the trondhjemite (Figure 4.33) shows a shallow slope towards an enrichment in HREE, with La values in line with typical magmatic zircons (< 0.90) (Long et al., 2012). Additionally, the zircons reveal high $(Sm/La)_N$ values (median = 10.5) indicating that aqueous fluids or hydrous melts was not present in their formation (the subscript N denotes normalized to chondrite). A typical hydrothermal zircon will have lower values with $(Sm/La)_N$ = 1.5-4.4 (Hoskin, 2005). Enrichment in HREE relative to LREE also point to no garnet being present during the formation of these magmas, further indicating a formation process not dictated by partial melting of deep crustal rocks. The typical magmatic zircon values of the sample suggest that they have not been significantly affected by metamorphism subsequent to their formation.

The zircons from the Geitung Unit show a steeper positive slope towards the HREE, and lower LREE values than the trondhjemite (by magnitude of 10). This slope, however, aligns perfectly with what has been revealed for typical igneous zircon patterns, including the prominent Ce and Eu anomalies (Whitehouse, 2003).

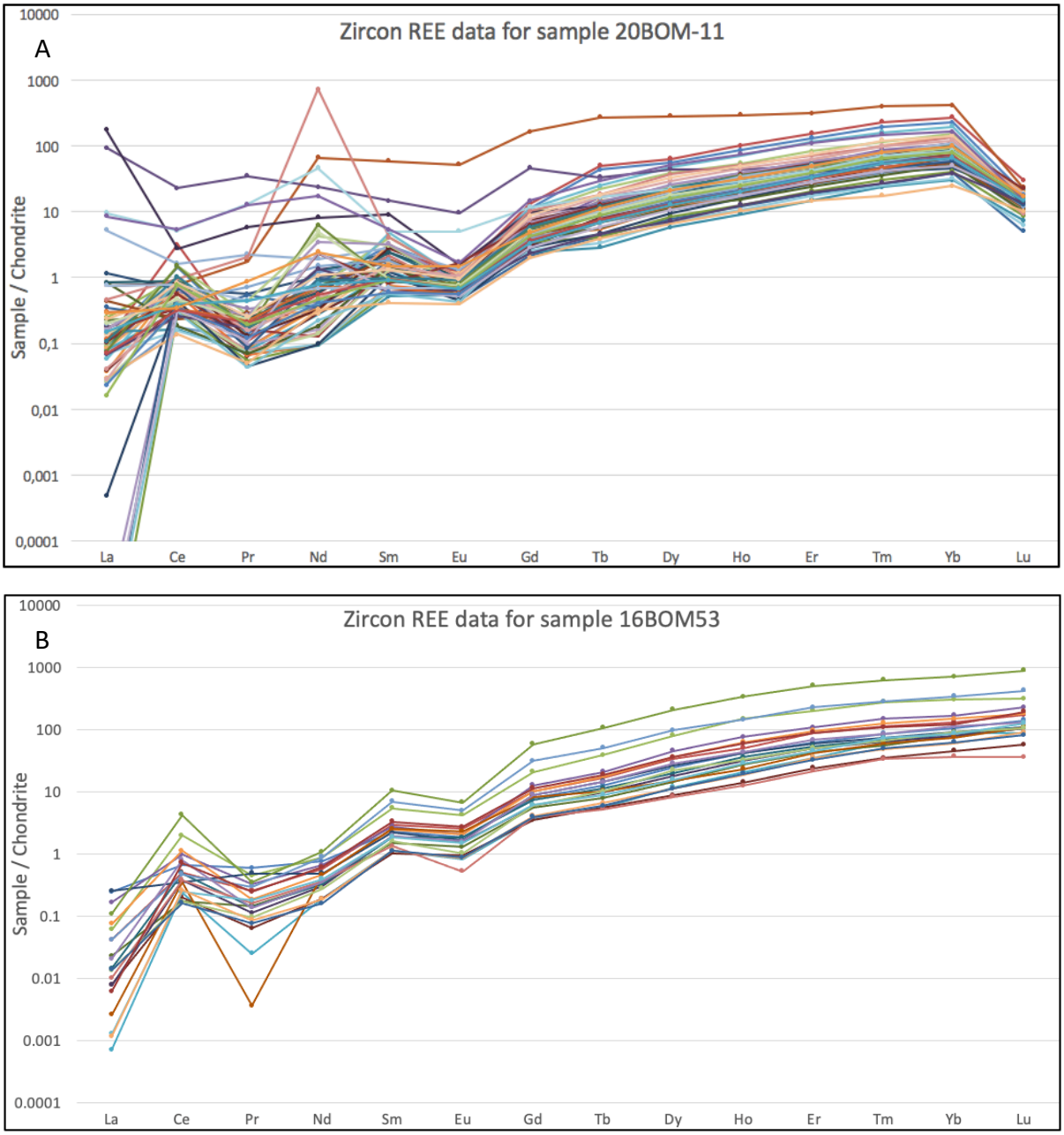

Figure 4.33. REE data analyzed on zircon grains for samples (**A**) 20BOM-11 and (**B**) 16BOM53 (Data acquired from Viken, 2017). Each REE pattern represents separate zircon grains. Normalized to chondrite.

5. Discussion

Following is a discussion surrounding the geochemical characteristics of the trondhjemites and tonalites and how they cast light on the early development of the island arc crust. This is achieved through a detailed research on these intrusions, and how they relate to the other occurring lithologies in the area, the ophiolite gabbros and Geitung Unit volcanics. Together with whole rock geochemistry, zircon geochemistry is used to discuss petrogenesis of the trondhjemites, as well as crustal thickness reconstructions. Lastly, an evolutionary history of the arc system is proposed.

5.1 Geochemistry of trondhjemites and tonalite, the Geitung Unit volcanics and gabbros of the Lykling Ophiolite Complex

The new geochemical data presented in this work demonstrates that the trondhjemites that intrude the gabbroic rocks of the ophiolite complex have almost identical trace element compositions as the dacitic volcanic rocks of the Geitung Unit (Figure 5.1). This indicates that they are the intrusive and extrusive components of the same magmatic event. These new data therefore support the conclusions made by Brekke et al. (1984) who suggested that the voluminous intrusions of trondhjemite and tonalite are geochemically similar to the extrusive volcanics of the Geitung Unit. This only applies for the dacitic extrusives however, as the brecciated rhyolites and andesites associated with the Geitung Unit are slightly enriched in REE relative to the dacites and trondhjemites (Figure 4.20).

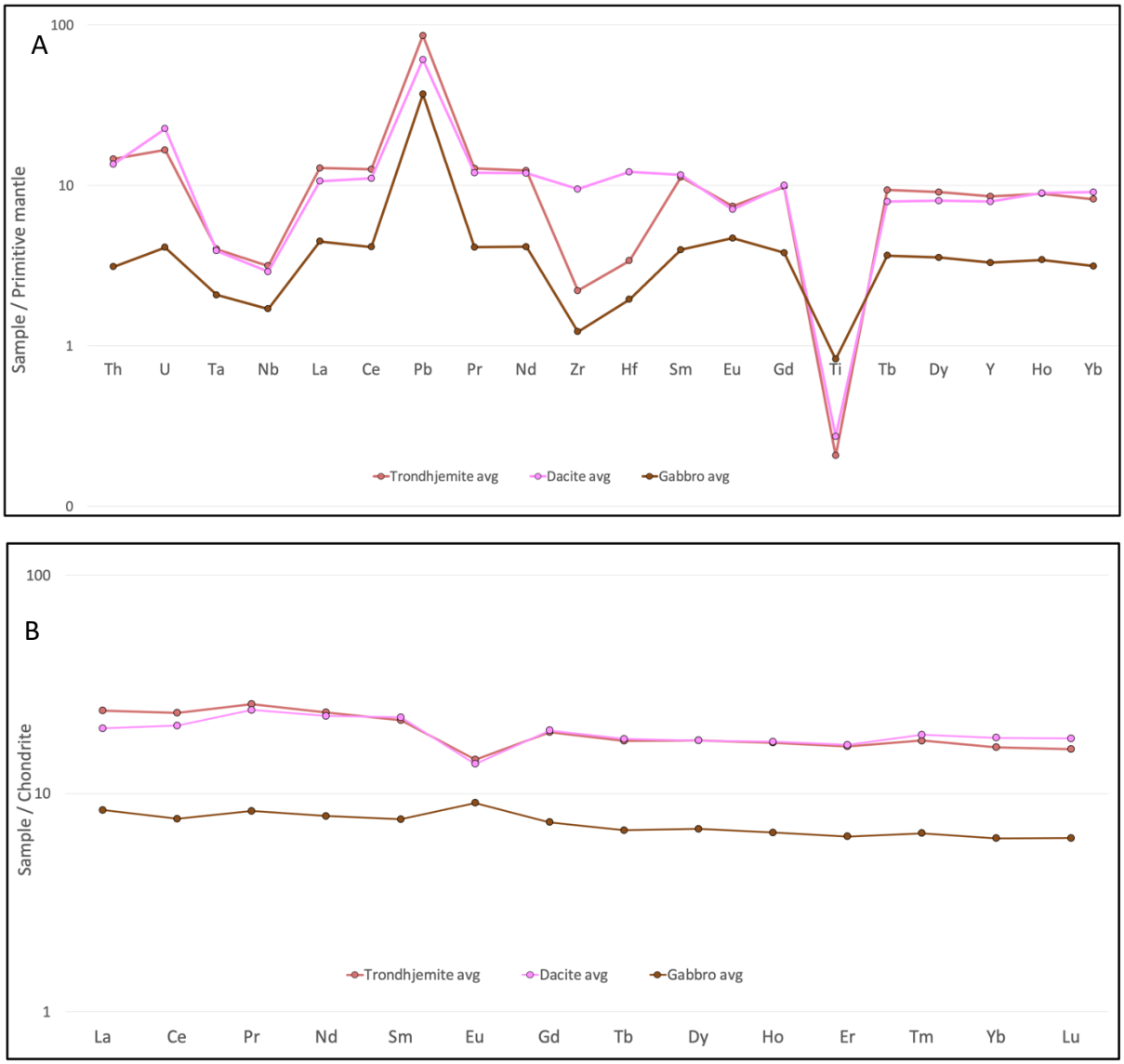

Figure 5.1. (**A**) Average trace element compositions and (**B**) REE patterns for trondhjemites compared to average patterns for dacites of the Geitung Unit and the ophiolite gabbros. Trace elements normalized to primitive mantle values from Sun and McDonough (1989). Rare earth elements normalized to chondrite.

In previous chapters and in figure 4.15 and 4.16 the dacitic extrusives of the Geitung Unit were divided into two distinct groups based on their slight geochemical variations involving their K_2O concentrations. The two groups are sampled in two separate geographical locations. The first group sampled solely on the island of Geitung exhibit slightly higher K_2O contents than the dacites sampled near Finnås and Lykling on Bømlo. The Geitung island samples show more developed magmatic arc signatures of a calc-alkaline magmatic source, whereas the Finnås dacites exhibit island arc tholeiite (IAT) signatures similar to the trondhjemites and tonalites (Figure 4.16). While still very fine grained the crystal growth and texture of the Finnås dacites is slightly more developed and coarser than the Geitung samples (determined in field) and a

transitional phase from the intrusive trondhjemites to extrusive dacites is suggested. These internal variations within the Geitung Unit have not been reported in earlier studies.

Pedersen & Dunning (1997) reported that island arc build up continued for approximately 20 My, and evolved from IAT to high-K calc-alkaline magma. The new analytical results on the volcanics of the Geitung Unit suggests that parts of the unit may represent a more mature island arc than previously recognized.

Extended spider diagram for trondhjemites and Geitung dacites exhibit positive anomalies for Th, U and Pb and negative anomalies for Ta and Nb. This is a typical trace element pattern of immature island arc tholeiitic volcanics (Pearce et al., 1984). Pearce et al. (1984) termed ophiolitic fragments with such compositional signatures for supra-subduction zone ophiolites (SSZ). The geochemical characteristics typical for a supra-subduction zone ophiolite are basaltic rocks with enrichments in Sr, K, Rb, Ba, Th ± Ce ± Sm, and depletions in Ta, Nb, Hf, Zr, Ti, Y and Yb relative to typical Mid-Ocean Ridge basalts (MORB). The granitic intrusions on Bømlo exhibits the same trace element patterns as that of a supra-subduction zone and is suggested to have formed in this type of formation environment.

The average composition of all gabbros sampled is plotted together with averages for trondhjemites and dacites in figure 5.1. The lithologies parallels one another with the exact same pattern, and the gabbros are distinguished from the trondhjemites and the dacites only by an overall enrichment of all trace elements for the latter. All three exhibit positive anomalies for U, Pb and Sm as well as negative anomalies for Ta, Nb, and Ti. In the REE spider diagram both trends are equally flat separated only by concentrations of REE. The gabbros shows values just below 10 times chondrite while the trondhjemites and dacites exhibit values 30–40 times chondrite. This can be explained by fractional crystallization where the trondhjemites represent the residual melt after the gabbros have crystallized. It is therefore suggested that the trondhjemites are derived from the residual melt of the ophiolite gabbro.

5.2 U/Pb geochronology of trondhjemites

The overall temporal evolution of this ophiolitic terrane have been documented by U/Pb zircon chronology (Dunning & Pedersen, 1988, Pedersen & Dunning 1997). Plagiogranites (trondhjemites) associated with the Karmøy- and the Gullfjellet ophiolite complexes have been dated to 493 +7/-4 Ma and 489 +/-3 Ma respectively (Dunning & Pedersen, 1988). It is well documented that the dated plagiogranites represent differentiation products of the basaltic magmas that formed the ophiolite complexes, and that these ages therefore date the formation of the initial arc crust that constitute the oldest parts of this oceanic terrane (Pedersen & Malpas, 1984; Dunning & Pedersen, 1988; Pedersen & Hertogen 1990; Dunning & Pedersen, 1997). The 494 ± 2 Ma age of a basaltic andesite flow at the Finnås area is consistent with this, and shows that the basaltic to rhyolitic volcanics of the Geitung Unit formed at the same time as the ophiolitic crust (Figure 5.4).

At Karmøy and in the Gullfjellet area, the juvenile oceanic crust was intruded by younger trondhjemites and quartz diorites. At Karmøy, diorites and tonalites intruded the ophiolite complex at 485 ± 2 Ma (Dunning & Pedersen, 1988), and the Gullfjellet ophiolite complex was intruded by tonalites at 482 +6/-4 Ma (Dunning & Pedersen, 1988). Nd and Sr isotopic data suggest that the mantle wedge by then had become enriched by a subducted continental component (Pedersen & Hertogen, 1990). The intrusion of quartz diorite plutons containing inherited Precambrian zircons at 479 ± 5 Ma, and the subsequent intrusion at 474 +3/-2 Ma of S-type granites that are loaded with old continental zircons, are interpreted to reflect the subduction of a continental shelf below the oceanic arc as a result of arc-continent collision (Pedersen et al., 1992; Pedersen & Dunning, 1997; Hamnes, 1998; Fonneland, 2002; Slotnes, 2021).

In this study three trondhjemite samples was dated by U/Pb geochronology revealing estimated concordia ages of 488 ± 9 Ma, 479 ± 5 Ma and 482 ± 5 Ma. A mean age for the three samples analyzed yielded an estimated U/Pb age for the trondhjemitic intrusion at 484 ± 6 Ma (Figure 5.2). A probability density plot and density plot is accompanied revealing a concentration peak at 478 Ma, and that most grains fall within the 468-482 Ma and 454-468 Ma intervals (Figure 5.3). Based on age distribution of individual zircons it was concluded that no inherited zircons were present in any of the three samples (Figure 5.3). No inherited zircons indicate that

magmatism occurred before arc-continent collision and thus giving crucial information on the time constraints to the evolution of the island arc system.

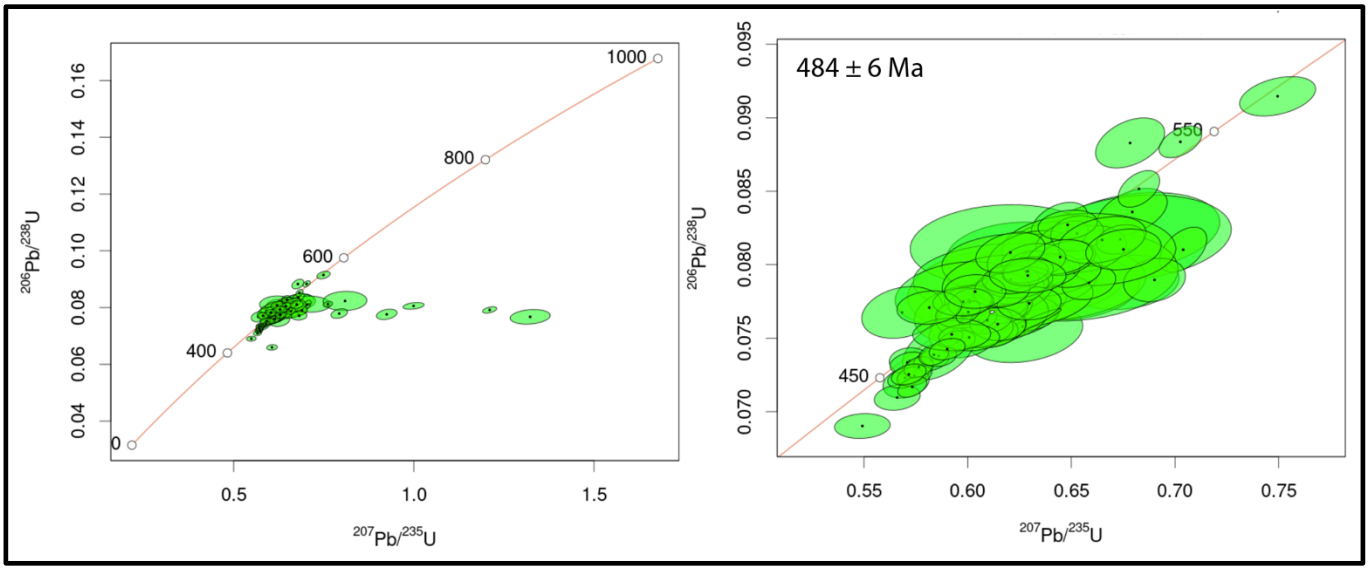

Figure 5.2. Concordia diagrams of the collective data set including all three samples (20BOM-9A, 20BOM-11, 20BOM-12A). Before data filtering and discordance cutoff (left). After 10% discordance cutoff (right). A few analyses were slightly <10% discordant, but stood out from the concordia line and was therefore not included in the final data set.

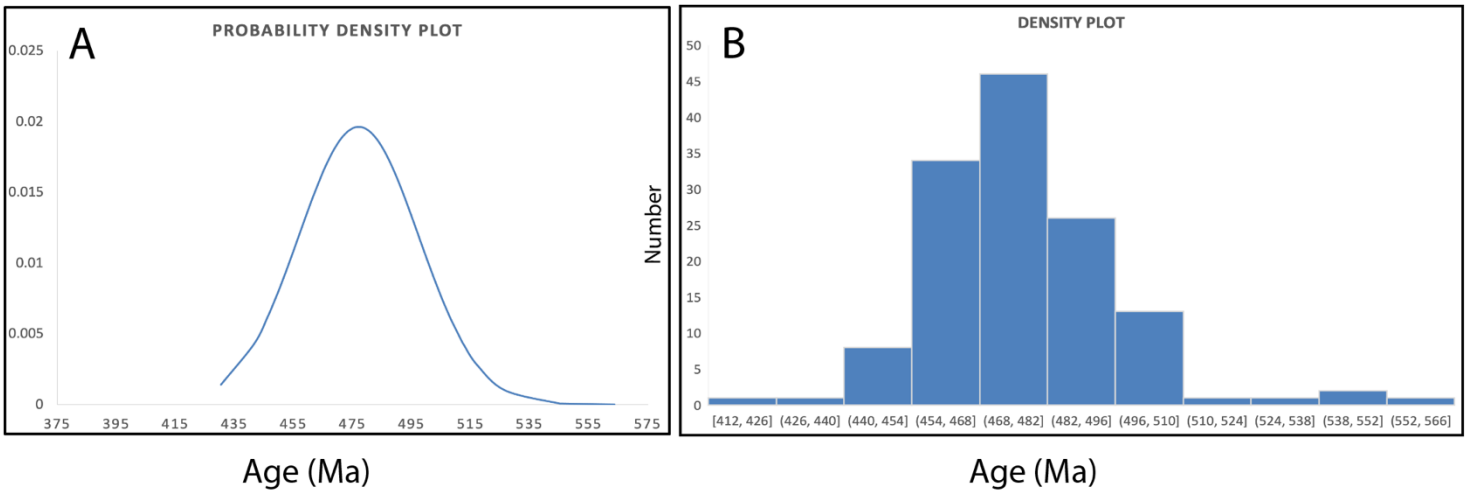

Figure 5.3. (**A**) Probability density plot for all three samples with a concentration peak at 478 Ma, and (**B**) density plot showing primarily abundance of grains within the 468 – 482 Ma and 454 – 468 Ma intervals.

The geochemical similarities between the trondhjemites and dacites (Geitung Unit) of Bømlo and the plagiogranite differentiates of the Karmøy ophiolite indicate that they are genetically related magmas. However, U/Pb dating revealed intervals in the ages at which these rocks formed (Figure 5.4). Between the two gabbro differentiates 9 My separate the two intrusions, and 10 My separate the trondhjemites from the Geitung dacites. This age gap can be explained by the uncertainties surrounding the dating performed on the trondhjemites where Pb loss most likely occurred, and was consequently masked by the relatively large uncertainty the analysis produced. The radiometric age of 484 ± 6 Ma most likely represents the minimum formation age of the trondhjemite intrusion, and that formation possibly occurred closer to 490 Ma.

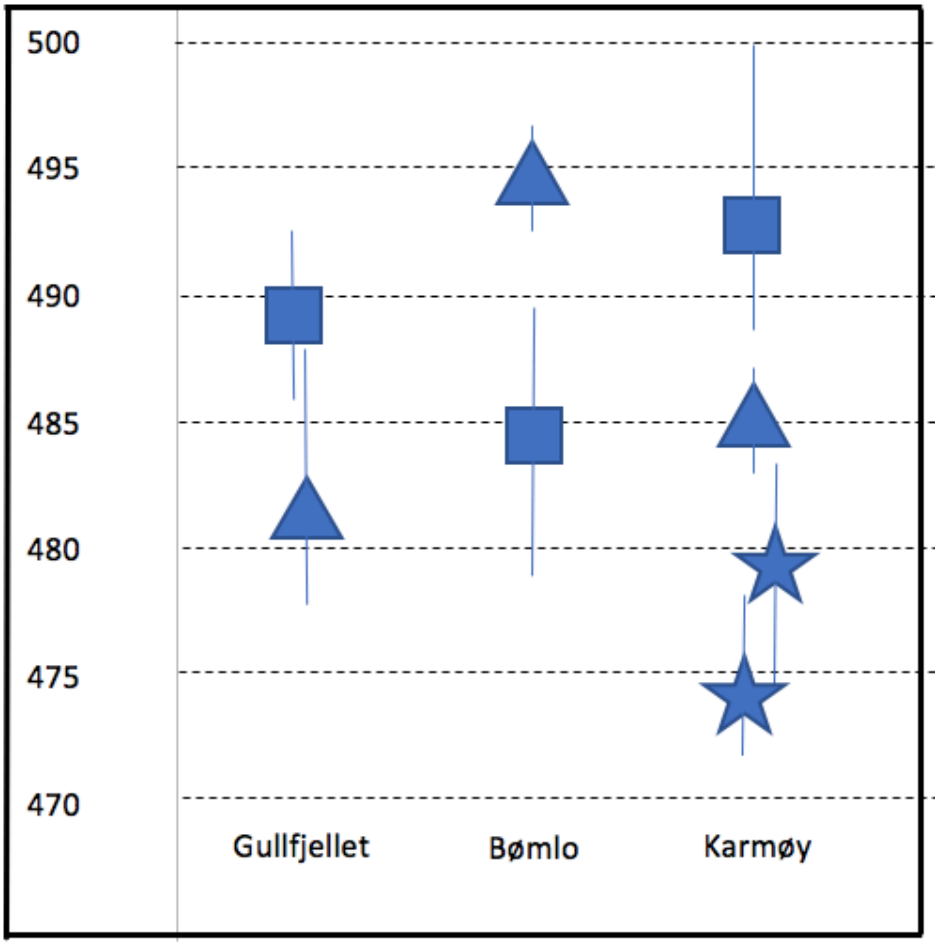

Figure 5.4 Ages of all three ophiolite complexes of SW Norway plotted against each other. **Square:** Trondhjemite (494 ± 6 Ma) and plagiogranites (493 +7/-4, Karmøy; 489 ± 3 Ma, Gullfjellet) differentiated from ophiolite gabbro. **Triangle:** Granitic intrusions/extrusions associated with the ophiolite complexes (482 +6/-4 Ma, Gullfjellet; 494 ± 2 Ma, Bømlo; 485 ± 2 Ma, Karmøy). **Star:** Intrusions containing inherited zircons marking the time interval at which subduction related magmatism became dominant (479 ± 5 Ma and 474 +3/-2 Ma).

5.3 Petrogenesis of trondhjemites and tonalite

Trondhjemitic and tonalitic rocks are exposed over large parts of the Lykling area (Figure 4.1). In the field the rocks are distinguishable by their absence of K-feldspar, and geochemically these rocks follow the low-K magmatic series (Figure 4.16). K-poor felsic rocks are common in ophiolite complexes where they represent a minor component of the crustal sequence (Coleman & Donato, 1979). Trace element compositions of the Lykling trondhjemites indicate both island arc tholeiitic (IAT) and calc-alkaline affinities (Figure 4.17). They also show that the trondhjemites of the Lykling ophiolite have geochemical characteristics that straddle the boundary of ocean ridge granites and island arc granites (Figure 4.19).

Ocean ridge granites (oceanic plagiogranites) typically form by the differentiation of basaltic magma (e.g. Coleman & Peterman, 1975; Pedersen & Malpas, 1984). Island arc granites, on the other hand, may form in many ways: 1) by melting of subducted lithosphere and sediments; 2) by differentiation of volatile rich arc magmas; and 3) by the interaction between lower crustal rocks and mantle derived melts that are underplating the developing arc crust (e.g. Takahashi et al., 2018). No inherited zircons are found in the trondhjemite samples that have been analyzed, indicating that silicate melts derived from subducted sediments were not involved in the petrogenesis of these rocks. The magmatic zircons that are present in the trondhjemites are enriched in HREE (Figure 4.33). As garnets have very high partition coefficients for HREE it seems clear that the petrogenesis of these rocks did not involve garnets, and that the trondhjemitic magmas therefore formed under relative low-pressure conditions.

It was previously reported from whole rock geochemistry that the trondhjemites was derived from residual melts after the ophiolitic gabbros have crystallized, and this complies with this conclusion. The slightly LREE depleted, but otherwise flat bulk rock REE pattern of the trondhjemites, is overall similar to the REE pattern of the microgabbros that they are associated with (Figure 5.1). The higher REE concentrations of the trondhjemites relative to the gabbros, and their distinct negative Eu anomalies, suggest that these trondhjemites formed by fractional crystallization of a basaltic magma that overall was similar to the gabbros that they intrude. The fact that the trondhjemites are cross-cut by basaltic dikes with similar compositions as these gabbros (Figure 4.24) shows that MORB-IAT like magmatism occurred both before and after these granitic intrusions formed.

The intruding basalt dikes on Lykling, Bømlo have been separated into two distinct groups (Figure 4.23 and 4.24) based on their geochemical characteristics. A younger generation of

basalts showing signatures to that of a mature island arc, and an older grouping showing signatures to that of an immature island arc. This is supported by in-field observations, REE patterns in spider diagrams, formation setting diagrams and SiO_2 vs. K_2O diagrams (Figure 4.21, 4.23 and 4.24). The older generation of basalt dikes can be spotted in the field as predominantly E-W cutting dikes with minor to major amounts of greenstone deformation. Geochemically they exhibit flat REE patterns similar to the gabbros of the Lykling Ophiolite Complex (Figure 5.5). Additionally, a diagram discriminating magmatic origin reveal that the older basalt dikes have an oceanic arc origin, as well as plotting as low-K basalts and calc-alkaline basalts. These plots give indicators that this generation of dikes were intruded in the very early stages of arc development while oceanic crust was still forming. It is proposed that these dikes are related to the development of the ophiolite complex.

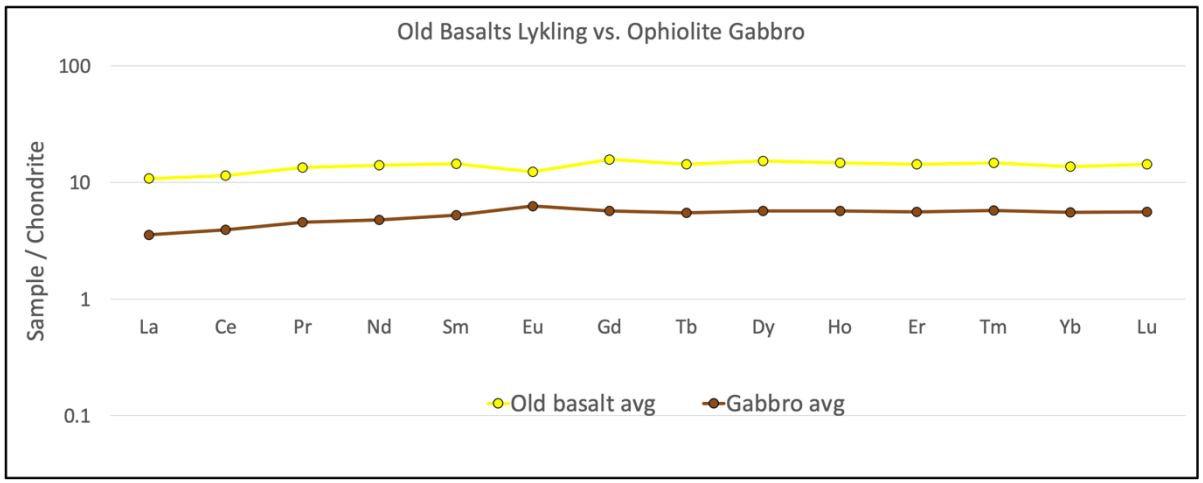

Figure 5.5. Average REE patterns for the older generation basalt dikes on Lykling compared to average patterns of ophiolite gabbro. Normalized to chondrite.

The younger generation of basalt dikes are in this thesis correlated with the Siggjo Complex, Vikafjord Group and Vardafjell Gabbro. The geology and geochemistry of these volcano-sedimentary units and intrusive complexes have been reported earlier (e.g. Brekke et al., 1984; Viken, 2017; Stubseid, 2017; Slotnes, 2021). New results suggest that these complexes probably represent a younger phase of extensional volcanism that developed after arc-continent collision involving the Laurentian margin and the ophiolite complex, with the intrusive trondhjemites and the Geitung Unit (R.B. Pedersen, in. prep.).

Comparisons to other Caledonian ophiolites in SW Norway

Plagiogranite that are associated with the Karmøy Ophiolite Complex and that are cogenetic with the gabbros show very similar REE patterns as that of the trondhjemite pattern on Bømlo (Figure 5.6). This indicates that the trondhjemites on Bømlo and the plagiogranites on Karmøy are related geochemically. This plagiogranitic pod from the Karmøy ophiolite was dated to 493 +7/-4 Ma (Dunning & Pedersen, 1988) and can be correlated with the Bømlo trondhjemite within the time constraints. Given their geochemical similarities it is safe to assume that the trondhjemites are the final differentiation product of the basaltic magma that also the gabbro crystallized from, similar to how plagiogranites are differentiates of the gabbroic sequence on Karmøy.

Figure 5.6 also compares the Bømlo trondhjemites with other intrusive granitic rocks present within the Karmøy ophiolite. A plagiogranite associated with the intruding Sauøy Diorite (485 ± 2 Ma) and an associated dacitic dyke that also post-date the axis sequence show both U-shaped REE patterns that are distinctly different from the Bømlo trondhjemites. On Karmøy these younger granitic intrusions are related to a phase of boninitic magmatism that took place around 485 Ma, and that today typically occurs in fore-arc environments (Hickey & Frey, 1982; Pedersen & Hertogen, 1990; Pearce et al., 1992). Both the Lykling and Karmøy ophiolite complexes show many other indicators for subduction influence, and both are thought to have formed in a supra-subduction zone setting.

The magmatic development of the different units on Bømlo evolved from IAT to calc-alkaline and further to alkaline magmas. This magmatic development is also recorded in the plutonic and extrusive parts of the Karmøy Ophiolite Complex (Pedersen & Hertogen, 1990). IAT magmas are recorded in the Geitung Unit and granitic plutons on Bømlo are comparable to the Karmøy axis sequence. The Siggjo Complex, Vikafjord Group and young generation of basalt dikes represents the mature island arc calc-alkaline to high-K calc-alkaline magmas on Bømlo and can be correlated with high-K calc-alkaline magmas that intruded the Karmøy Ophiolite Complex (i.e. the Feøy Gabbros) (Pedersen & Dunning, 1997). Age findings correlate the Siggjo Complex to the Feøy Gabbros (470 ± 9/- 5 Ma) (Dunning & Pedersen, 1988).

The similarities between the Lykling Ophiolite Complex and Karmøy Ophiolite Complexes also incorporates the basalt dikes. The Karmøy Axis Sequence (KAS) is, similar to Lykling,

cross cut by dikes formed during and subsequent to the complex formation (Pedersen & Hertogen, 1990).

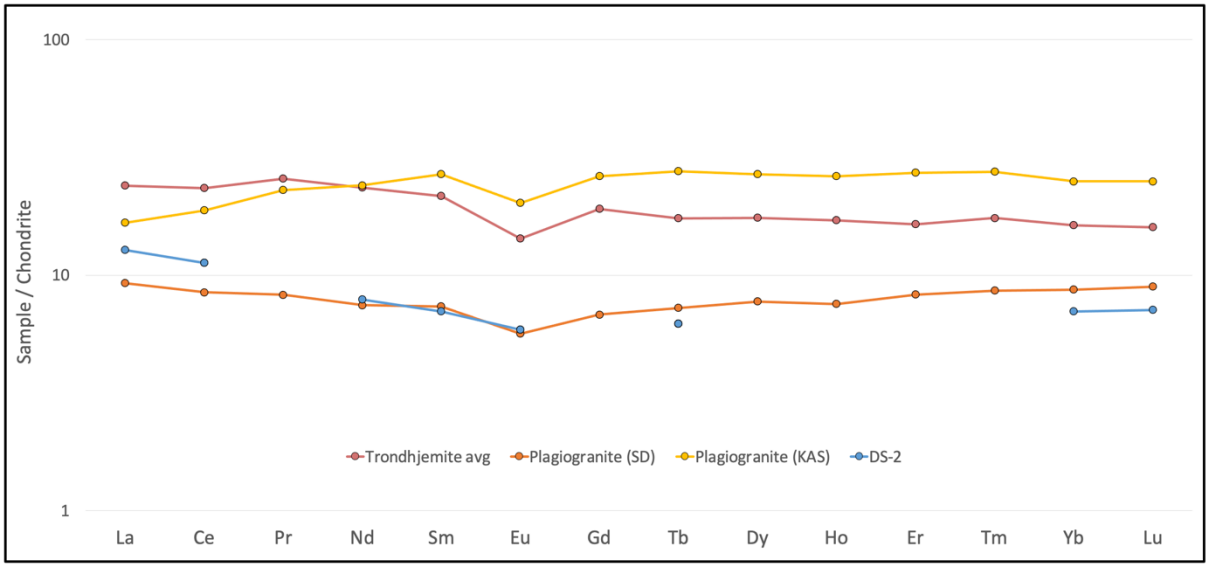

Figure 5.6. All trondhjemite samples averaged compared to similar plutonics in the Karmøy Ophiolite Complex. SD = Sauøy Diorite. KAS = Karmøy Axis Sequence. DS-2 = Duøy dike swarm. Data for SD, KAS and DS-2 from Pedersen and Hertogen (1990).

In summary, magmatic evolution of the Lykling and the Karmøy Ophiolite Complexes exhibits very much the same characteristics. The complexes evolved from IAT basaltic magmas that evolved to plagiogranite and trondhjemite complexes that have been dated to 493 + 7/- 4 and 484 ± 6 Ma. These were intruded by S-type granitic rocks that mark an arc-continent collisional event at around 475 Ma (e.g. Pedersen et al. 1992, Slotnes, 2021), and was followed by orogenic collapse and renewed extensional arc-magmatism represented by the calc-alkaline and high-K calc-alkaline like magmas of the Siggjo Complex, Vardafjell Gabbro and Feøy Gabbros (473 ± 2 Ma, 472 ± 2 and 470 + 9/- 4 Ma respectively).

5.4 Crustal thicknesses of the early arc system

Formation and evolution of island arc systems, as well as arc-continent collisions, is the single most important process for continental crust formation (Roberts et al., 2015). Initial crustal growth is determined by island arc build-up from oceanic crust. During island arc build-up the initial basaltic crust differentiates into intermediate crust, and further into a felsic crust with components of higher SiO_2 contents as the arc matures (Takahashi et al., 2007). The wide applicability of the mineral zircon makes it extremely useful in deciphering these systems, and

act as an important source for information surrounding continental crust evolution (Roberts & Spencer, 2015).

As a means of determining crustal thickness Tang et al. (2021) proposed that zircon Eu/Eu* anomalies can be used to infer crustal thickness. The rationale behind the calculation of crustal thickness from europium (Eu) anomaly lies in Eu behavior within the zircon lattice and melt. Eu/Eu* (Eu normalized to chondrite / $\sqrt{Sm\ x\ Gd}$) in zircon reflects the degree of plagioclase fractionation. Eu exists as both Eu^{2+} and Eu^{3+} in most magmatic systems and plagioclase strongly favors Eu^{2+} in its crystal lattice. Eu^{3+} is preferred in the zircon lattice. When plagioclase fractionates Eu (Eu^{2+}/Eu^{3+}) is depleted relative to neighboring Sm and Gd and this ratio infers crustal thickness from how much plagioclase is fractionated. Shallow crusts will have abundant plagioclase fractionations (low Eu/Eu*) and deep crustal thickenings will start fractionating garnet instead (high Eu/Eu*) (Tang et al., 2021).
This study attempts to apply this method to reconstruct the crustal thickness of the ancient cambro-ordovician arc represented by the Lykling Ophiolite Complex and the Geitung Unit. As part of this, rare earth elements were analyzed on zircon grains from one trondhjemite sample (484 ± 6 Ma, Figure 4.36), and from a siltstone from the Geitung Unit (494 ± 2 Ma). The equation used to calculate crustal thickness was formulated by Tang et al. (2021):

$z = (84.2 \pm 9.2)\ x\ Eu/Eu^*_{zircon} + (24.5 \pm 3.3)$, where z is crustal thickness in km.

Eu/Eu* averages for the selected samples are 0.31 (20BOM-11, trondhjemite) and 0.5 (16BOM-53, siltstone), yielding crustal thicknesses of 51 km and 66 km respectively (Figure 5.7).

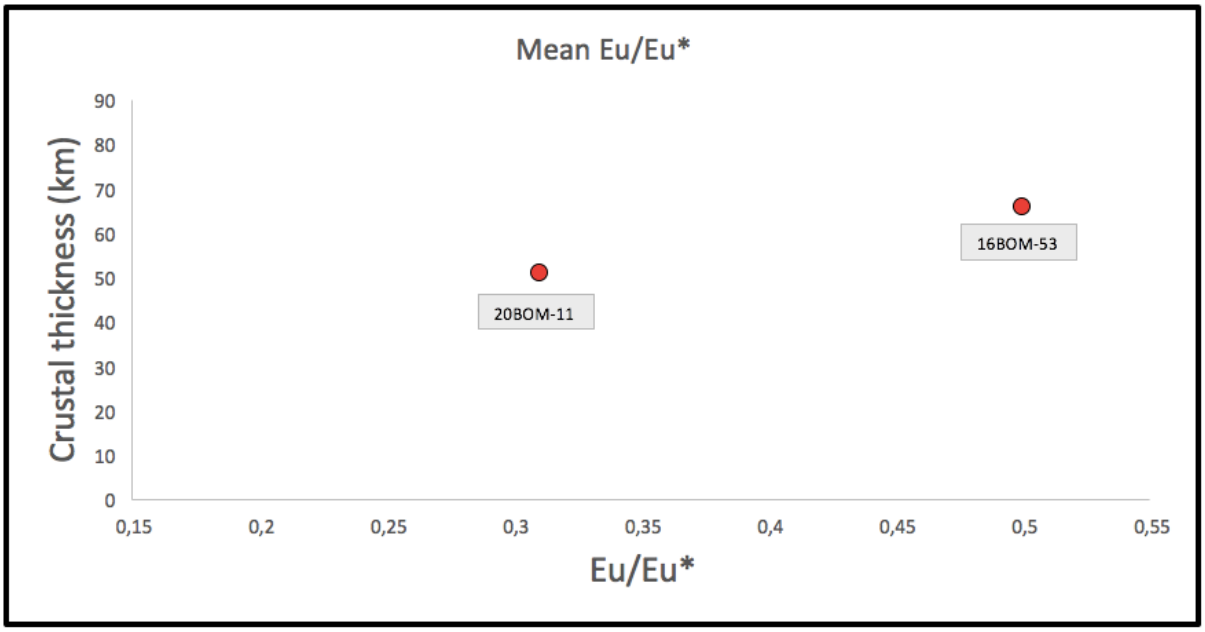

Figure 5.7. Mean Eu/Eu* values for samples 20BOM-11 (trondhjemite) and 16BOM-53 (siltstone) vs. Crustal thickness (in km).

The calculated crustal thicknesses of 51 km and 66 km seem unlikely large for a primitive island arc system that these rocks represent. To verify these thicknesses is difficult, but modern day equivalents, such as the Mariana Arc in the western Pacific, may be an appropriate system to compare them to. The Mariana Arc is a relatively young arc system (approx. 40-50 My) (Takahashi et al., 2007), and is considered a prime example of intra-oceanic island arc system where crustal anataxis, assimilation and continental contamination is non-existent (Woodhead, 1989). Takahashi et al. (2018) created velocity models of the Mariana Arc back-arc system, and revealed that 50 million years of arc magmatism in this setting have resulted in the formation of a 20 km thick crust (Figure 5.8). This vastly diverge from the 50-60 km thickness of the relatively immature ancient arc crust indicated by this study.

The method used to reconstruct the arc crust in this thesis is new and may therefore still be imprecise. It should also be noted that Tang et al. (2021) based their study on the analyses of detrital zircons from the Gangdese belt, southern Tibet, involving the Eurasia-India collision, and not pre-collision island arc systems.

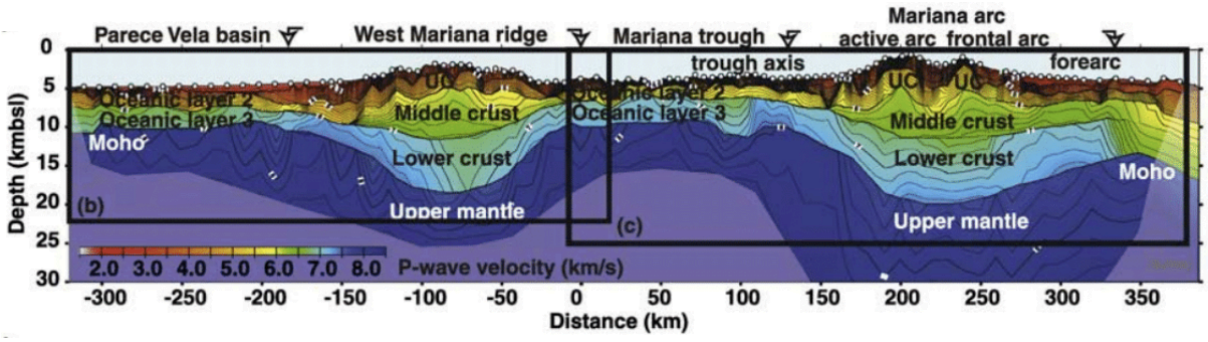

Figure 5.8. Cross-section of the Mariana Arc back-arc system from Parece Vela Basin through West Mariana ridge and Mariana through to the fore-arc of the Mariana Arc. This figure shows crustal thicknesses of a modern immature island arc system in the western Pacific where crustal thicknesses only reach approximately 20 km deep. Figure from Takahashi et al. (2018).

5.5 Tectonic environment and evolutionary history of the arc system

Based on results revealed in this thesis together with previous studies and known history of the geology of Bømlo we can reproduce an evolutionary history for the granitic intrusions and associated lithologies in the Bømlo and larger Sunnhordland area. The ophiolitic terrane that can be studied today on Bømlo, Karmøy and Gullfjellet began forming in the ancient paleo ocean of the Iapetus Ocean, the body of water in between the continents of Laurentia and Baltica. Concurrent with formation of this oceanic crust basaltic dikes intruded the gabbros of the complex. An immature island arc begins to build up around 494 Ma which is evident in the dacitic extrusives of the Geitung Unit overlying the ophiolite complex. Plutonic variations of these (trondhjemites and tonalites) intrude the arc system with a presumed minimum age of 484 ± 6 Ma. It is suggested in this thesis that crustal thicknesses for this arc reached approximately 50 km, but this is highly uncertain and may be due to methodical problems and assumptions. Two slight variations in the geochemistry of the Geitung Unit dacites, where the dacites on the island of Geitung show more developed arc signatures than their Finnås/Lykling counterparts (section 5.1) may reflect parts of the transition from immature to a more mature island arc. The island arc build-up continued for 20 My when arc-continent collision occurred (Pedersen et al. 1992; Pedersen & Dunning, 1997, Hamnes, 1998, Fonneland, 2002, Slotnes 2021) and later intruding bodies on Bømlo (the Siggjo Complex, the Vikafjord Group basalts and the youngest basalt dikes on Lykling) seem all to have formed after the arc-continent collision. This post orogenic phase involved orogenic collapse and extension with sub-aerial continental extensional type volcanism, renewed granitic magmatism and the development of a new marginal basin (Pedersen et al. in prep).

6. Concluding remarks

The present study shed light on the trondhjemitic and tonalitic intrusions associated with the Lykling Ophiolite Complex on Bømlo in SW Norway, as well as other lithological units in the Early Ordovician ophiolitic terrane. From this study, the following conclusions can be made:

- A mean age of three trondhjemite intrusions of the Lykling Ophiolite Complex yielded a U/Pb age of 484 ± 6 Ma. This age is in accordance with and can be correlated to similar plutonics dated in the Karmøy and Gullfjellet ophiolite complexes. All three complexes show geochemical similarities and the previous assumption that all belong to the same ophiolitic terrane and share a common history is further supported in this thesis.
- Trondhjemite and tonalite intrusions exhibit similar geochemical characteristics as the dacites of the Geitung Unit. It is proposed that both lithologies are sourced from the same magmatic event and that they are the intrusive and extrusive parts of the same magmatic system.
- Both trondhjemites and Geitung Unit dacites exhibit clear genetic relations with ophiolite gabbro indicating that they are differentiates of the residual melt after gabbro crystallization. This is supported by whole rock geochemistry, as well as zircon rare earth element analyses. This assumption is consistent with the development of time-equivalent plagiogranites found on Karmøy and Gullfjellet.
- The dacites of the Geitung Unit are separated into two groups based on their geochemical variations. The previously suggested immature island arc development setting for the Geitung Unit is supported in this thesis. However, dacites sampled on the island of Geitung suggests that this unit may represent a slightly more evolved magma as well.
- An older generation of basaltic dikes intrude the Lykling Ophiolite Complex. Trace- and rare earth element patterns indicate that these intrusions are concurrent with the development of the ophiolite complex.
- Crustal thicknesses were calculated for two different island arc rocks revealing crustal thicknesses of 51 km and 66 km. This thickness is highly unlikely to be the real thickness of the island arc, as a modern-day equivalent, the Mariana Arc, points to much thinner thicknesses in primitive island arcs. Our method of calculating thicknesses is

relatively recent and may be imprecise and faulty when applied to other settings than was used in the original case study.

7. Future work

It has been unveiled in this thesis that the Geitung Unit possibly represent parts of the transition phase from immature arc build up to mature island arc. Dacitic rocks on the island of Geitung show more developed geochemical signatures, and have been U/Pb dated to 494 ± 2 Ma. Their Finnås/Lykling counterparts have been correlated with the Geitung dacites, and therefore assumed the same age. It would be interesting to find out more whether these two groups exhibit sufficient differences in both geochemistry and geochronology, to assume they represent different stages of island arc build up.

Crustal thickness findings presented in this thesis seem unlikely high for primitive island arcs. It could be, however, that the method used to reconstruct these thicknesses is faulty with respect to this type of system, or the analyses carried out by this study are poorly executed. It could be interesting with a more in-depth look at crustal reconstructions of the Early Ordovician ophiolitc terrane, and compare them to modern-day equivalent arcs (e.g. the Mariana Arc).

References

Amaliksen, K. (1983) The geology of the Lykling Ophiolitic Complex, Bømlo, SW Norway Unpubl. Cand. Real. thesis, University of Bergen, Norway.

Andersen, T. B. & Jansen, Ø. J. (1987). The Sunnhordland Batholith, W. Norway: regional setting and internal structure, with emphasis on the granitoid plutons. *Norsk geologisk tidsskrift, 67*(3), 159-183.

Andersen, T. & Andresen, A. (1994). Stratigraphy, tectonostratigraphy and the accretion of outboard terranes in the Caledonides of Sunnhordland, W. Norway. *Tectonophysics, 231*(1-3), 71-84.

Andersen, T. B. (1998). Extensional tectonics in the Caledonides of southern Norway, an overview. *Tectonophysics, 285*(3-4), 333-351.

Belousova, E. A., Griffin, W. L., O'Reilly, S. Y., & Fisher, N. L. (2002). Igneous zircon: trace element composition as an indicator of source rock type. *Contributions to mineralogy and petrology*, *143*(5), 602-622.

Brekke, H., Furnes, H., Nordås, J. & Hertogen, J. (1984). Lower Palaeozoic convergent plate margin volcanism on Bømlo, SW Norway, and its bearing on the tectonic environments of the Norwegian Caledonides. *Journal of the Geological Society, 141*(6), 1015-1032.

Chew, D. M., Petrus, J. A., & Kamber, B. S. (2014). U–Pb LA–ICPMS dating using accessory mineral standards with variable common Pb. *Chemical Geology*, *363*, 185-199.

Coleman, R. G., & Peterman, Z. E. (1975). Oceanic plagiogranite. *Journal of Geophysical Research*, *80*(8), 1099-1108.

Coleman, R. G., & Donato, M. M. (1979). Oceanic plagiogranite revisited. In *Developments in petrology* (Vol. 6, pp. 149-168). Elsevier.

Corfu, F., Roberts, R. J., Torsvik, T. H., Ashwal, L. D. & Ramsay, D. M. (2007). Peri-Gondwanan elements in the Caledonian Nappes of Finnmark, Northern Norway: Implications for the paleogeographic framework of the Scandinavian Caledonides. *American Journal of Science, 307*(2), 434-458. doi:10.2475/02.2007.05

Corfu, F., & Roffeis, C. (2012). The Jotun and related nappe complexes, southern Norway. *Paper presented at the EGU General Assembly Conference Abstracts*.

Corfu, F., Gasser, D. & Chew, D. M. (2014). New perspectives on the Caledonides of Scandinavia and related areas: introduction. *Geological Society, London, Special Publications, 390*(1), 1-8.

Corfu, F., Andersen, T. & Gasser, D. (2014). The Scandinavian Caledonides: main features, conceptual advances and critical questions. *Geological Society, London, Special Publications, 390*(1), 9-43.

Dunning, G. & Pedersen, R. (1988). U/Pb ages of ophiolites and arc-related plutons of the Norwegian Caledonides: implications for the development of Iapetus. *Contributions to Mineralogy and Petrology, 98*(1), 13-23.

Ewart, Anthony. (1982). "The mineralogy and petrology of Tertiary-Recent orogenic volcanic rocks: with special reference to the andesitic-basaltic compositional range." *Andesites: Orogenic Andesites and Related Rocks* 7, 25-98

Fossen, H. (1992). The role of extensional tectonics in the Caledonides of south Norway. *Journal of structural geology, 14*(8-9), 1033-1046.

Fossen, H. & Hurich, C. A. (2005). The Hardangerfjord Shear Zone in SW Norway and the North Sea: a large-scale low-angle shear zone in the Caledonian crust. *Journal of the Geological Society, 162*(4), 675-687.

Furnes, H. & Lippard, S. J. (1979). On the significance of Caledonian pahoehoe, aa, and pillow lava from Bømlo, SW Norway. *Norsk geol. Tidsskr, 59*, 107-114.

Furnes, H. (1980). Ophiolite fragments in the Scandinavian Caledonides.

Furnes, H., Thon, A., Nordås, J. & Garmann, L. B. (1982). Geochemistry of Caledonian metabasalts from some Norwegian ophiolite fragments. *Contributions to Mineralogy and Petrology, 79*(3), 295-307.

Furnes, H. (1985). Geological and geochemical classification of the ophiolitic fragments in the Scandinavian Caledonides. *The Caledonide Orogen: Scandinavia and Related Areas*, 657-669.

Furnes, H., Brekke, H., Nordås, J. & Hertogen, J. (1986). Lower Palaeozoic convergent plate margin volcanism on Bømlo, southwest Norwegian Caledonides: geochemistry and petrogenesis. *Geological magazine, 123*(2), 123-142.

Furnes, H., Skjerlie, K., Pedersen, R., Andersen, T., Stillman, C. J., Suthren, R. & Garmann, L. (1990). The Solund–Stavfjord Ophiolite Complex and associated rocks, west Norwegian Caledonides: geology, geochemistry and tectonic environment. *Geological magazine, 127*(3), 209-224.

Fonneland, H. C. (2002). Radiogenic isotope systematics of clastic sedimentary rocks-with emphasis on detrital zircon geochronology. PhD Thesis, University of Bergen, Norway

Gee, D., Kumpulainen, R., Roberts, D., Stephens, M., Thon, A., & Zachrisson, E. (1985). Tectonostratigraphic Map, Scale 1: 2 000 000. In: John Wiley & Sons Chichester.

Gee, D. G., Janák, M., Majka, J., Robinson, P., & van Roermund, H. (2013). Subduction along and within the Baltoscandian margin during closing of the Iapetus Ocean and Baltica-Laurentia collision. *Lithosphere*, *5*(2), 169-178.

Griffin, W. L. (1985). High-pressure metamorphism in the Scandinavian Caledonides. *The Caledonide Orogens. Scandinavian and Related Areas*, 783-801.

Hamnes, G.M., 1998, Petrografi, Geokjemi og Petrogenese til Vest-Karmøy Intrusiv Kompleks [Cand. Scient. thesis]: Bergen, Norway, University of Bergen, 126 p.

Hastie, A. R., Kerr, A. C., Pearce, J. A., & Mitchell, S. F. (2007). Classification of altered volcanic island arc rocks using immobile trace elements: development of the Th–Co discrimination diagram. *Journal of petrology*, *48*(12), 2341-2357.

Hickey, R. L., & Frey, F. A. (1982). Geochemical characteristics of boninite series volcanics: implications for their source. *Geochimica et Cosmochimica Acta*, *46*(11), 2099-2115.

Hollocher, K., Robinson, P., Walsh, E., & Roberts, D. (2012). Geochemistry of amphibolite-facies volcanics and gabbros of the Støren Nappe in extensions west and southwest of Trondheim, Western Gneiss Region, Norway: a key to correlations and paleotectonic settings. *American Journal of Science*, *312*(4), 357-416.

Horstwood, M. S., Košler, J., Gehrels, G., Jackson, S. E., McLean, N. M., Paton, C., ... & Schoene, B. (2016). Community-derived standards for LA-ICP-MS U-(Th-) Pb geochronology–Uncertainty propagation, age interpretation and data reporting. *Geostandards and Geoanalytical Research*, *40*(3), 311-332.

Hoskin, P. W. (2005). Trace-element composition of hydrothermal zircon and the alteration of Hadean zircon from the Jack Hills, Australia. *Geochimica et cosmochimica acta*, *69*(3), 637-648.

Hossack, J., & Cooper, M. (1986). Collision tectonics in the Scandinavian Caledonides. *Geological Society, London, Special Publications, 19*(1), 285-304.

Ingdahl, S. E. (1989). The Upper Ordovician-Lower Silurian rocks in the Os area, Major Bergen Arc, Western Norway. *Norsk geologisk tidsskrift, 69*(3), 163-175.

Jackson, S. E., Pearson, N. J., Griffin, W. L., & Belousova, E. A. (2004). The application of laser ablation-inductively coupled plasma-mass spectrometry to in situ U–Pb zircon geochronology. *Chemical geology*, *211*(1-2), 47-69.

Long, X., Sun, M., Yuan, C., Kröner, A., & Hu, A. (2012). Zircon REE patterns and geochemical characteristics of Paleoproterozoic anatectic granite in the northern Tarim Craton, NW China: implications for the reconstruction of the Columbia supercontinent. *Precambrian Research*, *222*, 474-487.

Ludwig, K. R. (1994). Isoplot—A plotting and regression program for radiogenic-isotope data, US Geol. *Survey, Open-file Report*, 91-445.

Middlemost, E. A. (1994). Naming materials in the magma/igneous rock system. *Earth-science reviews*, *37*(3-4), 215-224.

Morad, S., El-Ghali, M. A. K., Caja, M. A., Sirat, M., Al-Ramadan, K., & Mansurbeg, H. (2010). Hydrothermal alteration of plagioclase in granitic rocks from Proterozoic basement of SE Sweden. *Geological Journal*, *45*(1), 105-116.

Nordås, J., Amaliksen, K., Brekke, H., Suthern, R., Furnes, H., Sturt, B. & Gee, D. (1985). Lithostratigraphy and petrochemistry of Caledonian rocks on Bømlo, SW Norway. *The Caledonide Orogen—Scandinavia and Related Areas: New York, John Wiley & Sons Ltd*, 679-692.

O'connor, J. T. (1965). A classification for quartz-rich igneous rocks based on feldspar ratios. *US geological survey professional paper B*, *525*, 79-84.

Paton, C., Hellstrom, J., Paul, B., Woodhead, J., & Hergt, J. (2011). Iolite: Freeware for the visualisation and processing of mass spectrometric data. *Journal of Analytical Atomic Spectrometry*, *26*(12), 2508-2518.

Pearce, J. A., Harris, N. B., & Tindle, A. G. (1984). Trace element discrimination diagrams for the tectonic interpretation of granitic rocks. *Journal of petrology*, *25*(4), 956-983.

Pearce, J. A., van der Laan, S. R., Arculus, R. J., Murton, B. J., Ishii, T., Peate, D. W., & Parkinson, I. J. (1992, December). Boninite and harzburgite from Leg 125 (Bonin-Mariana forearc): A case study of magma genesis during the initial stages of subduction. In *Proceedings of the ocean drilling program, scientific results* (Vol. 125, pp. 623-659). Ocean Drilling Program, College Station, TX.

Pedersen, R. B., & Malpas, J. (1984). The origin of oceanic plagiogranites from the Karmoy ophiolite, western Norway. *Contributions to Mineralogy and Petrology*, *88*(1-2), 36-52.

Pedersen, R.-F., Furnes, H., & Dunning, G. (1988). Some Norwegian ophiolite complexes reconsidered.

Pedersen, R. B., & Hertogen, J. (1990). Magmatic evolution of the Karmøy Ophiolite Complex, SW Norway: relationships between MORB-IAT-boninitic-calc-alkaline and alkaline magmatism. *Contributions to Mineralogy and Petrology, 104*(3), 277-293.

Pedersen, R., Bruton, D., & Furnes, H. (1992). Ordovician faunas, island arcs and ophiolites in the Scandinavian Caledonides. *Terra Nova, 4*(2), 217-222.

Pedersen, R. B., & Dunning, G. R. (1997). Evolution of arc crust and relations between contrasting sources: U-Pb (age), Nd and Sr isotope systematics of the ophiolitic terrain of SW Norway. *Contributions to Mineralogy and Petrology, 128*(1), 1-15.

Roberts, D., & Gee, D. G. (1985). An introduction to the structure of the Scandinavian Caledonides. *The Caledonide orogen–Scandinavia and related areas, 1*, 55-68.

Roberts, D., Melezhik, V., & Heldal, T. (2002). Carbonate formations and early NW-directed thrusting in the highest allochthons of the Norwegian Caledonides: evidence of a Laurentian ancestry. *Journal of the Geological Society, 159*(2), 117-120.

Roberts, D. (2003). The Scandinavian Caledonides: event chronology, palaeogeographic settings and likely, modern analogues. *Tectonophysics, 365*(1-4), 283-299. doi:10.1016/S0040-1951(03)00026-X

Roberts, N. M., & Spencer, C. J. (2015). The zircon archive of continent formation through time. *Geological Society, London, Special Publications*, *389*(1), 197-225.

Roberts, N. M., van Kranendonk, M. J., Parman, S., Clift, P. D. (2015). Continent formation through time. *Geological Society, London, Special Publication, 389*, 1-16.

Scheiber, T., Viola, G., Wilkinson, C. M., Ganerød, M., Skår, Ø. And Gasser, D. (2016). "Direct 40Ar/39Ar dating of Late Ordovician and Silurian brittle faulting in the southwestern Norwegian Caledonides." *Terra Nova 28*(5): 374-382.

Sivertsen, J. (1992). Stratigraphy and geochemistry of the extrusives of the Torvastad Group; marginal basin deposits associated with the Karmøy ophiolite complex, SW Norway. Cand. Scient, Thesis, Geologisk Institutt, Department A, University of Bergen.

Sláma, J., Košler, J., Condon, D. J., Crowley, J. L., Gerdes, A., Hanchar, J. M., ... & Whitehouse, M. J. (2008). Plešovice zircon—a new natural reference material for U–Pb and Hf isotopic microanalysis. *Chemical Geology*, *249*(1-2), 1-35.

Slama, J., & Pedersen, R. B. (2015). Zircon provenance of SW Caledonian phyllites reveals a distant Timanian sediment source. *Journal of the Geological Society, 172*(4), 465-478.

Slotnes, M. S. (2021). Detrital zircon provenance of the Bremnes Migmatite Complex on Bømlo, SW Norway. Master thesis. University of Bergen, Bergen, Norway.

Stephens, M., Furnes, H., Robins, B., & Sturt, B. (1985). Igneous activity within the Scandinavian Caledonides. *The Caledonide orogen—Scandinavia and related areas, 2*, 623-656.

Stephens, M. B., & Gee, D. G. (1989). Terranes and polyphase accretionary history in the Scandinavian Caledonides. *Geological Society of America, Special Paper, 230*, 17-30.

Stubseid, H. H. (2017). Geological evolution and stratigraphic relationships of the ophiolitic terrane in the outer Hardangerfjord area: evidence from geochronology and geochemistry, The University of Bergen.

Sturt, B. A., & Thon, A. (1978). Caledonides of southern Norway. *Caledonian- Appalachian orogen of the North Atlantic region, IGCP project, 27*, 39-47.

Sun, S. S., & McDonough, W. F. (1989). Chemical and isotopic systematics of oceanic basalts: implications for mantle composition and processes. *Geological Society, London, Special Publications*, *42*(1), 313-345.

Takahashi, N., Kodaira, S., Klemperer, S. L., Tatsumi, Y., Kaneda, Y., & Suyehiro, K. (2007). Crustal structure and evolution of the Mariana intra-oceanic island arc. *Geology*, *35*(3), 203-206.

Tang, M., Ji, W. Q., Chu, X., Wu, A., & Chen, C. (2021). Reconstructing crustal thickness evolution from europium anomalies in detrital zircons. *Geology*, *49*(1), 76-80.

Vermeesch, P. (2018). IsoplotR: A free and open toolbox for geochronology. *Geoscience Frontiers*, *9*(5), 1479-1493.

Viken, A. L., Vaagan, S., Vea, J. A., Larsen, T. N., Jiang, Y., Helgerud, H., ... & Broese van Groenou, Y. A. (2017). Accretionary history of Lower Ordovician island arc complexes on Bømlo: evidence from detrital zircon dating and geochemical data. *Master's thesis, University of Bergen, Bergen, Norway*.

Whitehouse, M. J. (2003). Rare earth elements in zircon: a review of applications and case studies from the Outer Hebridean Lewisian Complex, NW Scotland. *Geological Society, London, Special Publications*, *220*(1), 49-64.

Wiedenbeck, M., Corfu, F., Griffin, W. L., Meier, M., Oberli., F., von Quadt, A., Roddick, J. C. And Spiegel, W. (1995). Three natural zircon standards for U-Th-Pb, Lu-Hf, trace element and REE analyses, *Geostandards Newsletter, 19*(1), pp. 1-23.

Woodhead, J. D. (1989). Geochemistry of the Mariana arc (western Pacific): source composition and processes. *Chemical Geology*, *76*(1-2), 1-24.

Online resources:

NGU, 2021, Berggrunnskart N250, Bømlo: https://geo.ngu.no/kart/berggrunn_mobil/ (accessed: 24.09.2021)

Appendices

Appendix 1 – Sample descriptions and sample locations

Appendix 2 – Major- and trace element data

Appendix 3 – Geochronology data (LA-ICP-MS)

Appendix 1 – Sample descriptions and sample locations

Sample	Locality	Locality description	Coordinates	Lithostratigraphic Unit	Lithology
20BOM-1	Lykling	Relatively dark trondhjemite sampled south on Lykling in a mound of blocks from a landslide	59° 42' 6.81" N 005° 10' 30.21" E	Granitic intrusion	Trondhjemite
20BOM-2		Relatively dark trondhjemite sampled south on Lykling in a mound of blocks from a landslide	59° 42' 6.81" N 005° 10' 30.21" E	Granitic intrusion	Trondhjemite
20BOM-4		Quarry outcrop	59° 43' 1.05" N 005° 10' 24.79" E	Granitic intrusion	Trondhjemite
20BOM-6		Coastal outcrop close to Gullvegen. Central Lykling	59° 43' 4.84" N 005° 10' 15.61" E	Granitic intrusion	Trondhjemite
20BOM-7		Sampled in central Lykling along a hiking path.	59° 43' 12.37" N 005° 11' 46.39" E	Granitic intrusion	Trondhjemite
20BOM-15B		Roadcut along Gullvegen north on Lykling. Minor pyrite mineralization	59° 44' 11.21" N 005° 12' 33.47" E	Granitic intrusion	Trondhjemite
20BOM-22A		Coastal outcrop with basalt dike oriented N-S. Intrudes gabbro. Central Lykling close to Risvika	59° 43' 1.34" N 005° 10' 9.79" E	Dike intrusion	Basalt
20BOM-22B		Coastal outcrop with basalt dike oriented NE-SW. Intrudes gabbro. Central Lykling close to Risvika	59° 43' 0.89" N 005° 10' 8.83" E	Dike intrusion	Basalt
20BOM-23B		Coastal outcrop between Risvika and Tverrborgvika. Sampled close to ophiolite gabbro	59° 43' 7.86" N 005° 10' 20.96" E	Granitic intrusion	Trondhjemite
20BOM-27C		Coastal outcrop south on Lykling. Sampled in the contact with ophiolite gabbro	59° 42' 14.02" N 005° 09' 51.98" E	Granitic intrusion	Trondhjemite
20BOM-27D		Coastal outcrop south on Lykling. Sampled in the contact with trondhjemite intrusion	59° 42' 14.02" N 005° 09' 51.98" E	Lykling Ophiolite Complex	Gabbro
20BOM-9A	*Nymark*	Roadcut along Gullvegen on central Lykling.	59° 42' 28.28" N 005° 10' 25.11" E	Granitic intrusion	Trondhjemite
20BOM-9C		Roadcut along Gullvegen on central Lykling. Sampled close to contact with trondhjemite intrusion	59° 42' 28.28" N 005° 10' 25.11" E	Lykling Ophiolite Complex	Monzodiorite
20BOM-9E		Roadcut along Gullvegen on central Lykling. Sampled close to contact with trondhjemite intrusion	59° 42' 28.28" N 005° 10' 25.11" E	Lykling Ophiolite Complex	Gabbro

20BOM-11	*Øvre-Tverrborgvik*	Roadcut along Gullvegen south of Tverrborgvika.	59° 43' 8.34" N 005° 10' 39.03" E	Granitic intrusion	Trondhjemite
20BOM-10		Roadcut along Gullvegen south of Tverrborgvika.	59° 43' 7.39" N 005° 10' 37.08" E	Lykling Ophiolite Complex	Gabbro
20BOM-26A		Folded dike intruding gabbro. Roadcut along Gullvegen south of Tverrborgvika	59° 43' 13.55" N 005° 10' 49.56" E	Dike intrusion	Basalt
20BOM-12A	*Hellevika*	Coastal outcrop north of Hellevika. Several basalt dikes intrude the area.	59° 43' 37.57 N 005° 11' 1.40" E	Granitic intrusion	Trondhjemite
20BOM-13A		Big dike intruding trondhjemite north of Hellevika	59° 43' 37.57 N 005° 11' 1.40" E	Dike intrusion	Basalt
20BOM-24A		Coastal outcrop south of Hellevika. Intrudes trondhjemite	59° 43' 27.40" N 005° 10' 41.49" E	Dike intrusion	Basalt
20BOM-24B		Coastal outcrop south of Hellevika. Intrudes trondhjemite	59° 43' 29.41" N 005° 10' 35.99" E	Dike intrusion	Basalt
20BOM-24C		Coastal outcrop south of Hellevika. Deformed basalt.	59° 43' 29.41" N 005° 10' 35.99" E	Dike intrusion	Basalt
20BOM-8	Lindøya	Coastal outcrop close to the pier on Lindøya	59° 45' 17.68" N 005° 13' 28.83" E	Granitic intrusion	Trondhjemite
20BOM-19	Gjerdavåg-en	Roadcut outcrop along Sakseidvegen south of Erslandsvatnet	59° 45' 41.48" N 005° 14' 59.79" E	Geitung Unit (volcanosedimentary unit)	Dacite
20BOM-21D		Pocket of gabbro in the roadcut outcrop along Sakseidvegen north of Gjerdavågen	59° 45' 47.56" N 005° 14' 9.20" E	Lykling Ophiolite Complex	Gabbro
20BOM-21E		Roadcut outcrop close to Sakseidvegen north of Gjerdavågen	59° 45' 47.56" N 005° 14' 9.20" E	Granitic intrusion	Trondhjemite
20BOM-21F		Roadcut outcrop close to Sakseidvegen north of Gjerdavågen	59° 45' 47.56" N 005° 14' 9.20" E	Granitic intrusion	Trondhjemite
20BOM-20A	Ådnanes	Roadcut outcrop south of Sakseidvegen located between Pøyla and Straumsvika	59° 45' 37.28" N 005° 12' 15.20" E	Granitic intrusion	Tonalite
20BOM-20B		Roadcut outcrop south of Sakseidvegen located between Pøyla and Straumsvika	59° 45' 37.28" N 005° 12' 15.20" E	Lykling Ophiolite Complex	Gabbro
20BOM-25		Roadcut outcrop along Giljevegen	59° 46' 27.77" N 005° 12' 11.35" E	Vardafjellgabbro (Sunnhordland Batholith)	Gabbro
20BOM-17A	Finnås	Roadcut outcrop along Bømlavegen west of Hidletjørna	59° 43' 53.90" N 005° 14' 19.10" E	Geitung Unit (volcanosedimentary unit)	Rhyolite
20BOM-18		Roadcut outcrop along Finnåsvegen north of Finnåsvika	59° 44' 52.08" N 005° 15' 17.28" E	Geitung Unit (volcanosedimentary unit)	Basaltic andesite
20FINNÅS-1		Coastal outcrop in Finnåsvika	59° 44' 34.90" N 005° 15' 18.70" E	Geitung Unit (volcanosedimentary unit)	Dacite

20FINNÅS-2		Coastal outcrop in Finnåsvika	59° 44' 39.88" N 005° 15' 7.32" E	Geitung Unit (volcanosedimentary unit)	Dacite
20GEIT-1	Geitung	Outcrop along a path. In contact with andesite	59° 41' 28.78" N 005° 07' 41.54" E	Geitung Unit (volcanosedimentary unit)	Rhyolite
20GEIT-2		Outcrop along a path. In contact with Rhyolite	59° 41' 28.78" N 005° 07' 41.54" E	Geitung Unit (volcanosedimentary unit)	Andesite
20GEIT-4		Coastal outcrop south on the Island of Geitung	59° 41' 21.27" N 005° 07' 46.48" E	Geitung Unit (volcanosedimentary unit)	Dacite
20GEIT-5		Coastal outcrop south on the Island of Geitung	59° 41' 21.27" N 005° 07' 46.48" E	Geitung Unit (volcanosedimentary unit)	Dacite
20GEIT-6		Coastal outcrop south on the Island of Geitung	59° 41' 21.16" N 005° 07' 51.09" E	Geitung Unit (volcanosedimentary unit)	Dacite

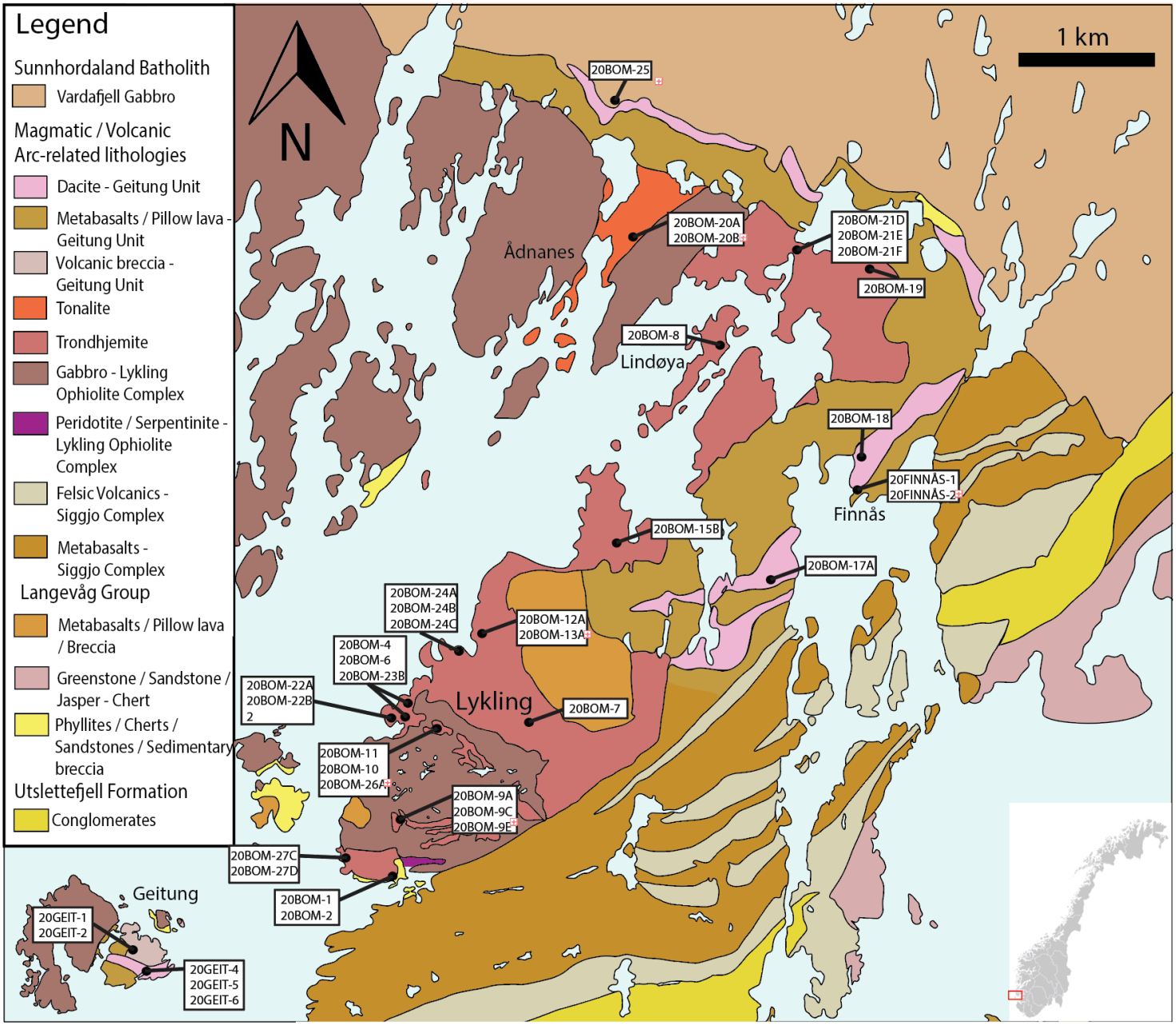
Legend
Sunnhordaland Batholith
Vardafjell Gabbro
Magmatic / Volcanic Arc-related lithologies
Dacite - Geitung Unit
Metabasalts / Pillow lava - Geitung Unit
Volcanic breccia - Geitung Unit
Tonalite
Trondhjemite
Gabbro - Lykling Ophiolite Complex
Peridotite / Serpentinite - Lykling Ophiolite Complex
Felsic Volcanics - Siggjo Complex
Metabasalts - Siggjo Complex
Langevåg Group
Metabasalts / Pillow lava / Breccia
Greenstone / Sandstone / Jasper - Chert
Phyllites / Cherts / Sandstones / Sedimentary breccia
Utslettefjell Formation
Conglomerates
N
1 km
Ådnanes
Lindøya
Finnås
Lykling
Geitung
20BOM-25
20BOM-20A
20BOM-20B
20BOM-21D
20BOM-21E
20BOM-21F
20BOM-19
20BOM-8
20BOM-18
20FINNÅS-1
20FINNÅS-2
20BOM-15B
20BOM-17A
20BOM-24A
20BOM-24B
20BOM-24C
20BOM-12A
20BOM-13A
20BOM-4
20BOM-6
20BOM-23B
20BOM-22A
20BOM-22B
2
20BOM-7
20BOM-11
20BOM-10
20BOM-26A
20BOM-9A
20BOM-9C
20BOM-9E
20BOM-27C
20BOM-27D
20BOM-1
20BOM-2
20GEIT-1
20GEIT-2
20GEIT-4
20GEIT-5
20GEIT-6

Appendix 2 – Major- and trace element data

Major elements

Sample ID	Na_2O	MgO	Al_2O_3	SiO_2	P_2O_5	K_2O	CaO	TiO_2	MnO	Fe_2O_3	% LOI	SUM
20BOM-1	4.98	0.87	11.84	75.22	0.06	0.17	0.56	0.24	0.10	4.18	1.17	99.38
20BOM-2	5.11	0.91	11.28	76.40	0.06	0.09	0.99	0.24	0.07	2.58	1.47	99.20
20BOM-4	4.75	0.52	12.87	75.04	0.05	0.96	1.14	0.24	0.07	2.76	1.29	99.69
20BOM-6	4.70	0.78	11.62	74.78	0.08	0.33	1.00	0.27	0.08	2.88	0.83	97.36
20BOM-7	5.51	0.60	11.89	77.99	0.06	0.19	0.80	0.22	0.07	1.86	0.76	99.96
20BOM-8	4.86	0.99	11.58	74.28	0.07	0.35	1.32	0.21	0.07	1.93	0.92	96.58
20BOM-9A	5.42	0.48	11.64	79.98	0.06	0.32	0.43	0.18	0.05	1.23	0.45	100.23
20BOM-9C	7.05	2.16	16.78	52.43	0.20	0.15	4.71	0.86	0.13	7.46	3.81	95.74
20BOM-9E	2.19	6.01	12.55	38.29	0.06	0.05	7.60	2.08	0.24	16.27	9.09	94.43
20BOM-10	2.34	9.69	14.60	48.30	0.05	0.34	14.15	0.32	0.14	6.26	2.98	99.19
20BOM-11	5.21	0.37	11.21	73.84	0.06	0.29	1.29	0.20	0.06	2.33	1.06	95.92
20BOM-12A	4.99	0.61	12.35	74.85	0.07	0.94	0.51	0.24	0.06	2.39	0.80	97.81
20BOM-13A	3.32	2.82	13.63	53.30	0.33	1.49	5.66	2.19	0.17	10.26	4.81	97.97
20BOM-15B	5.49	0.54	11.23	73.14	0.07	0.23	1.04	0.23	0.05	1.14	0.89	94.05
20BOM-17A	4.79	0.79	9.92	77.05	0.06	0.38	0.89	0.21	0.05	1.13	0.86	96.14
20BOM-18	3.72	3.78	15.82	54.53	0.08	1.05	7.19	0.37	0.22	8.10	1.38	96.24
20BOM-19	2.85	2.46	11.83	72.21	0.09	0.84	2.45	0.29	0.09	3.04	1.48	97.63

20BOM-20A	2.99	0.79	13.09	70.15	0.09	0.39	4.76	0.46	0.09	5.37	0.96	99.14
20BOM-20B	2.57	6.69	15.39	51.44	0.07	0.64	10.06	0.43	0.17	8.61	1.82	97.89
20BOM-21D	4.03	5.35	14.09	51.78	0.11	0.71	7.10	0.89	0.20	10.03	1.83	96.12
20BOM-21E	5.34	1.13	13.31	69.51	0.10	0.24	2.07	0.44	0.10	4.43	1.00	97.69
20BOM-21F	4.97	0.82	12.78	73.59	0.09	0.39	1.62	0.31	0.08	3.11	0.93	98.69
20BOM-22A	2.23	6.49	14.38	39.17	0.16	0.23	6.18	2.19	0.29	16.75	8.84	96.90
20BOM-22B	2.70	5.81	13.82	46.94	0.10	0.78	7.73	0.70	0.20	9.59	9.07	97.44
20BOM-23B	4.23	1.40	11.12	72.07	0.08	0.32	0.93	0.27	0.09	4.28	1.43	96.23
20BOM-24A	3.04	2.61	12.63	49.90	0.41	1.05	6.11	2.43	0.19	12.87	6.33	97.56
20BOM-24B	3.09	4.57	16.27	48.71	0.43	1.77	8.03	0.92	0.16	9.28	4.63	97.85
20BOM-24C	2.79	7.54	14.42	50.92	0.58	0.21	2.80	1.51	0.16	13.73	4.17	98.83
20BOM-25	1.88	6.93	16.26	48.00	0.15	0.98	12.27	1.03	0.16	8.41	2.04	98.10
20BOM-26A	3.64	4.40	12.77	48.03	0.13	0.39	7.32	1.41	0.18	11.53	7.92	97.72
20BOM-27C	4.83	1.03	11.02	76.40	0.06	0.09	0.88	0.20	0.06	3.38	1.16	99.12
20BOM-27D	1.41	8.50	11.99	40.80	0.07	0.11	10.70	1.72	0.21	19.57	2.63	97.72
20FINNÅS-1	4.06	0.28	7.54	70.88	0.05	0.19	0.44	0.12	0.04	0.62	0.32	84.54
20FINNÅS-2	3.91	0.88	9.49	72.69	0.07	0.14	0.97	0.28	0.08	2.53	1.11	92.16
20GEIT-1	4.63	0.43	9.72	81.71	0.06	0.11	0.52	0.16	0.05	1.51	0.53	99.42
20GEIT-2	1.87	3.52	15.30	57.39	0.06	3.72	0.53	0.25	0.07	5.18	3.36	91.25
20GEIT-4	4.48	0.62	10.91	66.98	0.07	1.98	1.57	0.30	0.07	3.40	0.94	91.33
20GEIT-5	4.97	2.44	12.86	63.59	0.17	1.08	2.15	0.88	0.11	8.69	1.40	98.36

20GEIT-6	3.35	0.53	8.54	65.41	0.06	1.66	1.11	0.21	0.09	2.72	0.77	84.45						

Trace elements

Sample ID	Li	Sc	V	Cr	Co	Ni	Cu	Zn	Rb	Sr	Zr	Nb	Cs	Ba	Hf	Ta	Pb	Th	U
20BOM-1	13.80	6.57	0.270	0.314	0.570	0.401	3.97	24.35	2.91	74.29	12.55	1.85	0.137	30.42	0.473	0.118	1.20	0.415	0.143
20BOM-2	10.19	7.00	0.108	0.244	0.500	0.221	7.03	18.92	1.01	96.49	23.34	1.72	0.105	17.04	0.739	0.120	0.741	0.584	0.120
20BOM-4	4.40	3.70	0.694	<0.12	0.124	<0.25	1.17	38.12	18.20	109.9	7.79	0.744	0.454	103.3	0.404	0.062	2.39	0.227	0.109
20BOM-6	6.32	9.37	13.17	0.787	2.27	0.560	3.06	59.26	3.16	66.08	12.60	1.38	0.157	59.23	0.812	0.097	2.33	0.674	0.270
20BOM-7	4.41	7.32	1.12	0.648	1.19	0.533	2.14	20.03	1.77	90.18	35.95	3.81	0.075	39.61	1.28	0.272	0.918	2.45	0.543
20BOM-8	8.16	5.22	3.63	0.421	1.39	0.350	0.610	23.36	8.13	98.36	39.12	2.87	0.294	90.83	1.68	0.224	3.71	2.18	0.575
20BOM-9A	2.53	3.82	6.00	0.324	1.93	0.291	164.9	9.77	7.45	87.17	4.87	0.159	0.164	50.91	0.306	0.022	68.13	0.078	0.059
20BOM-9C	8.16	15.72	32.04	2.04	9.29	1.43	4.16	65.45	1.95	138.8	7.98	1.18	0.104	49.00	0.327	0.059	4.98	0.038	0.023
20BOM-9E	10.58	50.73	317.4	53.63	44.99	29.32	1.56	105.6	0.430	141.2	6.01	0.182	0.210	9.09	0.243	0.024	2.04	<0.003	0.005
20BOM-10	16.30	71.15	194.5	330.2	36.02	68.24	218.7	30.99	5.99	197.4	4.13	0.027	0.273	40.76	0.214	0.006	1.11	0.018	0.006
20BOM-11	1.18	2.90	2.82	0.646	0.615	0.359	6.21	15.58	2.76	64.42	19.94	2.67	0.091	92.43	1.14	0.207	1.06	1.48	0.409
20BOM-12A	2.73	6.56	4.56	0.515	1.53	0.531	2.57	18.36	14.36	72.51	35.71	3.44	0.251	235.0	1.45	0.245	1.31	2.22	0.66

20BOM-13A	15.27	24.66	229.7	4.04	21.89	2.22	11.35	103.2	48.57	166.2	223.7	22.00	1.36	367.0	6.32	1.54	16.62	11.22	2.68
20BOM-15B	2.64	4.83	2.98	0.523	1.82	0.586	15.57	8.69	3.32	80.26	31.07	2.87	0.136	36.57	1.17	0.220	1.79	1.90	0.437
20BOM-17A	2.12	11.60	8.25	0.539	2.07	2.43	16.68	33.66	2.90	83.51	152.5	2.35	0.077	81.55	4.88	0.213	2.32	2.40	1.16
20BOM-18	10.81	17.35	59.11	5.23	11.37	8.24	0.779	104.7	25.75	217.5	268.3	4.90	0.532	91.46	8.14	0.374	2.81	3.17	1.24
20BOM-19	19.55	5.48	17.61	1.66	3.99	2.02	1.64	36.62	28.10	141.1	35.90	2.17	1.35	162.0	1.22	0.168	2.26	1.47	0.332
20BOM-20A	2.63	6.69	28.94	0.491	4.78	0.541	2.59	45.34	5.79	124.8	2.79	0.325	0.379	31.23	0.158	0.038	0.916	0.18	0.106
20BOM-20B	13.38	34.23	192.7	28.10	36.10	36.27	31.30	60.86	14.42	113.4	14.10	0.273	0.608	41.24	0.601	0.022	1.28	0.087	0.041
20BOM-21D	22.64	32.69	273.5	3.78	35.21	11.47	103.2	124.3	18.06	172.1	29.61	1.29	0.834	139.1	1.50	0.099	2.90	0.719	0.284
20BOM-21E	9.33	10.23	43.60	3.35	6.98	1.77	2.72	49.34	3.49	95.83	48.38	3.27	0.354	49.70	2.55	0.282	1.53	2.20	0.771
20BOM-21F	10.21	7.72	8.81	0.939	2.84	0.697	3.58	36.29	10.24	108.9	38.88	3.22	0.588	70.49	1.42	0.224	1.62	2.21	0.552
20BOM-22A	46.34	49.61	508.7	47.87	45.60	31.10	12.17	246.9	5.80	106.2	64.90	0.920	0.264	28.72	2.07	0.072	3.16	0.210	0.201
20BOM-22B	45.36	34.27	255.5	29.24	31.23	24.38	29.27	96.02	17.08	71.25	36.34	0.414	0.598	89.10	1.23	0.033	1.81	0.222	0.221
20BOM-23B	10.15	11.45	11.85	0.619	2.48	0.482	1.27	97.23	4.91	56.26	7.88	1.83	0.202	46.61	0.535	0.107	1.80	0.497	0.221
20BOM-24A	11.87	24.09	165.2	1.38	25.08	1.36	16.66	144.8	29.79	229.7	300.7	24.40	0.561	350.6	7.89	1.66	16.33	12.63	2.74
20BOM-24B	12.17	19.09	222.4	34.24	26.04	25.73	16.96	75.09	45.78	718.0	90.20	12.20	1.32	487.8	2.51	0.698	12.12	8.31	2.38
20BOM-24C	26.14	37.49	96.84	1.43	21.79	3.31	77.29	96.05	4.43	108.8	102.2	1.53	0.403	41.71	3.01	0.098	4.15	0.648	0.295

20BOM-25	31.65	38.99	200.6	325.9	33.82	22.40	17.31	68.00	44.59	333.8	24.55	5.36	1.15	178.5	0.934	0.361	4.73	0.979	0.228
20BOM-26A	24.17	43.71	306.9	1.19	48.59	5.47	95.12	45.76	9.46	208.2	44.28	0.648	0.444	67.88	1.41	0.048	2.62	0.231	0.662
20BOM-27C	9.74	7.87	0.638	<0.12	3.29	<0.25	16.78	34.93	0.764	65.53	50.00	3.51	0.057	12.94	1.61	0.229	1.92	1.29	0.26
20BOM-27D	11.95	69.07		217.3	73.04	42.76	92.16	76.07	0.589	228.0	9.76	0.168	0.063	8.72	0.389	0.024	1.33	0.011	0.017
20FINNÅS-1	1.57	1.01	0.840	0.316	0.321	1.06	2.87	224.0	2.02	48.74	156.8	3.19	0.051	38.83	5.75	0.271	2.88	1.86	0.693
20FINNÅS-2	9.35	10.18	0.375	0.427	1.15	0.504	1.64	70.11	2.58	45.75	129.6	2.35	0.083	19.37	4.29	0.163	15.64	1.43	0.730
20GEIT-1	3.54	7.01	0.9	<0.12	0.633	<0.25	2.28	29.61	1.21	77.95	146.1	2.26	0.037	23.86	5.16	0.175	2.14	1.53	1.03
20GEIT-2	47.77	13.81	6.66	5.79	1.47	1.58	5.82	80.36	115.3	72.52	255.6	5.13	1.30	380.5	9.87	0.438	2.35	3.29	1.49
20GEIT-4	2.61	6.88	29.87	0.496	2.11	0.968	1.04	24.28	20.52	83.69	127.5	1.95	0.243	195.5	4.69	0.151	1.22	0.972	0.377
20GEIT-5	12.11	21.04	119.9	2.70	12.28	3.07	4.04	75.88	13.60	57.07	77.37	1.45	0.396	105.9	2.81	0.109	1.48	0.627	0.247
20GEIT-6	3.67	6.35	13.74	0.955	0.758	1.32	3.46	80.17	10.45	71.27	108.9	1.31	0.099	220.4	3.69	0.100	2.38	0.561	0.466

Rare earth elements (REE)

Sample ID	Y	La	Ce	Pr	Nd	Sm	Eu	Gd	Tb	Dy	Ho	Er	Tm	Yb	Lu
20BOM-1	41.65	8.22	22.25	3.76	18.86	5.91	1.67	6.86	1.13	7.39	1.54	4.17	0.632	4.02	0.570
20BOM-2	37.92	9.06	24.67	4.19	21.70	6.35	1.36	7.16	1.20	7.05	1.51	4.20	0.582	3.58	0.532
20BOM-4	21.54	2.43	6.62	1.08	5.50	1.90	1.45	2.49	0.452	3.19	0.709	2.12	0.331	2.26	0.352
20BOM-6	43.63	4.41	13.19	2.26	12.09	4.46	1.07	6.17	1.13	7.98	1.65	4.56	0.701	4.42	0.655
20BOM-7	52.04	15.28	33.61	5.33	23.56	6.39	1.09	7.49	1.29	8.45	1.90	5.39	0.844	5.55	0.838
20BOM-8	45.39	14.20	32.14	4.30	18.79	4.80	1.04	6.06	1.03	7.50	1.60	4.68	0.686	4.36	0.665
20BOM-9A	4.69	3.64	7.60	0.990	5.13	1.06	0.361	1.09	0.147	0.842	0.173	0.503	0.066	0.403	0.067
20BOM-9C	23.09	2.35	6.99	1.24	7.13	2.66	1.48	3.50	0.602	4.08	0.857	2.37	0.372	2.47	0.385
20BOM-9E	8.17	0.279	0.902	0.176	1.35	0.619	0.526	1.02	0.204	1.39	0.303	0.889	0.134	0.863	0.136
20BOM-10	7.59	0.202	0.722	0.148	1.23	0.596	0.306	1.05	0.202	1.35	0.301	0.842	0.118	0.717	0.109
20BOM-11	50.85	9.26	24.55	4.29	20.13	6.52	2.09	7.63	1.32	8.31	1.89	5.24	0.831	5.43	0.823
20BOM-12A	40.12	10.27	26.80	3.54	15.47	4.58	0.892	5.47	1.00	6.75	1.53	4.51	0.722	4.68	0.706
20BOM-13A	38.61	44.10	90.26	10.84	42.66	8.76	2.08	8.46	1.23	7.31	1.40	3.85	0.544	3.38	0.485
20BOM-15B	31.99	10.10	27.68	4.12	18.58	4.95	0.696	5.49	0.859	5.55	1.17	3.24	0.481	3.08	0.420
20BOM-17A	23.06	5.65	13.92	1.96	8.79	2.46	0.480	3.08	0.552	3.86	0.839	2.61	0.417	2.83	0.446
20BOM-18	77.75	13.46	33.23	5.21	23.48	7.27	1.78	9.09	1.65	11.40	2.71	8.13	1.32	9.05	1.42
20BOM-19	27.66	8.41	19.86	3.25	14.27	4.29	1.14	4.87	0.779	4.60	0.984	2.68	0.413	2.78	0.401
20BOM-20A	6.89	2.26	5.03	0.681	3.35	0.865	0.990	1.06	0.175	1.08	0.237	0.711	0.107	0.705	0.115

20BOM-20B	10.07	1.11	3.06	0.467	2.38	0.901	0.420	1.29	0.230	1.65	0.376	1.05	0.165	1.14	0.182
20BOM-21D	27.76	4.36	12.37	2.00	9.74	2.98	1.06	3.80	0.663	4.56	1.02	2.91	0.434	2.97	0.457
20BOM-21E	45.60	9.93	25.51	3.99	19.21	5.52	1.23	6.64	1.16	7.81	1.69	5.03	0.781	5.16	0.787
20BOM-21F	40.51	15.85	37.92	5.53	23.74	6.32	1.29	6.61	1.13	7.31	1.52	4.40	0.690	4.64	0.690
20BOM-22A	29.01	3.02	9.40	1.70	9.21	2.93	0.717	4.06	0.705	4.85	1.12	3.24	0.486	3.07	0.500
20BOM-22B	20.78	2.23	6.02	0.950	5.13	1.86	0.663	2.78	0.505	3.52	0.750	2.20	0.328	2.20	0.340
20BOM-23B	59.19	4.27	13.13	2.52	14.12	5.61	1.25	7.53	1.48	10.10	2.27	6.08	0.913	5.59	0.841
20BOM-24A	45.98	46.40	95.89	11.96	46.93	9.71	2.29	9.58	1.47	8.71	1.73	4.70	0.682	4.35	0.646
20BOM-24B	23.10	34.28	63.99	8.48	30.27	6.36	1.87	5.40	0.814	4.38	0.895	2.31	0.335	2.14	0.309
20BOM-24C	50.84	6.13	17.33	2.96	16.70	5.72	1.92	8.02	1.33	8.79	1.84	4.97	0.728	4.39	0.675
20BOM-25	16.85	12.68	25.55	3.61	15.15	3.63	1.32	3.65	0.566	3.38	0.656	1.77	0.248	1.52	0.216
20BOM-26A	35.09	4.49	11.25	1.76	9.01	2.89	0.986	4.44	0.793	6.07	1.29	3.79	0.568	3.93	0.669
20BOM-27C	59.86	12.96	34.92	6.22	30.98	9.73	2.15	9.96	1.66	10.92	2.45	6.65	1.07	6.75	1.04
20BOM-27D	11.51	0.567	1.77	0.329	2.26	0.953	0.408	1.53	0.291	1.95	0.427	1.25	0.185	1.15	0.179
20FINNÅS-1	31.09	12.11	32.75	5.72	25.70	7.87	1.48	6.78	1.10	6.18	1.45	4.00	0.723	5.26	0.827
20FINNÅS-2	37.14	7.00	17.42	2.74	13.84	4.34	0.960	5.69	1.01	6.82	1.49	4.33	0.673	4.52	0.713
20GEIT-1	104.63	8.11	21.14	3.62	16.94	5.77	0.792	8.63	1.96	14.36	3.58	10.60	1.79	11.97	1.87
20GEIT-2	61.49	13.69	36.70	6.15	28.98	8.60	0.977	9.78	1.80	12.30	2.51	7.24	1.17	8.05	1.27
20GEIT-4	39.46	5.80	16.58	2.92	14.55	5.20	1.17	6.10	1.16	7.52	1.71	4.59	0.770	4.93	0.724
20GEIT-5	45.21	5.56	16.34	2.76	15.24	5.17	1.31	7.12	1.25	8.50	1.79	5.07	0.763	4.76	0.707
20GEIT-6	36.03	4.96	14.65	2.47	13.13	4.07	1.07	5.15	0.899	6.40	1.40	4.31	0.667	4.56	0.702

Appendix 3 – Geochronology data (LA-ICP-MS)

Laboratory & Sample Preparation	
Laboratory name	Department of Earth Science, University of Bergen
Sample type/mineral	Zircon
Sample preparation	Conventional mineral separation, 2.5 cm resin mount, 0.025 □m polish to finish
Imaging	CL, Zeiss Supra55 VP, 15 kV, 1 nA, 15mm working distance
Laser ablation system	
Make, Model & type	RESOlution M-50 LR with a Coherent COMPexPRO® 110 193 nm ArF excimer laser
Ablation cell & volume	Two volume
Laser wavelength	193 nm
Pulse duration	20 ns
Fluence	2.2 - 2.5 J.cm^{-2}
Repetition rate	5 Hz
Ablation duration	30 secs
Spot diameter	19 and 26 µm
Sampling mode / pattern	Static spot ablation/circular
Carrier gas	He (0.75 l/min) with small amounts of N2 (0.004 ml/min) mixed in before entering the ICP-MS to increase sensitivity.
Signal smoothing device	"Squid" connected between the laser and the ICP-MS
ICP-MS Instrument	
Make, Model & type	Nu Instruments, Nu Attom HR, SC-ICP-MS
Sample introduction	Ablation aerosol from laser ablation
RF power	1300W
Cool gas	Ar 13 l/min
Aux gas	Ar 0.7 l/min
Make-up gas flow	Ar 0.49 l/min
Detection system	MasCom Electron Multiplier
Masses measured	^{202}Hg, ^{204}(Hg + Pb), ^{206}Pb, ^{207}Pb, ^{208}Pb, ^{232}Th, ^{238}U
Integration time per peak/dwell times	200µs for ^{202}Hg, ^{204}(Hg + Pb), ^{206}Pb, ^{208}Pb, ^{232}Th, ^{238}U 800 µs for ^{207}Pb and ^{235}U
Number of sweeps per cycle	10
Total time per cycle	0.0493 s
Analysis method	Deflector jump
IC Dead time	14 ns
Detection Mode	Ion counting mode and ion-attenuated mode
Data Processing	
Gas blank	15 s

Calibration strategy	91500 (Wiedenbeck et al., 1995) used as primary reference material, while Plesovice (Sláma et al., 2008), Mud Tank (Horstwood et al., 2016), & GJ1 (nr. 63; Jackson et al., 2004) are used as secondaries.
Data processing package used / Correction for LIEF	Iolite4 (v. 4.4.5) for data normalization, uncertainty propagation and age calculation. LIEF correction assumes reference material and samples behave identically.
Common-Pb correction	No common-Pb correction applied to the data.
Data reduction	VizualAge UComPbine (Chew et al. 2014)
Down-hole correction model	Exponential or Exponential + linear
Uncertainty level & propagation	Ages are quoted at 2*s* absolute, propagation is by quadratic addition.
Quality control / Validation	**Run1 – LAS391 and LAS392** *Plesovice* – Wtd ave $^{206}Pb/^{238}U$ age = 340 ± 3 (2*s*, MSWD = 12, n=22) *GJ-1* – Wtd ave $^{206}Pb/^{238}U$ age = 592 ± 4 (2*s*, MSWD = 87, n=20) *91500* – Wtd ave $^{206}Pb/^{238}U$ age = 1061 ± 11 (2*s*, MSWD = 0.66, n=21) Systematic uncertainty for propagation is 2% (2*s*). **Run2 –LAS390** *Plesovice* – Wtd ave $^{206}Pb/^{238}U$ age = 347 ± 4 (2*s*, MSWD = 4.5, n=32) *GJ-1* – Wtd ave $^{206}Pb/^{238}U$ age = 611 ± 8 (2*s*, MSWD = 1.6, n=33) *91500* – Wtd ave $^{206}Pb/^{238}U$ age = 1061 ± 15 (2*s*, MSWD = 0.78, n=63) *Mudtank* – Wtd ave $^{206}Pb/^{238}U$ age = 720 ± 20 (2*s*, MSWD = 0.41, n=33) Systematic uncertainty for propagation is 2% (2*s*).
Data reporting	Reported in the format of the plasmage.org data reporting template (http://www.plasmage.org/recommendations/home.html) using a python script made by Joe Petrus (https://github.com/iolite-LA-ICP-MS/iolite4-python-examples/blob/master/export/PlasmAge.py).
Data visualization	Plotting of concordia and weighted mean using IsoplotR (Vermeesch, 2018)

LAS390 (20BOM-9A)														
	Isotopic ratios							Calculated ages (Ma)						
ID	$^{207}Pb/^{235}U$	1σ	$^{206}Pb/^{238}U$	1σ	Rho	$^{207}Pb/^{206}Pb$	1σ	$^{207}Pb/^{206}Pb$	2σ	$^{206}Pb/^{238}U$	2σ	$^{207}Pb/^{235}U$	2σ	%conc
LAS390_1	0.6226	1.0	0.07893	0.8	0.12	0.05829	1.0	567	38	489	8	489	8	92.1
LAS390_2	0.6306	1.0	0.07952	0.7	0.33	0.05896	1.0	587	41	494	7	494	8	92.1
LAS390_3	0.6272	1.7	0.07905	1.1	0.23	0.05916	1.8	761	62	491	10	488	13	92.1
LAS390_4	0.6523	1.7	0.08088	1.2	0.22	0.06051	1.8	807	59	501	11	506	14	91.9
LAS390_5-1	0.6792	2.5	0.08218	1.4	0.26	0.06128	2.7	924	80	508	13	513	20	91.7
LAS390_5-2	0.6800	2.8	0.08184	1.4	0.19	0.06211	3.0	1049	90	506	14	511	23	91.7
LAS390_5-3	0.6057	2.3	0.07822	1.4	0.16	0.05801	2.5	899	79	486	13	470	18	92.3
LAS390_6	0.6082	1.8	0.07625	1.0	0.22	0.05830	1.8	751	59	473	9	476	13	92.0
LAS390_7-Core	0.6753	1.6	0.07880	1.0	0.16	0.06453	1.8	880	61	488	9	520	14	91.4
LAS390_8-Rim	0.7096	3.4	0.08121	1.4	-0.03	0.06860	3.8	1252	97	502	14	517	29	91.3
LAS390_9	0.6241	2.2	0.08061	1.2	0.10	0.05796	2.4	829	83	500	11	481	17	92.3
LAS390_10-sprekker	0.6783	1.0	0.08829	0.8	0.40	0.05691	1.0	543	36	545	8	524	8	92.3
LAS390_11	0.6333	2.8	0.07894	1.3	0.14	0.05969	2.9	1009	84	489	12	481	22	92.0
LAS390_12-morkcl	0.7039	0.7	0.08102	0.8	0.47	0.06316	0.8	697	32	502	7	540	6	91.3
LAS390_13	0.6073	1.5	0.07666	0.9	0.36	0.05769	1.4	647	50	477	9	477	11	92.1
LAS390_14	0.6272	1.8	0.07538	1.1	0.23	0.06138	2.0	823	67	469	10	488	14	91.7
LAS390_15	0.6318	0.9	0.08012	0.7	0.37	0.05841	0.9	569	37	497	7	495	7	92.1
LAS390_16-1	0.6477	2.2	0.07844	1.1	0.11	0.06265	2.4	969	74	487	11	500	18	91.7
LAS390_16-2	0.6177	3.0	0.08130	1.4	0.08	0.05736	3.2	1044	100	503	14	469	23	92.4
LAS390_17	0.6184	0.8	0.07677	0.7	0.50	0.05939	0.7	567	32	477	6	487	6	91.9
LAS390_18	0.6428	2.7	0.07872	1.3	0.17	0.05943	2.7	942	86	488	12	489	22	91.8
LAS390_19	0.6524	3.1	0.07925	1.6	0.15	0.06205	3.3	1187	99	490	15	490	25	91.8
LAS390_20	0.6212	1.1	0.07926	0.9	0.38	0.05793	1.2	588	44	491	8	489	9	92.2
LAS390_21	0.6359	1.2	0.08112	0.9	0.36	0.05804	1.3	622	48	502	9	497	10	92.2
LAS390_22	0.8092	3.1	0.08233	1.7	0.06	0.07736	3.4	1412	99	510	17	586	28	90.2
LAS390_23	0.6794	1.0	0.08359	0.8	0.42	0.05954	1.0	617	39	517	8	524	8	91.9
LAS390_24	0.6435	0.9	0.08153	0.7	0.47	0.05772	0.8	538	34	505	7	503	7	92.1
LAS390_25	0.6166	1.5	0.07681	1.1	0.41	0.05942	1.5	705	56	477	10	484	12	92.0
LAS390_26-sprekk	1.3230	1.7	0.07674	1.4	0.19	0.13136	1.9	2031	72	476	13	843	21	82.8
LAS390_27-inkl	0.6128	2.0	0.07683	1.0	0.07	0.05946	2.2	864	71	477	9	476	16	92.0

LAS390_27-inkl	0.6219	1.7	0.07760	0.9	0.19	0.05952	1.7	777	60	482	9	486	13	92.0
LAS390_28	0.6165	1.1	0.07787	0.9	0.41	0.05873	1.1	595	41	483	8	485	8	92.1
LAS390_29-1	0.9248	1.3	0.07761	1.0	0.32	0.08810	1.3	1345	52	481	9	662	12	88.1
LAS390_29-2	0.7931	1.2	0.07789	0.9	0.34	0.07485	1.2	1042	47	483	8	590	11	89.8
LAS390_30-sprekk-inkl	0.6093	1.6	0.07727	1.1	0.27	0.05830	1.6	724	57	479	10	477	13	92.1
LAS390_31-inkl	0.5999	1.0	0.07507	0.8	0.27	0.05898	1.1	611	40	466	7	475	8	92.0
LAS390_32	0.6181	2.9	0.07906	1.2	0.10	0.05834	3.0	968	88	490	12	473	23	92.2
LAS390_33-core	0.6442	0.9	0.08281	0.7	0.39	0.05786	0.9	554	34	513	7	503	7	92.2
LAS390_34-rim	0.6901	0.9	0.07897	0.8	0.17	0.06476	0.9	754	35	490	7	531	7	91.3
LAS390_35	0.6584	2.6	0.08103	1.2	0.03	0.06202	2.8	1042	79	501	12	500	22	91.9
LAS390_36	0.6285	1.0	0.07664	0.6	0.17	0.06078	1.1	656	43	476	6	494	8	91.8
LAS390_37	0.6261	2.5	0.07993	1.1	0.00	0.05911	2.7	955	83	495	11	483	20	92.2
LAS390_38	0.5964	2.2	0.07802	1.1	0.21	0.05699	2.3	803	75	484	11	467	16	92.4
LAS390_1-2	0.6185	0.8	0.07807	0.7	0.40	0.05835	0.8	540	32	484	6	488	6	92.1
LAS390_39	0.6261	2.2	0.07761	1.0	0.25	0.06202	2.4	917	76	481	10	483	17	91.9
LAS390_40	0.5987	1.7	0.07664	1.1	0.20	0.05852	1.7	762	58	475	10	472	13	92.2
LAS390_41	0.6146	1.8	0.07861	1.1	0.11	0.05903	1.9	791	64	487	10	483	14	92.2
LAS390_42	0.5684	1.4	0.07675	0.9	0.23	0.05573	1.5	630	53	476	9	454	10	92.6
LAS390_43	0.6004	1.3	0.07623	1.1	0.55	0.05808	1.1	596	40	473	10	476	10	92.1
LAS390_44	1.2105	0.7	0.07917	0.6	0.46	0.11271	0.7	1830	24	491	6	803	7	84.7
LAS390_45	0.6329	1.5	0.08033	1.0	0.18	0.05873	1.6	733	60	498	10	495	12	92.1
LAS390_46	0.6118	1.8	0.07655	1.0	0.16	0.06000	1.9	802	66	475	9	479	14	92.0
LAS390_47	0.6265	1.2	0.07579	0.7	0.96	0.06067	1.3	719	47	471	6	491	10	91.7
LAS390_48-1	0.6131	1.0	0.07571	0.7	0.27	0.05957	1.1	625	41	470	6	484	8	91.9
LAS390_48-2	0.5862	1.2	0.07419	1.1	0.44	0.05917	1.2	655	43	461	10	467	9	92.1
LAS390_49-inkl-sprekk	0.6170	0.8	0.07781	0.7	0.47	0.05815	0.8	541	33	483	6	487	6	92.1

LAS391 (20BOM-11)														
	Isotopic ratios							Calculated ages (Ma)						
ID	$^{207}Pb/^{235}U$	1σ	$^{206}Pb/^{238}U$	1σ	Rho	$^{207}Pb/^{206}Pb$	1σ	$^{207}Pb/^{206}Pb$	2σ	$^{206}Pb/^{238}U$	2σ	$^{207}Pb/^{235}U$	2σ	%conc
LAS391_1	0.6572	1.2	0.08109	0.8	0.19	0.0598	1.33	877	44	502	8	503	10	99.7
LAS391_2	0.6160	0.8	0.07721	0.5	0.21	0.0582	0.89	668	30	479	5	484	6	98.9
LAS391_3	0.6130	0.9	0.07753	0.6	0.17	0.0581	1.03	712	35	481	5	483	7	99.7
LAS391_4	0.5703	0.8	0.07198	0.6	0.23	0.0577	0.90	631	33	448	5	457	6	98.1
LAS391_5	0.6214	0.9	0.07805	0.6	0.29	0.0582	0.91	674	32	484	6	487	7	99.4
LAS391_6	0.6070	0.9	0.07767	0.5	0.01	0.0573	0.97	667	32	482	5	477	7	101.1
LAS391_7	0.6051	0.6	0.07626	0.4	0.27	0.0580	0.62	592	23	474	4	478	5	99.0
LAS391_8	0.6085	0.8	0.07698	0.5	0.37	0.0569	0.80	588	29	478	5	481	6	99.3
LAS391_9	0.6094	1.0	0.07544	0.6	0.10	0.0597	1.10	798	35	468	5	477	8	98.1
LAS391_10	0.6102	0.8	0.07697	0.5	0.20	0.0581	0.77	630	28	478	5	481	6	99.4
LAS391_11	0.6333	0.7	0.07996	0.5	0.17	0.0578	0.80	616	29	496	5	495	6	100.0
LAS391_12	0.6175	0.9	0.07717	0.6	0.16	0.0582	1.00	673	35	479	5	484	7	98.9
LAS391_13	0.9994	1.2	0.08059	0.6	0.33	0.0905	1.13	1374	43	499	6	696	12	71.7
LAS391_14	0.6126	1.1	0.07737	0.6	0.08	0.0586	1.26	824	40	480	6	477	9	100.7
LAS391_15	0.6112	0.7	0.07760	0.5	0.33	0.0574	0.75	585	28	481	5	483	5	99.7
LAS391_16	0.6585	0.8	0.07878	0.6	0.24	0.0614	0.87	741	31	488	5	511	7	95.6
LAS391_17	0.5720	0.7	0.07345	0.5	0.05	0.0573	0.78	614	27	457	4	456	5	100.1
LAS391_18	0.6278	0.7	0.07838	0.5	0.35	0.0585	0.69	612	25	487	5	493	5	98.8
LAS391_19	0.5749	0.6	0.07273	0.5	0.48	0.0576	0.61	570	22	452	5	460	5	98.4
LAS391_20	0.6455	0.8	0.08178	0.6	0.50	0.0578	0.70	612	25	506	6	503	6	100.7
LAS391_21	0.6117	0.6	0.07793	0.5	0.31	0.0574	0.67	587	25	483	4	483	5	100.1
LAS391_22	0.6184	0.7	0.07829	0.5	0.16	0.0574	0.71	572	26	486	5	486	5	99.8
LAS391_23	0.7495	1.0	0.09146	0.6	0.37	0.0603	0.96	763	32	564	7	562	9	100.4
LAS391_24	0.5709	0.6	0.07334	0.4	0.35	0.0570	0.59	557	22	456	4	457	4	99.9
LAS391_25	0.6826	0.6	0.08516	0.6	0.45	0.0587	0.47	564	19	527	6	526	5	100.1
LAS391_26	0.5825	0.6	0.07349	0.4	0.31	0.0579	0.59	581	22	457	3	464	4	98.4
LAS391_27	0.6515	0.8	0.07942	0.5	0.29	0.0595	0.82	683	30	492	5	505	6	97.4
LAS391_28	0.6156	0.9	0.07714	0.6	0.06	0.0583	0.95	654	33	479	6	483	7	99.2
LAS391_29	0.5492	1.0	0.06902	0.5	0.10	0.0582	1.11	737	35	430	4	439	8	98.1
LAS391_30	0.5660	0.8	0.07096	0.5	0.18	0.0582	0.77	636	27	442	5	452	6	97.7
LAS391_31	0.5698	0.6	0.07230	0.4	0.32	0.0573	0.61	564	23	450	4	456	4	98.6
LAS391_32	0.6071	1.0	0.07548	0.6	0.25	0.0580	0.97	665	33	469	5	478	7	98.0

LAS391_33	0.5743	0.6	0.07244	0.4	0.35	0.0579	0.56	574	21	451	3	460	4	98.1
LAS391_34	0.6528	0.8	0.08212	0.6	0.12	0.0578	0.85	613	29	508	6	506	6	100.4
LAS391_35	0.5733	0.5	0.07168	0.4	0.44	0.0581	0.49	553	19	446	4	459	4	97.3
LAS391_36	0.6103	0.6	0.07749	0.4	0.32	0.0573	0.64	580	24	466	7	482	5	99.9
LAS391_37	0.5949	0.6	0.07478	0.4	0.27	0.0577	0.59	576	22	490	12	473	4	98.2
LAS391_38	0.6288	0.7	0.07997	0.5	0.33	0.0577	0.74	627	27	513	7	492	6	100.7
LAS391_39	0.5764	0.5	0.07303	0.4	0.30	0.0573	0.52	541	20	490	7	461	4	98.6
LAS391_40	0.7026	0.6	0.08836	0.5	0.47	0.0578	0.54	550	21	501	12	539	5	101.2
LAS391_41	0.6190	0.8	0.07835	0.6	0.28	0.0575	0.84	628	30	476	6	487	6	99.8
LAS391_42	0.6302	0.7	0.07929	0.5	0.34	0.0579	0.68	603	25	495	11	494	5	99.6
LAS391_43	0.6052	0.6	0.07619	0.4	0.41	0.0573	0.62	559	23	484	11	479	5	98.9
LAS391_44	0.5860	0.6	0.07379	0.4	0.14	0.0580	0.67	595	24	484	6	466	5	98.5
LAS391_45	0.6736	0.7	0.08172	0.5	0.26	0.0601	0.78	671	28	481	10	520	6	97.3

LAS392 (20BOM-12A)														
Isotopic ratios								Calculated ages (Ma)						
ID	$^{207}Pb/^{235}U$	1σ	$^{206}Pb/^{238}U$	1σ	Rho	$^{207}Pb/^{206}Pb$	1σ	$^{207}Pb/^{206}Pb$	2σ	$^{206}Pb/^{238}U$	2σ	$^{207}Pb/^{235}U$	2σ	%conc
LAS392_1	0.6005	0.8	0.07762	0.5	0.17	0.0565	0.88	653	31	482	4	474	6	101.5
LAS392_2	0.6386	1.0	0.07957	0.6	0.25	0.0587	0.98	726	32	493	5	496	8	99.4
LAS392_3	0.6094	0.8	0.07623	0.5	0.22	0.0581	0.88	697	31	473	5	480	6	98.6
LAS392_4	0.5837	0.5	0.07387	0.4	0.26	0.0571	0.50	507	19	459	3	466	4	98.6
LAS392_5	0.5919	0.4	0.07495	0.3	0.54	0.0573	0.36	505	15	466	3	472	3	98.7
LAS392_6	0.6474	0.9	0.08044	0.6	0.29	0.0588	0.91	696	31	499	6	502	7	99.4
LAS392_7	0.6482	0.9	0.08271	0.5	0.20	0.0571	0.97	666	33	512	5	502	7	101.9
LAS392_8	0.6649	1.3	0.08168	0.8	0.32	0.0609	1.42	899	43	505	7	504	10	100.2
LAS392_9	0.6318	1.0	0.08027	0.6	0.19	0.0573	1.05	703	35	498	5	492	8	101.1
LAS392_10	0.6446	1.0	0.08052	0.6	0.24	0.0590	1.04	737	34	499	6	502	8	99.3
LAS392_11	0.6257	1.0	0.07893	0.5	0.13	0.0573	1.05	691	36	489	5	488	8	100.3
LAS392_12	0.6203	1.1	0.07847	0.6	0.06	0.0582	1.12	753	35	487	5	482	8	100.9
LAS392_13	0.5976	0.9	0.07662	0.5	0.12	0.0567	0.97	706	32	476	5	471	7	100.9
LAS392_14	0.6239	1.0	0.07869	0.5	0.13	0.0579	1.00	726	33	488	5	487	7	100.1
LAS392_15	0.7617	0.7	0.08118	0.5	0.30	0.0683	0.72	881	27	503	5	572	6	88.0
LAS392_16	0.6145	0.9	0.07595	0.6	-0.03	0.0594	0.99	722	33	472	5	481	7	98.1
LAS392_17	0.6297	1.0	0.07737	0.6	0.10	0.0592	1.08	728	35	480	6	490	8	98.0
LAS392_18	0.6164	0.9	0.07826	0.6	0.14	0.0574	0.98	715	33	486	5	483	7	100.5
LAS392_19	2.0997	1.5	0.08841	0.7	0.53	0.1685	1.28	2480	46	546	7	1100	23	49.6
LAS392_20	0.6207	0.9	0.07899	0.5	0.07	0.0573	0.92	664	31	490	4	485	7	101.0
LAS392_21	0.6011	0.7	0.07742	0.5	0.22	0.0565	0.76	598	26	480	4	476	6	101.0
LAS392_22	0.5716	0.6	0.07253	0.4	0.38	0.0571	0.52	535	20	451	3	458	4	98.6
LAS392_23	0.6281	0.7	0.07953	0.4	0.23	0.0574	0.76	623	27	493	4	492	6	100.3
LAS392_24	0.6290	0.8	0.07955	0.5	0.18	0.0575	0.85	660	29	493	5	492	6	100.2
LAS392_25	0.6007	1.0	0.07505	0.5	0.02	0.0586	1.02	733	33	466	5	472	7	98.8
LAS392_26	0.6820	1.3	0.07709	0.8	0.10	0.0662	1.48	1024	47	478	7	518	10	92.3
LAS392_27	0.6206	1.1	0.08083	0.7	0.29	0.0565	1.15	737	37	500	6	486	8	103.0
LAS392_28	0.6751	1.1	0.08104	0.7	0.19	0.0611	1.12	795	37	502	6	516	8	97.4
LAS392_29	0.5923	1.3	0.07526	0.6	0.04	0.0589	1.49	884	44	468	6	463	10	101.0
LAS392_30	0.6003	0.4	0.07678	0.4	0.41	0.0567	0.39	484	16	477	3	477	3	100.0
LAS392_31	0.5978	1.0	0.07747	0.5	0.09	0.0567	1.00	674	32	481	5	470	7	102.3
LAS392_32	0.5901	0.6	0.07425	0.4	0.30	0.0572	0.59	543	22	462	3	470	4	98.2
LAS392_33	0.6066	1.0	0.06596	0.6	0.14	0.0677	1.11	927	37	412	5	475	8	86.7

LAS392_34	0.5815	1.1	0.07708	0.6	0.13	0.0565	1.24	800	39	478	6	460	9	104.0
LAS392_35	0.6036	1.0	0.07817	0.6	0.03	0.0569	1.10	683	33	485	5	474	7	102.2
LAS392_36	0.6290	1.2	0.07926	0.6	-0.01	0.0582	1.22	747	36	491	6	486	8	101.2